Evaluation of occupational exposures in Endoscopic Retrograde Cholangiopancreatography using Monte Carlo Simulation

Lucas Wilian Gonçalves de Souza

Universidade Federal de Uberlândia
Faculdade de Engenharia Elétrica
Programa de Pós-Graduação em Engenharia Biomédica

Uberlândia
2020

Lucas Wilian Gonçalves de Souza

Evaluation of occupational exposures in Endoscopic Retrograde Cholangiopancreatography using Monte Carlo Simulation

Thesis presented to the Programa de Pós-graduação em Engenharia Biomédica from the Faculdade de Engenharia Elétrica of the Universidade Federal de Uberlândia as partial requirement to obtain the title of Master of Sciences.

Study field: Biomedical Engineering

Supervisor: Prof. Dr. Lucio Pereira Neves
Co-supervisor: Prof. Dr. Ana Paula Perini

Uberlândia
2020

Ficha Catalográfica Online do Sistema de Bibliotecas da UFU
com dados informados pelo(a) próprio(a) autor(a).

S729 Souza, Lucas Wilian Goncalves de, 1990-
2020 Evaluation of occupational exposures in Endoscopic Retrograde Cholangiopancreatography using Monte Carlo Simulation [recurso eletrônico] / Lucas Wilian Goncalves de Souza. - 2020.

Orientador: Lucio Pereira Neves.
Coorientadora: Ana Paula Perini.
Dissertação (Mestrado) - Universidade Federal de Uberlândia, Pós-graduação em Engenharia Biomédica.
Modo de acesso: Internet.
Disponível em: http://doi.org/10.14393/ufu.di.2020.295
Inclui bibliografia.
Inclui ilustrações.

1. Engenharia biomédica. I. Neves, Lucio Pereira,1982-, (Orient.). II. Perini, Ana Paula,1981-, (Coorient.). III. Universidade Federal de Uberlândia. Pós-graduação em Engenharia Biomédica. IV. Título.

CDU: 62:61

Bibliotecários responsáveis pela estrutura de acordo com o AACR2:
Gizele Cristine Nunes do Couto - CRB6/2091
Nelson Marcos Ferreira - CRB6/3074

I dedicate this work to Jandira, my loving and caring mom, who has always done everything she could to provide me a happy life.

Acknowledgments

To my family for the support and incentive in every single time I needed.
To Paula Justino for all her initial help with the MCNP code.
To my friends who gave me many moments of joy, support and collective crying. I won't dare listing names for I will surely forget someone.
To Rosângela and Gustavo for their medical support on my mental illness, advice and incentives that were fundamental for me staying on this path.
To Edson Mundin for all his hard work, patience and advice at the PPGEB office.
To Prof. Dr. William de Souza Santos for all his help with the phantom manipulations and MCNP classes.
To my supervisors Prof. Dr. Lucio Pereira Neves and Prof. Dr. Ana Paula Perini who always supported me on my academic and personal lives. You make feel part of your family.
To the Overleaf™ team for making my writing process MUCH easier.
To USP and FACOM-UFU professors for creating the Latex dissertation template in English that I used.
To Roberto, my boyfriend, for all his support, love and kindness in these turbulent final months of research.
To all people who fought and still fight for the right of education for all human beings.
To FAPEMIG for the financial support through "FAPEMIG Projetos Demanda UNIVERSAL FAPEMIG nº APQ-02934-15 and APQ-03049-15."
To CNPq for the financial support through "Projetos UNIVERSAL CNPq nº 421603/2016-0 and 420699/2016-3."
To the Programa de Pós Graduação em Engenharia Biomédica (PPGEB).
To the Universidade Federal de Uberlândia.

"If I have seen further, it is by standing upon the shoulders of giants"
(Isaac Newton)

Resumo

O modo de vida contemporâneo em conjunto com o envelhecimento da população mundial criam um cenário favorável ao aumento das doenças hepatobiliárias e pancreáticas. A Colangiopancreatografia Endoscópica Retrógrada (ERCP) é uma das principais técnicas médicas aplicadas no diagnóstico e tratamento dessas doenças. A ERCP é um procedimento guiado por fluoroscopia, portanto ela expõe paciente e profissionais à radiação ionizante. Essa exposição pode provocar reações teciduais e câncer tardio. O objetivo desse trabalho foi aplicar simulações de Monte Carlo (MC) para avaliar a exposição à radiação de pacientes e profissionais durante procedimentos de ERCP. O cenário simulado reproduziu uma sala típica de ERCP equipada com um sistema de raios-x com tubo acima da mesa. Os simuladores virtuais antropomórficos MASH3 e FASH3 foram utilizados para representar paciente, médico e médico assistente. O paciente foi simulado na posição prona sobre a mesa. Os profissionais utilizaram avental com equivalência de 0.5 mm de Pb, protetor de tireoide e óculos plumbífero. Os parâmetros fluoroscópicos foram tensão do tubo de 70, 80, 90, 100 e 110 kVp; tamanho de campo irradiado de 15×15 cm^2, 17×17 cm^2, 22×22 cm^2, 25×25 cm^2, 31×31 cm^2 e 38×38 cm^2. Os espectros de raios-x foram simulados no programa SRS 78 e as simulações de Monte Carlo foram implementadas no código *Monte Carlo N-Particle eXtenteded* (MCNPX) (versão 2.7.0). Os resultados mostram que, para uma tensão do tubo, os coeficientes de conversão para dose efetiva CC[E] do paciente aumentaram até que a área irradiada se tornou maior do que a área do paciente que deveria ter sido irradiada. Para um campo fixo, os CC[E] do paciente aumentaram à medida que a tensão do tubo foi aumentada. Considerando os profissionais, os valores de CC[E] também aumentaram quando o campo aumentou, mas a tensão do tubo foi inalterada. Os valores de CC[E], para um tamanho do campo fixo, aumentaram quando a tensão do tubo foi elevada. As doses efetivas estimadas com os valores médios dos CC[E] e valores de Produto Dose Área (DAP) encontrados na literatura estão de acordo com os valores de trabalhos anteriores. Os valores dos coeficientes de conversão para dose equivalente CC[H_T] também estão de acordo com a literatura. Este trabalho apresenta os primeiros resultados de um projeto maior que foca na proteção

radiológica de um hospital universitário.

Palavras-chave: ERCP. Radiação Ionizante. Simulação de Monte Carlo. Dosimetria. Proteção Radiológica..

UNIVERSIDADE FEDERAL DE UBERLÂNDIA
Coordenação do Programa de Pós-Graduação em Engenharia Biomédica
Av. João Naves de Ávila, 2121, Bloco 3N, Sala 115 - Bairro Santa Mônica, Uberlândia-MG, CEP 38400-902
Telefone: (34) 3239-4761 - www.ppgeb.feelt.ufu.br - ppegb@feelt.ufu.br

ATA DE DEFESA - PÓS-GRADUAÇÃO

Programa de Pós-Graduação em:	Engenharia Biomédica				
Defesa de:	Dissertação de Mestrado Acadêmico, 058, PPGEB				
Data:	cinco de março de dois mil e vinte	Hora de início:	15 horas	Hora de encerramento:	17 horas
Matrícula do Discente:	11812EBI005				
Nome do Discente:	Lucas Wilian Gonçalves de Souza				
Título do Trabalho:	Evaluation of Occupational Exposures in Endoscopic Retrograde Cholangiopancreatography using Monte Carlo Simulation				
Área de concentração:	Engenharia Biomédica				
Linha de pesquisa:	Sistemas Computacionais e Dispositivos Aplicados à Saúde				
Projeto de Pesquisa de vinculação:	Dosimetria para exames de radiodiagnóstico convencional e tomossíntese mamária				

Reuniu-se no Anfiteatro do bloco 1E, Campus Santa Mônica, da Universidade Federal de Uberlândia, a Banca Examinadora, designada pelo Colegiado do Programa de Pós-graduação em Engenharia Biomédica, assim composta: Professores Doutores: Selma Terezinha Milagre - FEELT/UFU; Linda Viola Ehlin Caldas - IPEN; Lucio Pereira Neves - INFIS/UFU orientador do candidato.

Iniciando os trabalhos o presidente da mesa, Dr. Lucio Pereira Neves, apresentou a Comissão Examinadora e o candidato(a), agradeceu a presença do público, e concedeu ao Discente a palavra para a exposição do seu trabalho. A duração da apresentação do Discente e o tempo de arguição e resposta foram conforme as normas do Programa.

A seguir o senhor(a) presidente concedeu a palavra, pela ordem sucessivamente, aos(às) examinadores(as), que passaram a arguir o(a) candidato(a). Ultimada a arguição, que se desenvolveu dentro dos termos regimentais, a Banca, em sessão secreta, atribuiu o resultado final, considerando o(a) candidato(a):

Aprovado.

Esta defesa faz parte dos requisitos necessários à obtenção do título de Mestre.

O competente diploma será expedido após cumprimento dos demais requisitos, conforme as normas do Programa, a legislação pertinente e a regulamentação interna da UFU.

Nada mais havendo a tratar foram encerrados os trabalhos. Foi lavrada a presente ata que após lida e achada conforme foi assinada pela Banca Examinadora.

Documento assinado eletronicamente por **Lucio Pereira Neves**, **Professor(a) do Magistério Superior**, em 05/03/2020, às 17:06, conforme horário oficial de Brasília, com fundamento no art. 6º, § 1º, do Decreto nº 8.539, de 8 de outubro de 2015.

Documento assinado eletronicamente por **Selma Terezinha Milagre**, **Professor(a) do Magistério Superior**, em 05/03/2020, às 17:08, conforme horário oficial de Brasília, com fundamento no art. 6º, § 1º, do Decreto nº 8.539, de 8 de outubro de 2015.

Documento assinado eletronicamente por **Linda Viola Ehlin Caldas**, **Usuário Externo**, em 05/03/2020, às 17:14, conforme horário oficial de Brasília, com fundamento no art. 6º, § 1º, do Decreto nº 8.539, de 8 de outubro de 2015.

A autenticidade deste documento pode ser conferida no site https://www.sei.ufu.br/sei/controlador_externo.php?acao=documento_conferir&id_orgao_acesso_externo=0, informando o código verificador **1909991** e o código CRC **6D4D8CBE**.

Referência: Processo nº 23117.016046/2020-91 SEI nº 1909991

Abstract

The contemporary life style and the aging of world population have set a favorable scenario to the increase of hepatobiliary and pancreatic diseases. The Endoscopic Retrograde Cholangiopancreatography (ERCP) is one of the main medical techniques employed to diagnose and treat those diseases. ERCP is a fluoroscopy guided procedure, therefore it exposes patient and medical staff to ionizing radiation. This exposure may lead to tissue reactions and cancer later in life. The objective of this work was to apply Monte Carlo (MC) simulation to evaluate patient and staff radiation exposure during ERCP procedures. The simulated scenario reproduced a typical ERCP room equipped with an over-couch x-ray system. MASH3 and FASH3 virtual anthropomorphic phantoms were utilised to represent the patient, the physician and the assistant physician. The patient was placed in prone position on the table. The staff wore 0.5 mm Pb apron, thyroid collar and eyewear. The fluoroscopic parameters were tube voltage of 70, 80, 90, 100 and 110 kVp; the Field of View (FOV) sizes were 15×15 cm^2, 17×17 cm^2, 22×22 cm^2, 25×25 cm^2, 31×31 cm^2 and 38×38 cm^2. The x-ray spectra were simulated in SRS78 software and the Monte Carlo simulations were implemented in the Monte Carlo N-Particle eXtended (MCNPX) (version 2.7.0) code. For a given tube voltage, the results show an increase of patient conversion coefficients for effective dose CC[E] values for FOV sizes increments until the irradiated area suppressed patient area, then for larger FOV sizes, the CC[E] values decreased. For a defined FOV size, the patient CC[E] values raised as the tube voltage was increased. Concerning the staff, the CC[E] values increased for elevated tube voltages, given a fixed FOV size. Their CC[E] values also raised when the tube voltage was unchanged but the FOV sizes were expanded. The effective dose calculated from the mean CC[E] values and Dose Area Product (DAP) from the literature are in agreement with previous works. The estimated conversion coefficients for equivalent dose CC[H_T] values are also consistent with the literature. This work presents the first results of a greater project focused on the radiation protection at an university hospital.

Keywords: ERCP. Ionizing Radiation. Monte Carlo Simulation. Dosimetry. Radiation Protection.

List of Figures

List of Tables

Acronyms list

BMI Body Mass Index

BPD Biliary and Pancreatic Ducts

CC Conversion Coefficient

CPE Collective Protective Equipment

CC[E] Conversion Coefficient for Effective Dose

]CC[$\mathbf{H_T}$]]Conversion Coefficient for Equivalent Dose

DAP Dose Area Product

ESD Entrance Skin Dose

ERCP Endoscopic Retrograde Cholangiopancreatography

FOV Field of View

GPU Graphics Processing Unit

MC Monte Carlo

MCNPX Monte Carlo N-Particle eXtended

PPE Personal Protective Equipment

RBM Red Bone Marrow

Contents

Chapter 1

Introduction

The Biliary and Pancreatic Ducts (BPD) diseases are amongst the health problems responsible for many deaths, morbidity and economical losses (SHAFFER, 2006; SANDLER *et al.*, 2002; AERTS; PENNINCKX, 2003). In the last decades, the number of BPD diseases have increased due to the bad health habits and population aging. It is also important to highlight the prevalence of BPD in pregnant women as a consequence of the hormonal disbalance during pregnancy (VALDIVIESO *et al.*, 1993). These diseases are treated or diagnosed by laparoscopy or retrograde endoscopic cholangiopancreatography (ERCP). Laparoscopy is performed by means of a incision in the abdominal region where a physician can visualize and treat the problem. ERCP is an upper endoscopy guided by fluoroscopy. Both techniques present advantages and disadvantages. This dissertation focuses on ERCP since it exposes both patient and professionals to ionizing radiation.

The first successful canulation of the Vater Papilla was performed by McCune *et al.* (1968). This achievement enabled both diagnosis and treatment of BPD with minimal intervention due to the use of fluoroscopy and contrast agents. As seen in Figure 1, the procedure consists of the insertion of a duodenoscope in to the patient mouth (under sedation) passing through the oesophagus and stomach finally reaching the duodenum. In the left side wall of this organ is located the Vater Papilla which is the final billiary and pancreatic ducts access to the duodenum. A lateral camera placed in the tip of the duodenoscope enables the visualization of the site. Through the duodenoscope the physician can insert a cateter to investigate the ducts, the interventions are visualized trough the fluoroscopy. If necessary, contrast agents may be injected in the ducts.

The technique was primary used as a diagnosis tool, however, due to the technological advances it became a therapeutic procedure. Data from the *Sistema de Avaliação Ambulatorial* of the *Sistema Único de Saúde (SIA/SUS)* shows a 60% increase in the number of ERCP between 2008 and 2018 in Brazil as shown in a previous work of our group (SOUZA *et al.*, 2019). This trend is expected to keep growing as Brazilian population ages and bad health habits worsen. As a consequence, it can be also expected a increase of the occupational exposure to the ionizing radiation. It poses a concern since the ionizing

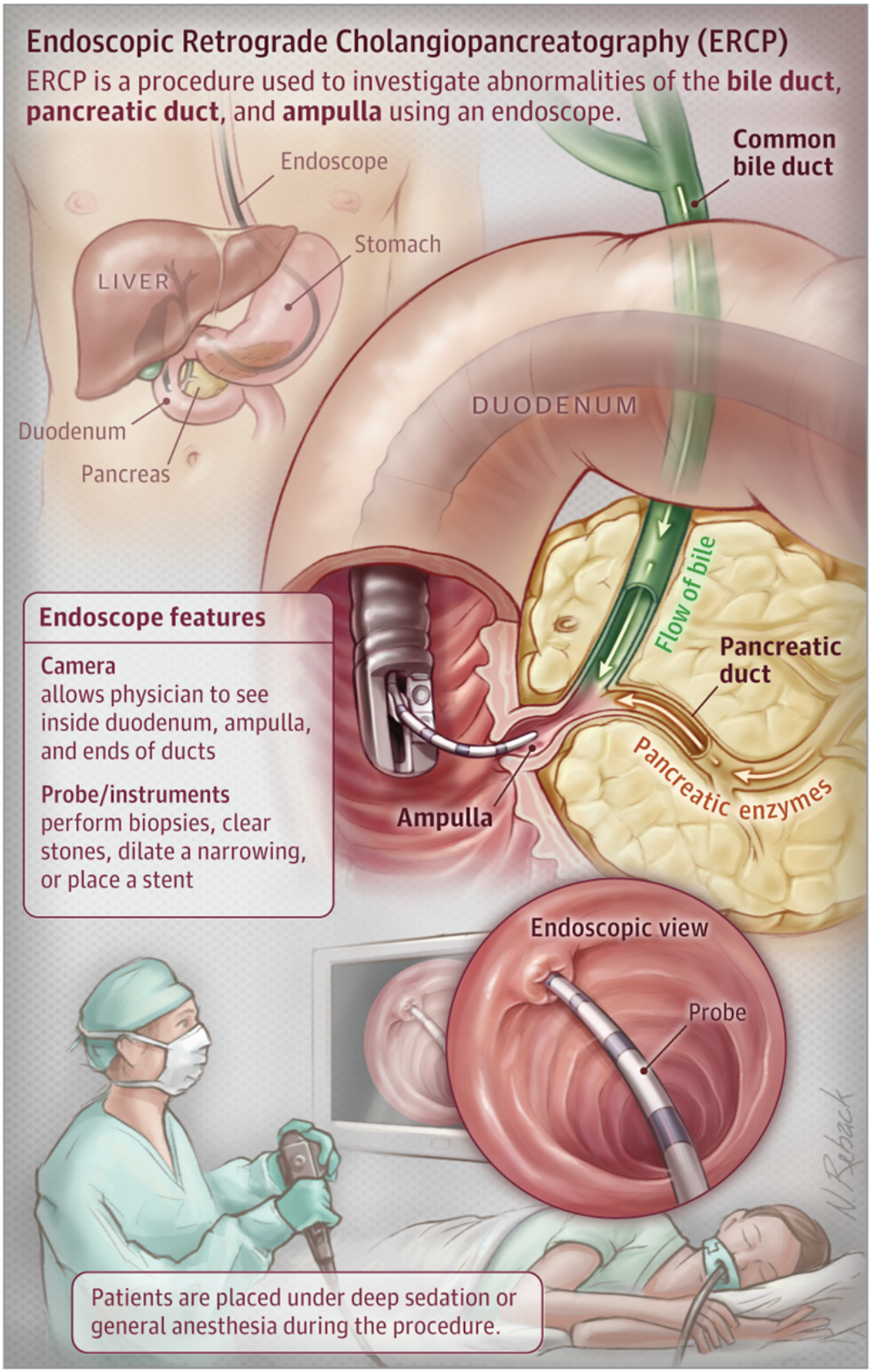

Figure 1 – Scheme of a ERCP procedure showing the details of the duodenoscope and organ structure. Figure from (BAIU; VISSER, 2018)

radiation has a potential to cause DNA damages that can lead to neoplasms and other health issues, such as eye lens opacity.

The occupational exposure in ERCP has already been studied by other scientists (SULIEMAN *et al.*, 2010; SEO *et al.*, 2016; HUDA *et al.*, 2016; MARTIN, 2011; CARINOU *et al.*, 2015). Most of the studies focus on the experimental evaluation of the dose levels. Although, experimental studies have the capacity of showing the real situation, they are not capable of measure the organs and tissues radiation doses, since it is not achievable to inserted dosimeters in the human body. This limitation is solved by means of computer based MC simulation, which enables the simulation of radiation exposure scenarios with high precision results. In the simulations, it is possible to realistically model both physical and biological structures irradiated during the procedure. Therefore, it is possible to estimate the absorbed doses by the organs and tissues using virtual anthropomorphic phantoms (XU, 2014).

The MC simulations are performed by computational codes specially designed to simulate the radiation-matter interactions. Among many codes, the Monte Carlo N-Particle eXtended MCNPX stands out due to its capability to simulate the interactions of about 34 particles in a wide energy range implemented in complex geometries (PELOWITZ, 2011). The MCNPX has been coupled with realistic virtual anthropomorphic phantoms to investigate the exposure to ionizing radiation in different situations (SILVA *et al.*, 2020; SOARES *et al.*, 2020; PEREIRA *et al.*, 2019; BELINATO *et al.*, 2018).

As presented in the Liao *et al.* (2015) study, the exposure during ERCP procedure, is related to the procedure complexity and endoscopist experience. In the treatment of Klatskin tumor, several stents are placed in the organ, which requires a long exposition time. In twenty minutes of fluoroscopy, the occupational doses can reach 30 mSv which is higher the annual limit of 20 mSv recommended by the International Commission on Radiological Protection (ICRP 103, 2007).

The need to reduce staff and patient exposure to ionizing radiation is supported by studies on the effects of radiation at cellular and tissue levels. High doses are associated with tissue reactions such erythema, burns and necrosis, that arise from the intense biochemical reactions induced by the radiation. Low doses are associated with the mutagenic effects of the ionizing radiation on the DNA. If these mutations are not corrected and the cell survives it may evolve to a cancer. These conclusions are based on cancer rates studies performed with the atomic bombs survivors and patients who went through radiation therapy (ICRP 103, 2007; BEIR VII, 2006).

Beyond the stochastic effects from ionizing radiation exposure to the staff, there is a concern on the patient tissue reaction. Zagorska *et al.* (2015) evaluated the eye lens exposure in a high demand Gastroenterology department during two months. The researchers evaluated the exposure for the four main positions occupied by the professionals. The fluoroscopy time ranged from 1.0 min to 28.8 min, averaging 4.6 min. Their findings

showed that if the proper protection in not used, the annual exposure can exceed the ICRP recommended limits, since their dose measurements varied between 34.9 μSv and 93.3 μSv (ZAGORSKA *et al.*, 2015). Considering the fluoroscopy time, the estimated cumulative dose for the gastroenterologist for 400 ERCP procedures can reach 25.6 mSv, also higher than the ICRP limits.

The DAP is a reliable and easily measured quantity to estimate patient effective dose and, thus, the radiogenic risks involved in a procedure (HERON, 1992; BOR *et al.*, 2004). Bor *et al.* (2004) compared the patient effective dose values obtained from DAP and kerma measurements and found that the DAP enables more reliable estimates. So, DAP measurements may provide a way to assess and optimize patient and staff doses. However, just measuring and recording the DAP does not directly result in the reduction of the exposure (KRUIT *et al.*, 2015). This finding suggests the need for more effective approaches to induce better practices in the interventional radiology room.

In this context, this work presents the first results of a greater project focused on the radiation protection during ERCP procedures in a large Brazilian university hospital. The present study aims to evaluate the effect of the tube voltages and the FOV on patient and staff exposure to ionizing radiation. For didactic purposes, we simulated situations of wrong FOV choices practices as the outcomes of this work will be applied to develop a training course for the staff.

1.1 Motivation

As previously discussed, the importance of the ERCP on the treatment and diagnosis of the pancreatic and biliary ducts diseases is expected to increase due to the trends in population aging, and bad health habits prevalence. In this scenario, it is very likely that more ERCP procedures will be performed which may increase both patient and staff exposure to ionizing radiation. In order to protect the professionals, from the risks of exposure to ionizing radiation, it is necessary to better understand the radiation levels involved during these procedures. This knowledge can be applied into the development of protocols, training courses, among other practices to reduce the radiation exposure, assuring good working conditions for the health professionals, keeping the quality of the ERCP procedure.

Chapter 2

Objectives

2.1 General Objective

The objective of this research is to estimate, by means of Monte Carlo simulations, the exposure to ionizing radiation, by health professionals and patients during an ERCP procedure.

2.2 Specific Objectives

- ❏ Understand the dosimetry and radioprotection principles involved in ERCP procedures;
- ❏ Understand the Monte Carlo simulations;
- ❏ Learn to use the MCNPX (2.7.0) code for radiation transport simulations;
- ❏ Review the literature on the occupational ionizing radiation exposure during ERCP procedures;
- ❏ Reproduce in the MCNPX Monte Carlo simulation software the geometry of a typical ERCP procedure room;
- ❏ Introduce virtual anthropomorphic phantoms in the modelled scenario to represent patient and professionals;
- ❏ Apply the SRS 78 software to simulate the x-ray spectra produced by the Axiom R100 equipment;
- ❏ Estimate the conversion coefficients for effective and equivalent patient doses;
- ❏ Estimate the conversion coefficients for effective and equivalent staff doses.

Chapter 3

Theoretical Background

3.1 Radiation Matter Interactions

The applications of the ionizing radiation in diagnostic medicine are possible due to the characteristics of the interactions of radiation and matter. These interactions enable the production of images as the radiation interacts with the patient tissues and then with the detector. In the radiology energy range, the main interactions are the Compton scattering and photoelectric effect as shown in Figure 2.

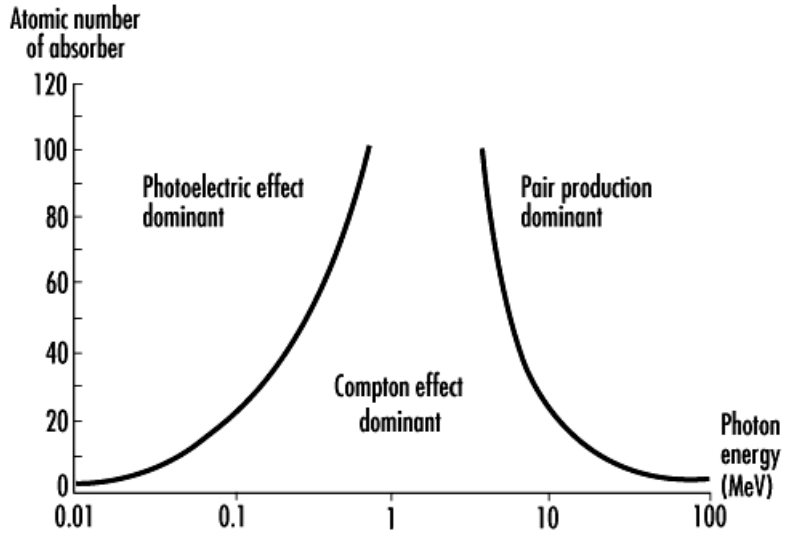

Figure 2 – Prevalence of Compton effect and Photoelectric effect according to photon energy and atomic number of the absorber. Photoelectric effect prevails for low energy photons and higher atomic number while Compton effect dominates for lower atomic number for all energy range, and higher atomic number and higher energies. Figure from (CHERRY, 1998).

3.1.1 Compton Effect

The Compton effect was discovered by Arthur H. Compton by observing the increase in x-ray wavelength after interacting with a graphite target (COMPTON, 1923). Compton explained this change as a result of an inelastic collision of a x-ray photon with an electron, another charged particle. As shown in Figure 3, the photon transfers some energy and momentum to the electron, which is recoiled and the photon is scattered with less energy, that means larger wavelength. This discovery reinforced the theory of the quantum nature of light. In radiology, the Compton effect is responsible for the production of scattered ionizing radiation which is the major cause of reduction in image quality and exposure to scattered radiation to both patient and staff (PERCUOCO, 2014).

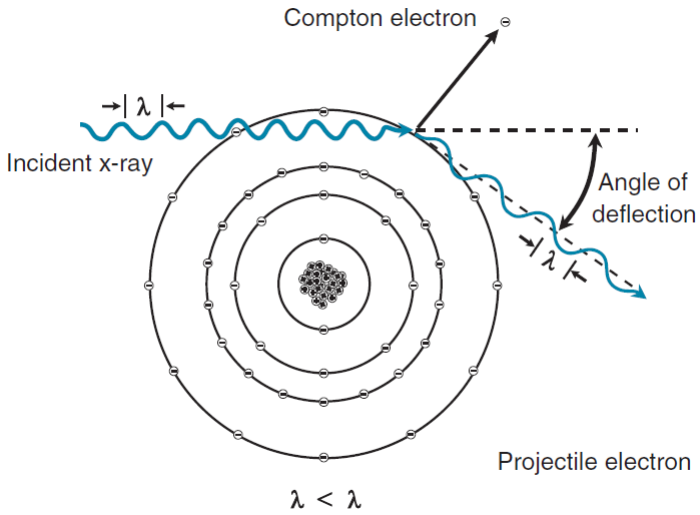

Figure 3 – Atom ionized through the Compton effect. The incident x-ray photon knocks an electron off the atom, the photon is deflected with lower energy. Figure from (PERCUOCO, 2014, p. 14).

3.1.2 Photoelectric Effect

The photoelectric effect was explained by Albert Einstein in 1905 (EINSTEIN, 1905) by applying the quantum theory developed by Max Planck to explain the Black-Body Radiation Emission (PLANCK, 1972). Einstein theorized the photoelectric effect as an complete absorption of photons by electrons. As shown in Figure 4, if the photon energy is higher than the binding energy (work function) of the electron with the atom, then the electron is ejected with energy corresponding to the difference between the photon energy and the electron binding energy. As a consequence the atom gets ionized.

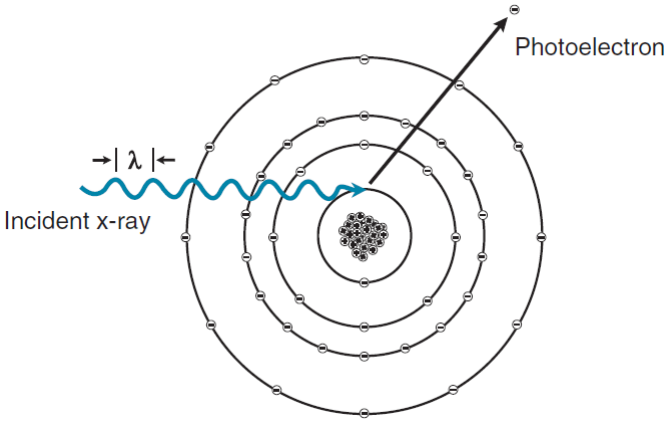

Figure 4 – Atom ionized through the Photoelectric Effect. The incident x-ray photon is completed absorbed by an electron, which is ejected off the atom. Figure from (PERCUOCO, 2014, p. 13).

In radiology, the photoelectric effect is responsible for the image formation. The x-ray photons interact with the patient tissues, transferring their energy to the patient atoms. In this way, less photons reach the film under higher density tissues, keeping the film area brighter than the film area hit by less attenuated photons. However, the ejected electrons may harm the patient by further ionizing the tissues, leading to DNA damages or tissue destruction (PERCUOCO, 2014).

3.2 Physical Quantities and Dosimetric Units in Radiology

3.2.1 Absorbed Dose

One of the main consequences of the interaction of radiation and matter is the energy transfer from the radiation to the irradiated surrounding. This effect is computed as the dosimetric quantity absorbed dose (D). As shown in Equation 1, the absorbed dose is defined as an function of the mean energy $d\bar{\epsilon}$ transferred from the radiation to the mass dm of the irradiated volume in a specific point P (ICRP 103, 2007). The unity of this quantity is Gy (J/kg).

$$D = \frac{d\bar{\epsilon}}{dm} \tag{1}$$

The absorbed dose is defined for all ionizing radiations, irradiation geometries and materials.

3.2.2 Equivalent Dose

The ionizing radiations may lead to different effects depending on factors such as electrical charge, mass, energy, etc. These differences are computed by the Equivalent dose (H_T), taking into account the effects of same absorbed dose from different types of ionizing radiations. As shown in Equation 2, the equivalent dose (H_T) is defined as the product of the absorbed dose in a organ/tissue T by the radiation weighting factor, w_R (ICRP 103, 2007). The unity of this quantity is Sv (J/kg).

$$H_T = \sum_R w_R D_{T,R} \tag{2}$$

Table 1 – Radiation weighting factors recommended by (ICRP 103, 2007).

Radiation type	Radiation weighting factor (w_R)
Photons	1
Electrons and muons	1
Protons and charged pions	2
Alpha particles, fission fragments, heavy ions	20
Neutrons	A continuous curve as a function of neutron energy

3.2.3 Effective Dose

Different tissues and organs respond differently for the same dose of a type of radiation, these differences are computed by the Effective dose (E) taking into account a weighting factor w_T based on the effects of same absorbed doses in different tissues. As shown in Equation 3, the effective dose (E) is defined as the product of the equivalent dose by the weighting factor w_T related to the organ/tissue radio sensitivity (ICRP 103, 2007). The unity of this quantity is Sv (J/kg).

$$E = \sum_T w_T H_T \tag{3}$$

The effective dose is averaged for gender and age, and the w_T, shown in Table 2, are calculated from epidemiological studies on cancer rates for individuals exposed to ionizing radiation (ICRP 103, 2007). The use of virtual anthropomorphic phantoms is fundamental for the estimate of the effective dose, since its measurement is impracticable. The effective dose is not intended to calculate the risk for a specific individual, genre or age, instead, it was conceived to better evaluate patient justification and optimization of examinations (ICRP 103, 2007).

Table 2 – Weighting factor w_T related to the organ/tissue radio sensitivity (ICRP 103, 2007).

Organ/tissue	w_T
Bone marrow	0.12
Colon	0.12
Lung	0.12
Stomach	0.12
Breast	0.12
Remainder tissues	0.12
Gonads	0.08
Bladder	0.04
Oesophagus	0.04
Liver	0.04
Thyroid	0.04
Bone surface	0.01
Brain	0.01
Salivary glands	0.01
Skin	0.01
Total	1.00

3.3 Monte Carlo Simulation

The Monte Carlo (MC) simulation is a fundamental tool, applied in a multitude of science and engineering fields, to simulate systems which can be represented by stochastic processes. In Nuclear Physics, this technique is utilized to simulate the radiation transport through matter (XU, 2014). In this way, it is possible to estimate many physical quantities involved in basic and applied studies in nuclear sciences.

The MC is an old technique, but its applications begun to increase during the Second World War in the context of the atomic bombs developed by the Manhattan Project. Another key factor for the spread of MC is the computing power revolution due to the invention of transistors. Since the MC is a statistical method, in which a sequence of random numbers are used to perform a simulation, the increase in computing power enabled the simulations of complex and more realistic scenarios, reducing time and financial costs. In nuclear physics, the random numbers are used to represent the coordinate position of particles due to the collisions and their energies (XU, 2014). The problem can be solved if it is possible to represent it by Probability Density Functions (PDF).

As the number of simulated events increase, the result approaches the medium value of the desired physical quantity.

3.3.1 Virtual Anthropomorphic Phantoms

In MC dosimetry studies, the main interest regards the radiation doses absorbed by the exposed individuals. In this scenario, it was necessary to develop virtual objects to simulate the characteristics of the organs and tissues, which composes the studied individuals. The development of such phantoms is a hot research field with ongoing breakthroughs. In this session, it will be discussed the main types of virtual anthropomorphic phantoms developed so far.

3.3.1.1 Stylised anthropomorphic phantoms

The stylized, or mathematical anthropomorphic phantoms, were the first virtual objects to simulate the human body in computational dosimetry during the 1960 decade. The first computational phantoms were comprised by simple shapes as slabs (SNYDER, 1950) and circular cylinders (AUXIER *et al.*, 1968). Due to the technology limitations, the human body was represented by geometric figures such as cones, spheres, cylinders, etc, as shown in Figures 5 and 6. This feature resulted in non realistic representations of the structures, the organs did not present the proper shape, and the distance between them were not compatible with the real human bodies. As a consequence, accurate results could not be achieved.

Despite their limitations, the stylised anthropomorphic phantoms were fundamental in the early studies in internal dosimetry, specially in nuclear medicine. The constant search for better phantoms lead to different types of stylised phantoms. Fisher e Snyder (1968) developed phantoms with internal structures representing the organs and tissues. Stabin *et al.* (1995) constructed a series of pregnant anthropomorphic phantoms in the last month of each gestational trimester. Further developments were achieved by Kramer (1982) who built gender specific anthropomorphic phantoms called ADAM and EVA based on the MIRD phantoms.

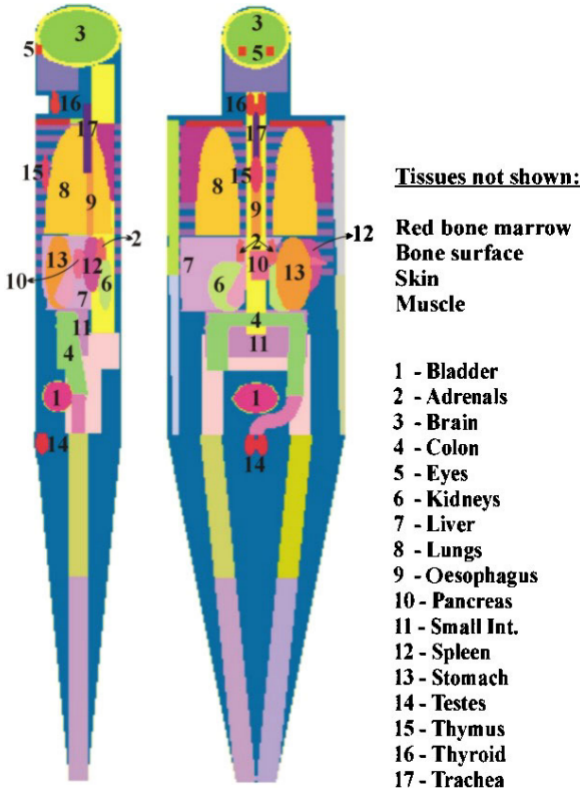

Figure 5 – Lateral and front view of ADAM stylised phantom. Figure from (KRAMER, 1982)

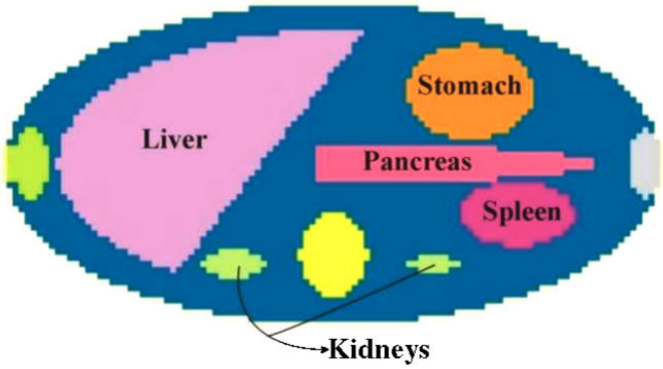

Figure 6 – Abdominal cross-section of ADAM stylised anthropomorphic phantom. Figure from (KRAMER, 1982)

3.3.1.2 Voxel virtual anthropomorphic phantoms

The development of Computational Tomography (CT), and the enhancement of computational power, enabled the implementation of voxel virtual anthropomorphic phantoms. This was a remarkable achievement since the phantoms could represent the body structures with higher accuracy than the stylised phantoms. The first voxel virtual anthropomorphic phantom was presented in a study of radiation exposure during dental radiology (GIBBS *et al.*, 1984a; GIBBS *et al.*, 1984b). Subsequent developments resulted

in a head and torso virtual anthropomorphic phantom (VEIT *et al.*, 1989; ZANKL *et al.*, 1988). This virtual phantom was used by Kramer *et al.* to develop MAX (KRAMER *et al.*, 2003) and FAX (KRAMER *et al.*, 2004). These phantoms are shown in Figure 7.

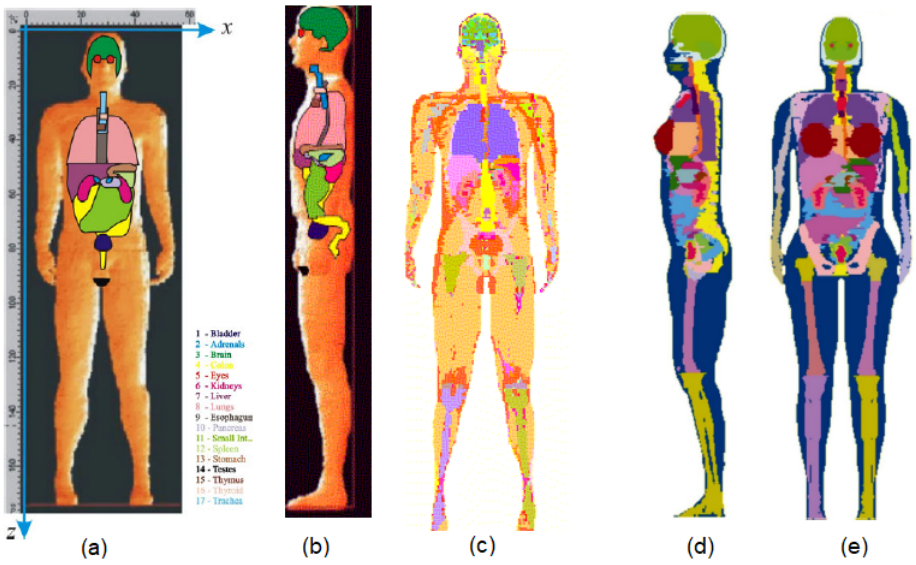

Figure 7 – Frontal (a), lateral (b) and central (c) plane view of MAX. Figure from (KRAMER *et al.*, 2003). Lateral (d) and frontal (e) view of FAX. Figure from (KRAMER *et al.*, 2004)

.

This type of anthropomorphic phantom can also be constructed from magnetic resonance (MR) (NAGAOKA *et al.*, 2003) and photographic images of sliced frozen bodies (ZHANG *et al.*, 2007). All the realistic details obtained with these technologies enables a better representation of the human body, therefore enhancing the confidence of the computational simulations. It has been shown a 25% decrease in effective dose estimate due to photon exposure as a result of adipose and muscular tissue, organs shapes and positions and complex skeletal representation in voxel virtual anthropomorphic phantoms compared to stylised phantoms (KRAMER *et al.*, 2004).

A drawback from voxel phantoms is the surface irregularity caused by the cubic voxel surfaces, in reality, the organs surfaces are smooth. Another problem is the limitation in the tomographic cuts thickness which restricts the representation of small structures, like the skin, eye lens and organs walls (GARDUMI *et al.*, 2012). Deforming or repositioning organs/tissues may be a work intensive or unachievable task. The large amount of data is also a concern, since it will cause memory allocation problems.

3.3.1.3 BREP anthropomorphic phantoms

The advances in graphic technologies enabled the development of another class of very realistically boundary representation (BREP) phantoms. These objects can be constructed in different 3D modelling technologies namely Non-Uniform Rational B-Splines

(NURBS) or polygonal meshes. The development of this new class of phantoms is a hot topic in Medical Physics, in fact, Xu (2014) reported the existence of 183 BREP models up to 2014. Softwares such as Blender™ and Rhinoceros™ are employed to model the phantoms based on atlases of human anatomy and images (CT, MR, photography). The ease in deforming and adapting the shapes of the models is one of the main advantages of BREP phantoms.

The NURBS phantoms are more realistic in the representation of the body than the mesh polygons due to its ability to represent smooth curves. However, mesh polygons are easier to work with since they directly create 3D structures while NURBS 3D structures are created by combining 2D patches to form complex 3D shapes. Attention must be paid while modelling NURBS complex structures because seams may appear when the 2D patches are combined (XU, 2014). Despite all the advantages of the BREP phantoms, their data format can not be handled by some of the Monte Carlo softwares, so the BREP phantoms have to be voxelized in order to be employed in the simulations. As shown in Figure 8 this process brings back some of the unrealistic representation of surface and organ/tissue found in the the virtual voxel phantoms. Some developments have been made to implement BREP phantoms in Monte Carlo codes, however the computing time can be raised by a factor of two (KIM *et al.*, 2011). As the research advances, some promising MC codes adaptations (HAN *et al.*, 2013) and new mesh modeling approaches (YEOM *et al.*, 2014) have reduced the BREP phantoms based simulations computing time. Finally, the advances in the Graphics Processing Unit (GPU) has opened a new era of fast MC simulations (XU, 2019).

Figure 8 – Comparison of MAX/FAX(voxel) with MASH/FASH(mesh) and MASH/FASH voxelised. Figure from (CASSOLA *et al.*, 2009)

Chapter 4

Materials and Methods

In this chapter, the MCNPX code (PELOWITZ, 2011), the SRS 78 spectra calculation software (CRANLEY, 1997), the exposure scenario, the FASH and MASH virtual anthropomorphic phantoms and the conversion coefficients calculation applied in this project are described.

4.1 The Monte Carlo N-Particle eXtended (MCNPX)

The MCNPX (version 2.7.0) code is a MC based computational tool developed by the Los Alamos National Laboratories (LANL) with the aim to simulate the transport of radiation (PELOWITZ, 2011). The code is provided with cross section libraries and powerful computing algorithms which enables precise and accurate calculations in Nuclear Physics. The code is implemented in Fortran 95 and the input files are written in text files. One of the greatest features of MCNPX is the possibility to simulate complex geometries, making it more realistic. Beyond that, MCNPX is capable of simulate 34 particles in a broad range of energies. Since MCNPX is a complex code, it is out of the scope of this section to fully explain all its features. A depth description of MCNPX applications in Medical Physics is provided by (REED, 2007). The input files of MCNPX are organized in lines, called cards, and columns. The first card is reserved to be a header of the file, the remaining cards are organized in three blocks as follows.

4.1.0.1 Block of cell cards

As shown in Figure 9, the cell block is introduced with a comment card (optional). The comment card begin with a "c" followed by a blank space and the desired comment, generally a title for the cell. The remaining cards are assigned to the cell parameters. The cells are volumes in space delimited by the surfaces created in the Surface Block, these volumes are filled with the materials defined in the Data Cards Block. In a cell card the ID number, material composition, density, surfaces and the particle transport importance

must be defined. The surfaces needed to build the cells are defined in the surface card and they are combined to built complex 3 dimensional shapes. The combination of surfaces is made by applying Boolean commands of intersection and union. The intersection is represented by a blank space between the surfaces one wants to combine. The first number (3) shown in Figure 9 is a mnemonic to identify the cell. The second number (2) represents the material that fills the cell. The third number (1.234e-3) is the density of the material. If this number is negative, the density is given in g/cm^3, and if it is positive, the density is given in $atom/cm^3$. The following number (-2) represents the surface that is used to create the cell. The negative sign implies that the cell is the volume of space negative to the surface 2, as it will be discussed in section 4.1.0.2. The last part of the card is the importance of particle, which is represented by the expression "imp:<pl>", where <pl> is a particle mnemonic (p=photons, e=electron, a=alpha, etc).

```
C     Cell Card
3 2 1.234e-3   -2    imp:n=1
```

Figure 9 – Basic components of a cell card. Figure from (REED, 2007)

4.1.0.2 Block of surface cards

Figure 10 shows an surface card example, the first number (1) is a mnemonic to identify the surface. The mnemonic "cz" identifies the surface, in this case an infinite cylinder centered on the z-axis with a 20 cm radius. The comment after the "$" sign is not read by MCNPX.

```
1    cz    20.0   $ infinite z cylinder
```

Figure 10 – Basic components of a surface card. Figure from (REED, 2007)

In MCNPX, the surfaces are defined by equations, points or macrobodies. The surfaces are featured with a "sense", all points at $f(x, y, z) > 0$ are positive to the surface, all points $f(x, y, z) < 0$ are negative to that surface and all points at $f(x, y, z) = 0$ are on the surface.

4.1.0.3 Block of data cards

All problem specifications not related to geometry are defined in the data card. The main definitions are: particle type, materials, radiation sources, relevant particle interactions, cross section libraries and tallies (how the results are scored. In this block lies the main physics specifications, and it is the most powerful feature of MCNPX. The parameters can be combined to simulate a multitude of nuclear physics phenomena and its applications. In the case of this study, which is interested on the particle interactions

in the energy range used in radiology, the transported particles are photons which are defined in the "mode card" by the letter "p". The source is defined by the "SDEF" card. The card "POS" defines the location of the particle source. The energy of the particles is defined by the "ERG" card and the values can be given by a number, for monoenergetic sources, or by a function that describes different energy for the particles. In the latter case, it is necessary to specify the energies in the "SI" card and its probability in the "SP" card. The direction of the particles flight is given by the "VEC" card. Since in radiology the x-ray beam has a conical shape, it is necessary to reduce the isotropic particle emission created by the "SDEF" card with a biasing function, which collapses the emission to a conical volume. In Figure 11 is shown the example of a point source located at the origin (POS=0 0 0) emitting photons (PAR=P) with energies defined by a distribution (ERG=D1). The source emits photons with 1.173 and 1.332 MeV with the same probability.

```
SDEF ERG=D1 POS=0 0 0 PAR=P
SI1   L 1.173 1.332
SP1   D 1 1
```

Figure 11 – Basic components of a data card. Figure from (REED, 2007)

Aside from the source, the Data Block also contains the materials, transformations, tallies, among other critical parameters. The material card begins with the letter "m" followed by a identification number for the material. The way the materials are described depends on the investigated phenomenon. In radiology only electrons and photons interaction are relevant. In this case, the material composition is defined by the atomic number of the element followed by "000". Two more numbers can be used to specify a cross section library. In front of the elemental identification is set its fraction, negative numbers represent massic fraction and positive represent atomic fraction. Then, is defined the way the calculation results are going to be scored. This is done by the Tally cards, which can accumulate the results of the interactions in different forms. In radiology studies, the Tally F6 is widely used since it scores the deposited energy in the cell with a easy translation to energy by mass, which is the quantity used to measure the absorbed dose (REED, 2007).

Finally, the number of particles to be generated using the "NPS" card is set up, the maximum number of particles is 1E9. The uncertainties of the simulation decrease as the number of histories increase, however the computational time is also increased. In this work we simulated 1E9 particles.

4.2 SRS 78 software for spectra calculation

One of the key factors to perform a reliable simulation of the particle interactions in a radiologic procedure is the correct generation of the x-ray spectra. Several codes were developed to perform this task. In this work, the SRS 78 software was applied which is a reliable software developed to generate x-ray spectra with energy range between 30 and 150 keV, with 0.5 keV increments (CRANLEY, 1997). The target can be set as molybdenum, tungsten and rhodium. SRS 78 software also enables the use of different filtration, anodic angles, and other radiological parameters.

In this project the spectra produced by the OPTILIX 150/30/50 HC-100 x-ray tube was simulated. This tube is used in the AXIOM ICONOS^{TM} R100 x-ray unit manufactured by SIEMENS. The total filtration was 2.5 mmAl, optical anode angle of 12° and tungsten target. The tube peak voltages were 70, 80, 90, 100 and 110 kVp as found in the literature (ANGSUWATCHARAKON *et al.*, 2018; MITCHELL; GRIMM, 2003). The fields of view (FOV) were also selected from previous works (BULS *et al.*, 2002; ALZIMAMI *et al.*, 2013) as follows: 15 × 15, 17 × 17, 22 × 22, 25 × 25, 31 × 31, and 38 × 38 cm^2. For the FOV sizes of 22 × 22 to 38 × 38 cm^2, the irradiated area is superior to the patient abdominal area. This situations were simulated to describe cases of accidental or wrong choice of FOV. The focus to patient distance was 77 cm, as measured in an ERCP room.

4.3 Exposure scenario

The simulated exposure scenario was modelled based on a typical radiology room at a large university hospital. The room is used to perform conventional and interventional radiology procedures using an Axiom R100 x-ray system, manufactured by SIEMENS. When the room is used for endoscopic procedures guided by fluoroscopy, additional equipment are gathered from other departments, changing the room geometry. For ERCP procedures, cauterization system, endoscopic equipment, sedation system and other minor utensils are brought into the room. It is important to emphasize these changes in geometry since these objects may affect the ionizing radiation scattering.

In Figure 12 is shown the general appearance of the simulated room. The patient lays on the bed in prone position and is exposed to an Antero Posterior (AP) x-ray beam projection. This incidence poses a concern in the occupational exposition doses since the patient is the main source of scattered radiation to the staff. In this case, the assistant physician is located 69 cm away from the center of the irradiated field, the physician is located 86 cm. Both professionals wear Personal Protective Equipment (PPE) such as lead apron (0.5 mm Pb), thyroid protection (0.5 mm Pb) and lead glass eyewear. No Collective Protective Equipment (CPE) were simulated. The lines leaving the x-ray tube

represent some radiation trajectories.

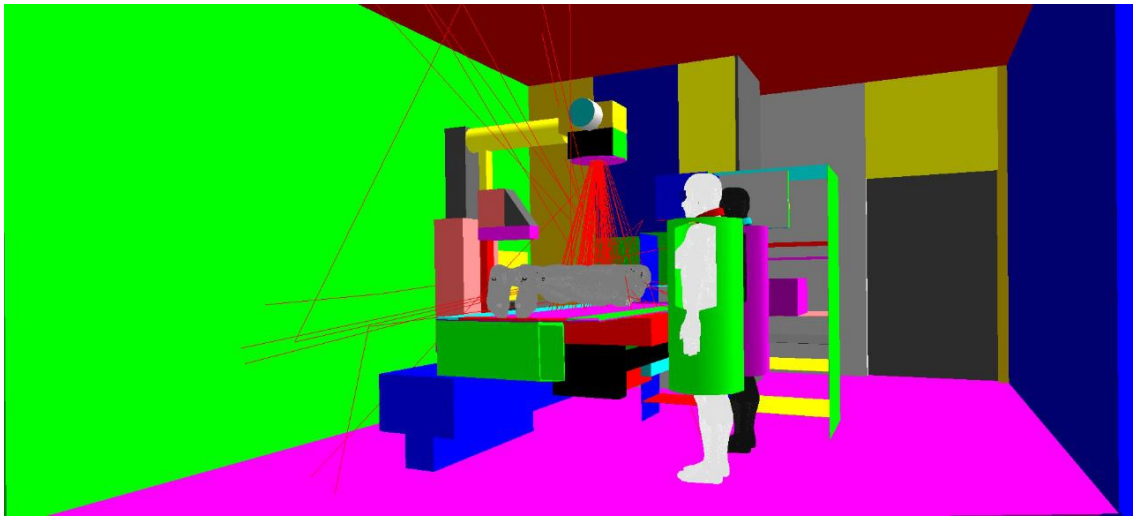

Figure 12 – Lateral view of the simulated scenario showing some scattered radiation trajectories.

In Figure 13 is shown a detailed view of the exposure scenario in which the virtual anthropomorphic phantoms were excluded to better depict the protective equipment. The assistant physician wears a lead eyewear (a), thyroid collar (b) and lead apron (c). The physician wears a lead eyewear (d), thyroid collar (e) and lead apron (f). The patient (not shown) is positioned on the table (h) and is irradiated by the x-ray tube primary beam (g).

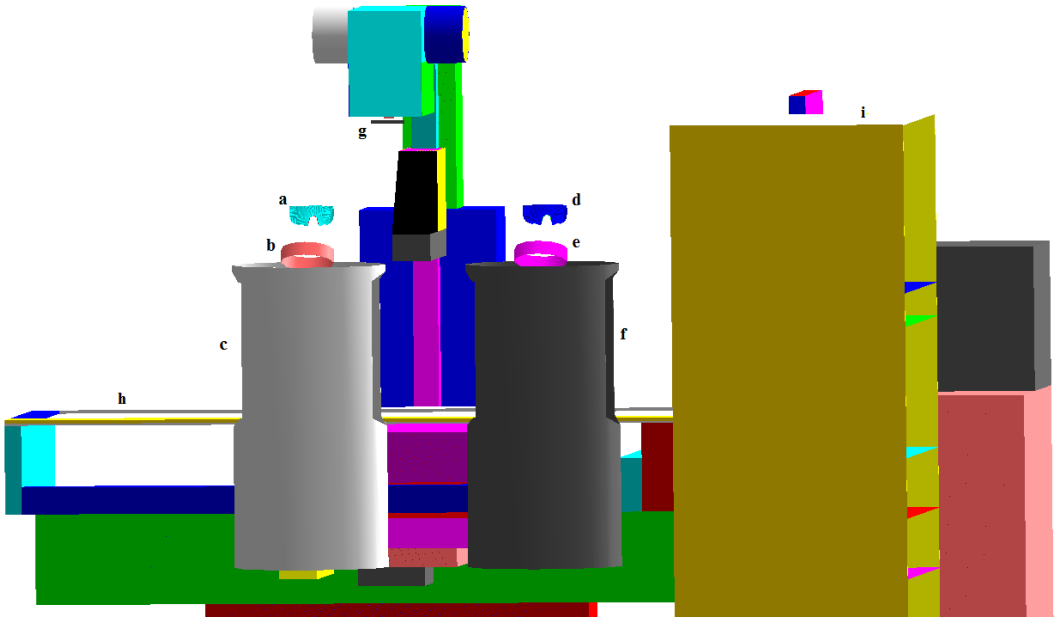

Figure 13 – Back view of the simulated scenario showing the PPI. Assistant physician: lead eyewear (a), thyroid collar (b) and lead apron (c). Physician: lead eyewear (d), thyroid collar (e) and lead apron (f). The patient (not shown) is positioned on the table (h) and is irradiated by the x-ray tube primary beam (g).

4.4 FASH and MASH virtual anthropomorphic phantoms

The virtual anthropomorphic phantoms applied in this project were developed by the *Departamento de Dosimetria Computacional* of the *Universidade Federal de Pernambuco* (CASSOLA *et al.*, 2009; KRAMER *et al.*, 2009). These phantoms, namely MASH3 (Male Adult meSH) and FASH3 (Female Adult meSH) were built using polygon mesh surfaces, according to the physiological and anatomical data from atlases and following the male and female references from ICRP 89 (VALENTIN, 2002). MASH3 and FASH3 features 113 organs, tissues and bones.

Most virtual anthropomorphic phantoms are modelled after MR, CT and colored photographs of sliced frozen bodies from volunteers. As a consequence, most of the phantoms, represent a body of a person in supine position, which leads to anatomical dislocations of organs and tissues. In that way, these phantoms do not realistically represent a person in standing position. The differences are more pronounced in the abdominal sagital diameter, compression of the lungs and distortions in walled organs shapes. The MASH3 and FASH3 virtual phantoms are based on atlases of people in the upright position, which eliminates the previous discussed distortions, which means that MASH3 and FASH3 are suitable to be applied in occupational radiation studies, since the professionals work in the upright position.

The phantoms were modelled with graphic computational tools developed for animation and scientific research, such as MakeHuman (BASTIONI *et al.*, 2007), Blender (HESS, 2007), Binvox (MIN, 2005?) and ImageJ (FERREIRA; RASBAND, 2012). Except for the trabecular bones, all structures of the phantoms are based in polygon mesh surfaces and not on MR, CT or photographs. MakeHuman is a virtual representation of the human body capable of some adjustments such as gender, height, and weight. This model was edited with Blender in order to fit the organs ans tissues which were downloaded from internet or built in Blender. Then, the resulting model was voxelised with Binvox in order to enable dose calculations with EGSnrc, and because the voxelised nature of the sponginosa required the whole virtual phantom to be also voxelised (CASSOLA *et al.*, 2009; KRAMER *et al.*, 2009). In Table 3 is shown the voxel number of the MASH3 phantom, in Table 4 is shown the voxel number of the FASH3 phantom. Adjustments of organs volume and position were performed with ImageJ. In Figure 14 is shown a comparison between a voxel virtual phantom based on CT scans and the mesh and voxelised mesh phantom.

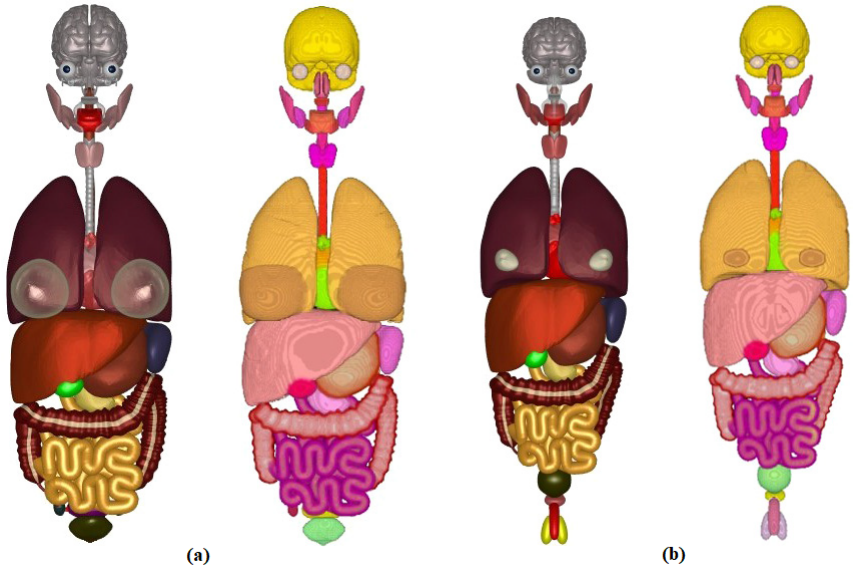

Figure 14 – Mesh and voxel versions of the internal organ/tissues of (a) FASH3 and (b) MASH3 phantoms (CASSOLA *et al.*, 2009).

Table 3 – Number of MASH3 voxels for the organs and tissues with dosimetric importance according to (ICRP 103, 2007).

	Physician	Assistant physician	Patient
Organ	*N*° Voxels	*N*° Voxels	*N*° Voxels
Bone marrow	161853	161853	161823
Colon	25644	25644	25777
Lung	347086	347086	319205
Stomach	10373	10373	10423
Breast	1142	1142	1187
Remainder tissues	2143229	2143229	2143070
Gonads	2440	2440	2433
Bladder	3494	3494	3467
Oesophagus	2766	2766	2795
Liver	123977	123977	123975
Thyroid	1384	1384	1384
Bone surface	522077	522077	523811
Brain	99838	99838	99838
Salivary glands	5986	5986	5986
Skin	219611	219611	218920
Eyes	1029	1029	1029

Table 4 – Number of FASH3 voxels for the organs and tissues with dosimetric importance according to (ICRP 103, 2007).

	Physician	Assistant physician	FASH3 Patient
Organ	$N°$ Voxels	$N°$ Voxels	$N°$ Voxels
Bone marrow	119485	119485	118971
Colon	25038	25038	24983
Lung	274827	274827	252824
Stomach	9698	9698	9731
Breast	22908	22908	22906
Remainder tissues	1555690	1555690	1555336
Gonads	760	760	773
Bladder	2780	2780	2794
Oesophagus	2433	2433	2473
Liver	96492	96492	96473
Thyroid	1157	1157	1196
Bone surface	388008	388008	387347
Brain	89513	89513	89618
Salivary glands	4952	4952	4904
Skin	153664	153664	154122
Eyes	1030	1030	1031

Both FASH3 and MASH3 have been extensively applied to evaluate ionizing radiation exposures since they were developed. The LInDa group has published many papers using these phantoms, or their subsequent developments (NEVES *et al.*, 2019; PERINI *et al.*, 2019; SANTOS *et al.*, 2018; BELINATO *et al.*, 2018).

4.5 Conversion coefficients calculation

The computational dosimetric studies generally rely on the calculation of Conversion Coefficient (CC) for presenting the data. The coefficients link the simulation with the clinical practice by the calculation of a ratio between the estimated value and the measurement. One of those easily measured quantities is the DAP. In this study, the data is presented in terms of Conversion Coefficient for Equivalent Dose ($CC[H_T]$) and the Conversion Coefficient for Effective Dose (CC[E]). The Red Bone Marrow (RBM) coefficients were estimated using the Tally F4 ($MeV/cm^2/particle$). For the other organs and tissues, the coefficients were calculated employing Tally F6 ($MeV/g/particle$). The product of the factor $1.602 \times 10^{-10}\ (J/kg) \times (g/MeV)$ by the Tally F6 value is used to calculate the absorbed dose. Since in this work only the effects of the x-ray photons are accounted, the absorbed dose is numerically equal to the equivalent dose. Therefore, the $CC[H_T]$ is given by Equation 4.

$$CC[H_T] = F6 \times 1.602 \times 10^{-10}(J/kg) \times (g/MeV) \tag{4}$$

The CC[E] for the professionals were found using Equation 5.

$$CC[E] = \sum_{T} w_T \frac{CC[H_T]_{Male} + CC[H_T]_{Female}}{2} \tag{5}$$

where w_T is the tissue weighting factor, $CC[H_T]_{Male}$ and $CC[H_T]_{Female}$ are, respectively, the conversion coefficient of equivalent doses of the male and female virtual phantoms. The CC values were normalized by the simulated DAP value obtained with the simulation of a 10×10×1 cm^3 DAP meter placed at the x-ray tube exit, 15 cm from the focus.

The CC[E] and $CC[H_T]$ obtained in this study can be used, in the clinical practice, to estimate the doses during ERCP procedures using Equation 6.

$$D = CC \times DAP \tag{6}$$

where D is the dose (equivalent or effective) and CC is the conversion coefficient (CC[E] or $CC[H_T]$).

Chapter 5

Results and Discussion

In this chapter the main results of this work are presented and discussed. Concerning both patient and staff doses, the reader should be advised that our results are specific to staff and a patient simulated in a determined situation. The quoted studies cover the real medical practice in which parameters such as case complexity, protective equipment, fluoroscopic technique, staff experience among many other play a significant role on the exposure levels and in the vast majority of these papers, these parameters are nor specified. These factors are specially important in interventional radiology procedures and may lead to dose differences factors of 50 to hundreds as reported by (MILLER, 2020).

5.1 Generated x-ray energy spectra

Figure 15 shows the x-ray spectra generated with the SRS 78 software (CRANLEY, 1997), with the parameters previously covered in Section 4.2. As shown in the Figure 15, each spectrum is composed of a continuum component (Bressthralung x-rays) and a discrete component (characteristic x-ray).

5.2 Evaluation of patient exposure

In the Appendix A the CC[H_T] are presented for of all patient organs and tissues with dosimetric importance. As observed in Tables 12 - 23, the CC[H_T] for the patient organ and tissues increase as the tube voltage increases. This pattern is expected since the rise in tube voltage results in the production of a higher amount of x-ray photons, while also increasing their energy. In this way, more energy is deposited in the organs and tissues due by, mostly, Compton scattering and photoelectric effect.

The higher CC[H_T] were found for organs situated closer to the gall bladder, the organs and tissues with larger areas and the most radio-sensitive organs. For the female patient, undergoing a procedure with a FOV size of 15 $\times$ 15 cm^2, the higher CC[H_T] values were found for the gonads, eyes and thyroid, which are high sensitive structures.

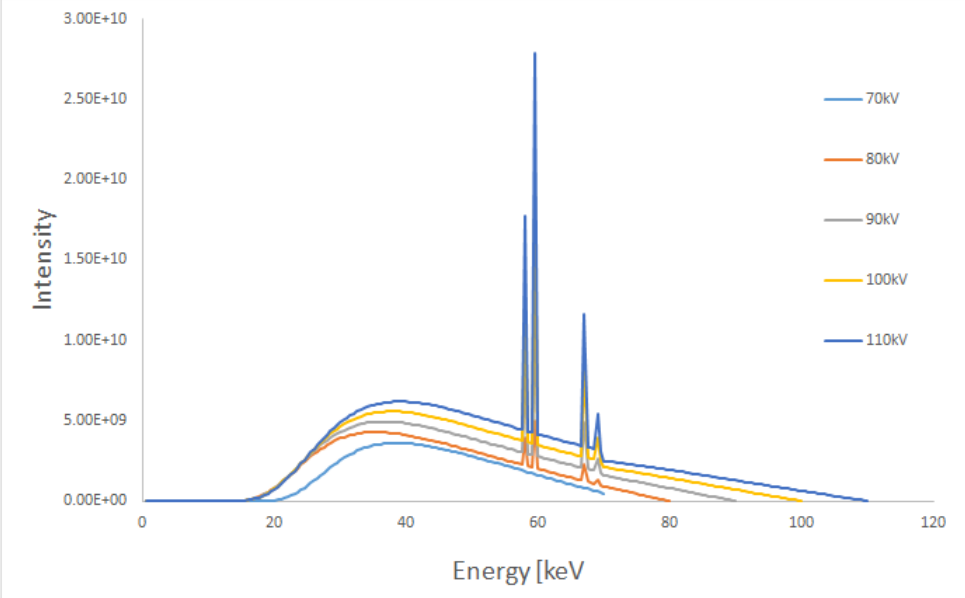

Figure 15 – X-ray spectra generated by SRS 78(CRANLEY, 1997) for 70, 80, 90, 100 and 110 kVp.

This pattern is kept as the tube voltage is increased from 70 to 110 kVp. For the male patient, the higher CC[H_T] are for the eyes, breast and thyroid, and this order also holds as the photon energy is increased. For all FOV, the higher CC[H_T] uncertainties where found for organ/tissues away from the irradiated area and for small or thin organs/tissues such as the eyes, gonads, thyroid and brain.

As seen in Table 5 there is a relationship between the increase in tube voltage and the CC[E]. This trend is caused by the increase in the photon energy, as the tube voltage increases, leading more photons to deposit higher energy levels in the patient body and tissues, increasing their CC[H_T]. As described in Equation 5, the CC[E] is calculated from the CC[H_T], as a consequence the CC[H_T] lead to a increase in the CC[E]. Samara *et al.* (2009) have also observed the increase of patient CC values as the tube voltage was increased from 80 to 100 kVp, in a stylised virtual anthropomorphic phantoms using the MCNP software.

Table 5 – CC[E] mean values (mSv/Gy.cm^2), as a function of tube voltage, for FOV sizes of 15 × 15 cm^2, 17 × 17 cm^2, 22 × 22 cm^2,25 × 25 cm^2, 31 × 31 cm^2 and 38 × 38 cm^2. The uncertainties are presented in parentheses (in %).

Tube Voltage	**15 × 15 cm^2**	**17 × 17 cm^2**	**22 × 22 cm^2**
Reference (70 kV)	8.4E-02(0.1)	8.6E-02(0.1)	8.0E-02(0.1)
(80 kV)	1.1E-01(0.1)	1.1E-01(0.1)	1.0E-01(0.1)
Difference (%)	26.8%	26.1%	25.1%
(90 kV)	1.3E-01(0.1)	1.3E-01(0.1)	1.2E-01(0.1)
Difference (%)	20.3%	19.8%	19.2%
(100 kV)	1.5E-01(0.1)	1.5E-01(0.1)	1.4E-01(0.1)
Difference (%)	15.3%	15.0%	14.5%
(110 kV)	1.7E-01(0.1)	1.7E-01(0.1)	1.5E-01(0.1)
Difference (%)	11.9%	11.7%	11.4%
	25 × 25 cm^2	**31 × 31 cm^2**	**38 × 38 cm^2**
Reference (70 kV)	7.6E-02(0.1)	6.4E-02(0.1)	5.6E-02(0.1)
(80 kV)	9.5E-02(0.1)	8.0E-02(0.1)	7.0E-02(0.1)
Difference (%)	25.2%	25.2%	25.0%
(90 kV)	1.1E-01(0.1)	9.6E-02(0.1)	8.3E-02(0.1)
Difference (%)	19.2%	19.2%	19.1%
(100 kV)	1.3E-01(0.1)	1.1E-01(0.1)	9.5E-02(0.1)
Difference (%)	14.6%	14.6%	14.5%
(110 kV)	1.4E-01(0.1)	1.2E-01(0.1)	1.1E-01(0.1)
Difference (%)	11.4%	11.4%	11.3%

The change of FOV size from 15 × 15 cm^2 to 17 × 17 cm^2 resulted in a 1.1% increase in the patient CC[E]. However, this tendency is reversed for further FOV sizes increments as observed in Table 5. In fact, comparing all remaining FOV sizes there is a reduction of 8.4% (17 to 22 cm), 4.8% (17 to 25 cm), 15.4% (25 to 31 cm) and 13.6% (31 to 38 cm). These reductions are consequences of the increase in the irradiated area with the same amount of x-ray photons. In this way, the energy deposition occurs in a larger area, covering other organs which are not included in the CC[E] calculations. Schueler *et al.* (2006) reported that the patient air kerma rate doubles as the FOV is reduced from 28 to 20 cm. Another reason for the decrease in the CC[E] as the FOV increases, is the irradiation of areas outside the patient body, colliding with the table. The different FOV areas can be observed in Figures 16 - 21. From Figures 19 - 21 it is possible to observe that the irradiated area reaches the table, reducing the absorbed dose to patient. However, the ionizing radiation exposure of the staff is increased (as it will be discussed in Section 5.3) without any further diagnostic or therapeutic benefit to the patient. This scenario, in which a FOV larger than the necessary is employed to represent a bad clinical practice, equipment failure or mistake in collimation selection. Figure 21 represents the worst situation, in which a FOV much larger than the necessary is employed.

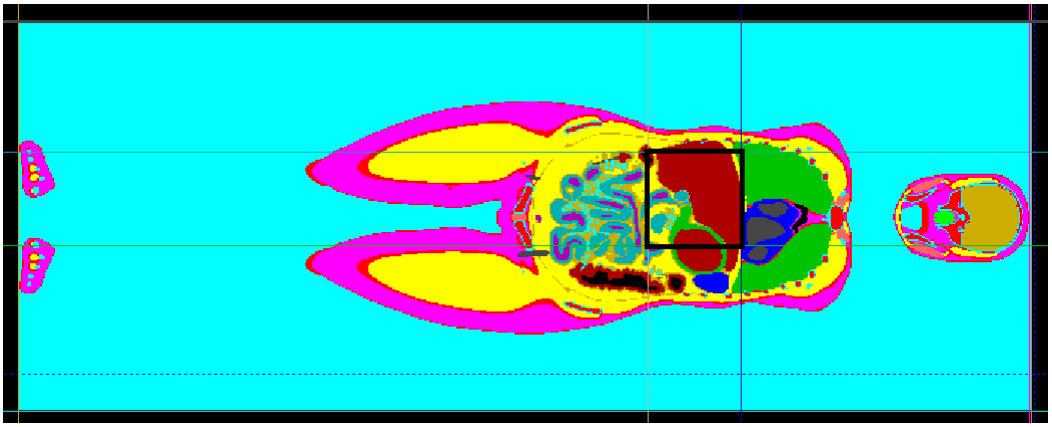

Figure 16 – Front view of the patient phantom showing FOV size of 15 × 15 cm^2.

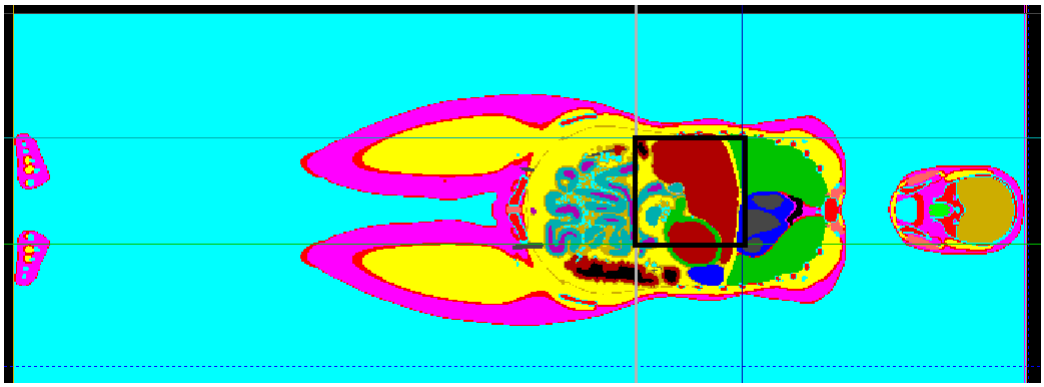

Figure 17 – Front view of the patient phantom showing FOV size of 17 × 17 cm^2.

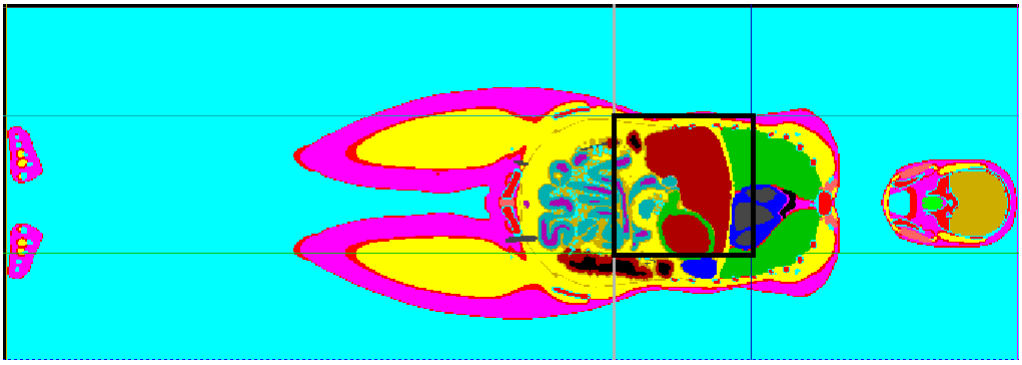

Figure 18 – Front view of the patient phantom showing FOV size of 22 × 22 cm^2.

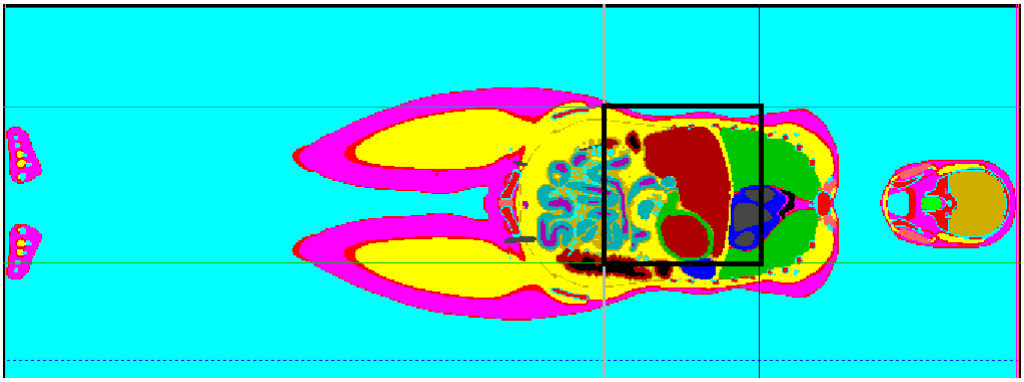

Figure 19 – Front view of the patient phantom showing FOV size of 25 × 25 cm^2.

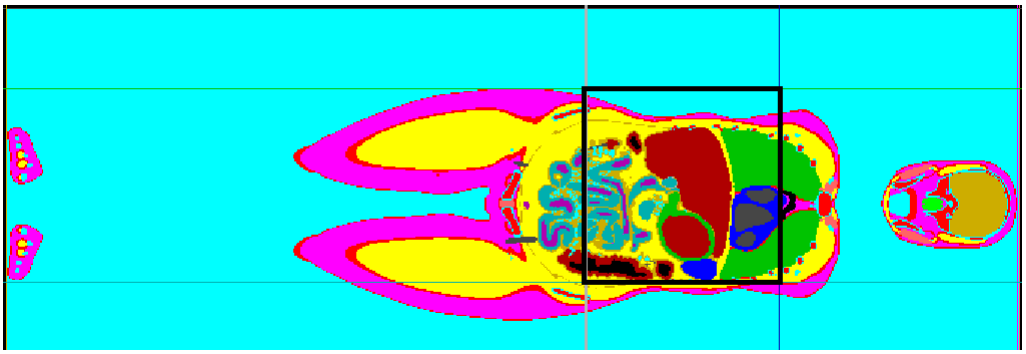

Figure 20 – Front view of the patient phantom showing FOV size of 31 × 31 cm^2.

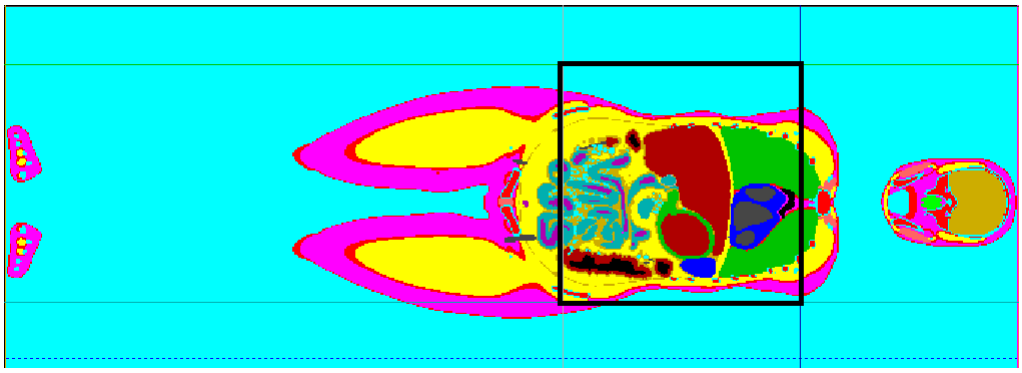

Figure 21 – Front view of the patient phantom showing FOV size of 38 × 38 cm^2.

DAP values from the literature were used to calculate the patient E based on the the CC[E] presented in Table 5, and the results are listed in Table 6. As observed, the effective dose varies greatly between the studies. These differences arise from factors depending on procedure complexity, x-ray system, endoscopist experience, among other procedure/staff factors. Patient anthropometric parameters such as height, mass and consequently the Body Mass Index (BMI) also effect the dose levels as reported in studies on other fluoroscopy guided procedures (CUSHMAN *et al.*, 2016; SANTOS *et al.*, 2018; HSI *et al.*, 2013).

Table 6 – Comparison of E values for patients with other studies and this one.

	Patient		
Study	DAP (Gy.cm^2)	E (mSv)	E this study (mSv)
Seo *et al.* (2016)	47.06	8.93 (0.33–56.63)	5.2
Buls *et al.* (2002)	49.9	9.9 (4.4-12*, max=35)	5.5
Hadjiconstanti *et al.* (2016)	2.03	0.39 (0.11 to 0.97)	0.2
Saukko *et al.* (2015)	5.15	1 (0.02-10.8)	0.6
Larkin *et al.* (2001)	13.5^D	3.1	1.5
	66.8^T	12.4	7.4
Saukko *et al.* (2018)	2.33	0.61 (0.02–3.69)	0.3
Liao *et al.* (2015)	13.98^L	3.63 (2.28-6.00)	1.5
	8.8^H	2.28 (1.36-3.76)	1.0
Churrango *et al.* (2015)	3.62	0.94 (0.34-1.05)	0.4

*First quartile-third quartile
^{D}Diagnostic
^{T}Therapeutic
^{L} Low volume endoscopist (LVE).
^{H} High volume endoscopist (HVE).

Buls *et al.* (2002) performed an evaluation of both patient and staff doses during 54 therapeutic ERCP procedures. Some parameters of the procedures were FOV sizes of 15×15 cm^2, 23×23 cm^2 and 38×38 cm^2 and tube potential ranging from 100-125 kVp. Staff doses were measured with TL dosimeters, while patient doses were estimated using male and female stylised anthropomorphic phantoms coupled with Monte Carlo simulations, and DAP values from the procedures. For patients, the median effective dose was 7.3 mSv (4.4 to 35 mSv). Our estimated values fit in this range even considering that in the cited study the patient was positioned in left lateral while we simulated the patient in the prone position. The equivalent dose for the liver (40.5 mGy), small intestines (29.1 mGy) and colon (28.4 mGy) were the highest. The female gonads (5.9 mGy) received a considerably higher dose than the male gonads (0.1 mGy).

In another study focused on the dosimetry of ERCP procedures, the authors utilised TL dosimeters to measure the radiation exposure of patients and staff over 126 ERCP procedures. They also found a wide variation of measured quantities between different patients caused by differences in patient characteristics, such as the BMI range of 15.6 to 44.5 kg.m^{-2} and procedure complexity, among other factors. On average, the patients received an effective dose of 8.93 mSv (0.33-56.63 mSv). The effective dose was calculated using the PCXMC (TAPIOVAARA; SIISKONEN, 2008), a Monte Carlo based software. The authors found, as expected, a strong correlation between fluoroscopy time and DAP, which influences the absorbed dose (SEO *et al.*, 2016). The E value in our work was 42% lower than the mean value reported to a mean DAP of 47.06 Gy.cm^2, however it falls into the interval presented in the study.

Sulieman *et al.* (2016) evaluated the entrance surface air kerma (ESAK) and effective doses for 55 ERCP patients in 3 hospitals in Khartoum (Sudan) using TL dosimeters.

They applied the National Radiological Protection Board (RNPB-SR262) software to estimate the effective doses. This code employs Monte Carlo simulations to estimate the doses in a hermaphrodite virtual stylised average adult phantom (m=70.9 kg, h=174 cm and BMI=23.12 kg/m^2). Their results found a mean patient effective dose of 1.94 mSv from 3 different hospitals: Fedail (1.60 mSv), Soba (1.56 mSv) and Ibn sena (2.67 mSv). The differences were attributed to factors such as staff experience, equipment, FOV sizes, clinical indication, type of procedure, patient age and tube filtration (2.5 to 4.0 mmAl). The fluoroscopy parameters also varied, as tube voltage from 57.0 to 116.0 kVp, tube current from 0.6 to 7.6 mA and screening time from 0.2 to 27.6 min. It is also important to point it out that this study did not use specific ERCP projection views. The authors based on the average conversion factors for PA kidney, stomach and duodenum views, to calculate the effective dose. The higher equivalent doses were found for the liver (9.51 mSv), pancreas (8.20 mSv) and ovaries (5.07 mSv) all in the Ibn Sena hospital. It is important to emphasize that this study included patients with a wide BMI range, different beam filtration (3.5, 4.0 and 2.5 mm Al) and a wider tube voltage range (40-125 kvp) than we simulated.

Hadjiconstanti *et al.* (2016) evaluated patient doses during 15 ERCP procedures for endoscopic sphincterotomy, stone extraction, bile duct dilation or stent placement. It was found an effective dose varying from 0.11 to 0.97 mSv with mean value of 0.39 mSv, which is 43% higher than our estimated effective dose, as shown in Table 6. The study included only therapeutic procedures, which are linked to higher dose levels (LARKIN *et al.*, 2001), moreover there was a significant patient BMI range (23.4 to 32.0 kg/m^2) and all patients were placed in the left lateral recumbent position. In this work, the patient was simulated in the prone position only, and as the same virtual anthropomorphic phantom was employed, there was only one BMI.

The higher effective dose difference of 58% was found applying the DAP reported by Saukko *et al.* (2018), however the value estimated in this work was in agreement with the reported E values range of 0.02 to 3.69 mSv. The authors studied the data from 638 procedures performed between 2013 and 2015 for different patient complexity. The results showed a higher dose for the male patients and for patients who needed a repeated ERCP procedure. Univariate analysis showed significant correlation between ERCP complexity level, cannulation difficulty grade, bile duct stricture, bile duct injury and pancreatic duct leakage with fluoroscopy time (FT) and DAP. Other variables such as age, gender, radiographer involved in ERCP, jaundice and suspicion of bile duct injury were related only to DAP. The endoscopist practice influenced only the FT. The authors concluded that the DAP and FT, which are the primary responsible for the exposure levels, are affected by multiple variables. In another prospective study on the predictive factors for 404 ERCP procedures, univariable analysis showed that alkaline phosphatase serum levels, balloon dilation, biliary stent placement and ERCP diagnosis are considerably

related to higher radiation exposure. However, another study employing multivariate analysis concluded that only the stent insertion is an independent predictor to prolonged fluoroscopy time (LORENZO-ZÚÑIGA *et al.*, 2013).

Regarding the parameters that affects the radiation exposure in ERCP, Heyd *et al.* (1996) found that patient dose is highly related to fluoroscopy time, it was also shown that, appropriate protection can significantly reduce the staff exposure to ionizing radiation (93%). These general findings are supported by another study (SAUKKO *et al.*, 2015) on the dosimetry of 227 ERCP procedures with 91% therapeutic cases. The patient BMI ranged from 15.6 to 44.5 $kg.m^{-2}$ and the DAP varied from 0.08 to 57 $Gy.cm^2$, these results evidence the great patient differences found in ERCP procedures. The estimated E value in this work also lies in the reported range of 0.02 to 10.8 mSv.

Jorgensen *et al.* (2010) also analyzed the fluoroscopy time for 8655 ERCP procedures, performed by 65 endoscopist in 6 countries, and found that the fluoroscopy time is highly influenced by the endoscopist experience. Liao *et al.* (2015) conducted a retrospective single-center study evolving 197 patients for 331 ERCP whose results supports the findings of (JORGENSEN *et al.*, 2010), on the endoscopist experience influence on the patient dose. The study reports a higher median total radiation dose (98.30 mGy vs 74.13 mGy), DAP (13.98 $Gy.cm^2$ vs 8.8 $Gy.cm^2$), and effective dose (3.63 mSv vs 2.28 mSv) when comparing less experienced endoscopist with the more experienced ones ($\geq$ 200 ERCP procedures/year). However, no significant FT differences were found.

The dose differences for therapeutic and diagnostic ERCP procedures were evaluated by Larkin *et al.* (2001). It was found a linear relationship between FT and DAP. Since the FT was longer for therapeutic (10.5 min) than diagnostic (2.3 min) procedures, the DAP were 66.8 and 13.5 $Gy.cm^2$, respectively. As a consequence of higher DAP, the therapeutic mean effective dose was 12.4 mSv while diagnostic was 3.1 mSv. Using the reported DAP and our mean CC values for all FOV sizes and tube voltages, the patient doses in our study are lower than the authors reported, as shown in Table 6. However, the ratio between the therapeutic to diagnostic mean E values (3.9) reported and our estimated values (4.9) are comparable. The older x-ray equipment employed in the Larkin *et al.* (2001) study could have played a major role in the differences between the reported E values and the ones found in the present work.

As discussed, the effective doses in ERCP procedures rely on a wide range of factors such as equipment, techniques, staff experience and case complexity. In order to enhances the techniques, Barakat *et al.* (2018) evaluated the effects of a brief (20 min) educational program on the optimization of radiation exposure during an ERCP procedure performed by high-volume endoscopists ($\geq$ 200 ERCP/year) or low-volume endoscopists ($<$ 200 ERCP/year). After completion, the FT for HVE reduced 48% while LVE reduced 30%, at the same time the total radiation dose reduced in 28% and 52% and the DAP values reduced by 35% and 48%. (CHURRANGO *et al.*, 2015) observed a significant re-

duction in patient E doses just by avoiding live or continuous fluoroscopy, our estimated E values are consistent with range communicated in the study. The results show that simple and effective action may reduce the patient exposure in ERCP procedures.

5.3 Evaluation of staff exposure

Appendix B and C present the CC[H_T] for the physician and assistant physician organs and tissues with dosimetric importance, respectively. The physician data are featured in Tables 24 to 35 and the assistant physician data are presented in Tables **??** to 47. As expected the staff CC[H_T] values are lower than the patient CC[H_T] values, since the patient is irradiated with the primary x-ray beam, while the staff is only exposed to the scattered radiation. Moreover, the staff wears protective equipment. The CC[H_T] values for the assistant physician are higher due to the closer distance (69 cm) to the x-ray beam center while the physician is positioned at 86 cm.

Table 7 presents the CC[E] values for both physicians. It is shown an increase in the CC[E] values for a fixed FOV size as function of the tube voltage. As the tube voltage is increased from 70 to 110 kV, in 10 kV steps, the physician CC[E] values increased by 56.7, 49.2, 43.5 and 33.5%. For the same tube voltage changes, the assistant physician CC[E] values increased by 40.6, 31.9, 25.8 and 20.6%. The reduction in CC[E] value changes may be explained by the deeper energy deposition done by more energetic x-ray photons, in this way some of the photons may deposited their energy beyond the staff bodies.

The change in FOV sizes also affects the scattered radiation from patient, thus interfering with the staff absorbed doses. Schueler *et al.* (2006) investigated the effects of FOV sizes and found a 30% reduction in the scattered radiation at the operator's waist and collar height, due to a FOV decrease from 28 × 28 cm^2 to 20 × 20 cm^2. A reduction of 50% was achieved as the FOV was reduced from 20 × 20 cm^2 to 14 × 14 cm^2. As observed in Table 7, the CC[E] values increase for larger FOV sizes, this effect may be caused by the larger patient area to interact with the x-ray beam. A larger area may also result in a smaller distance between the staff and the patient irradiated area.

As previously done to estimate the patient effective dose, the CC[E] presented in Table 7 were employed to compare our results with the literature. The estimates are presented in Table 8 and 9 for the physician and the assistant physician, respectively. There are few information about staff exposure in ERCP, fewer studies present the data for the assistant physician and the DAP values are not always reported. As observed, all estimates are lower than the quoted studies. These differences, as previously discussed are explained by the variability in staff position, case complexity, techniques, radiation protection practices, among another factors. The staff height also plays a crucial role on the dose levels as reported by (RIGATELLI *et al.*, 2016). The authors found that shorter (< 165 cm) individuals are exposed to significantly higher radiation levels than the taller

Table 7 – CC[E] mean values (μSv/Gy.cm^2) for physician and assistant physician, as a function of tube voltage, for different FOV sizes. The uncertainties are presented in parentheses (in %).

Tube Voltage	**15 × 15 cm^2**		**17 × 17 cm^2**	
	Physician	**Assistant**	**Physician**	**Assistant**
Reference (70 kV)	3.5E-02(4)	5.8E-02(5)	3.6E-02(4)	6.0E-02(5)
(80 kV)	5.4E-02(3)	8.2E-02(4)	5.5E-02(3)	8.5E-02(4)
Difference (%)	56.0	40.7	54.4	41.3
(90 kV)	8.0E-02(3)	1.1E-01(3)	8.1E-02(3)	1.1E-01(3)
Difference (%)	46.9	32.1	47.3	31.6
(100 kV)	1.1E-01(2)	1.4E-01(3)	1.2E-01(2)	1.4E-01(3)
Difference (%)	41.0	26.2	41.7	26.1
(110 kV)	1.5E-01(2)	1.6E-01(3)	1.5E-01(2)	1.7E-01(3)
Difference (%)	33.6	20.4	34.1	20.6
	22 × 22 cm^2		**25 × 25 cm^2**	
Reference (70 kV)	3.8E-02(4)	6.9E-02(5)	3.9E-02(3.6)	7.2E-02(4.4)
(80 kV)	6.0E-02(3)	9.7E-02(4)	6.1E-02(2.8)	1.0E-01(3.8)
Difference (%)	58.5	41.2	56.5	41.5
(90 kV)	9.0E-02(2)	1.3E-01(3)	9.2E-02(2.4)	1.3E-01(3.4)
Difference (%)	50.4	32.2	51.1	31.7
(100 kV)	1.3E-01(2)	1.6E-01(3)	1.3E-01(2.4)	1.7E-01(3.1)
Difference (%)	50.4	25.6	43.1	25.6
(110 kV)	1.7E-01(2)	2.0E-01(3)	1.8E-01(2.2)	2.0E-01(3.0)
Difference (%)	33.8	21.0	33.2	21.0
	31 × 31 cm^2		**38 × 38 cm^2**	
Reference (70 kV)	3.9E-02(4)	7.6E-02(4)	3.8E-02(4)	7.6E-02(4)
(80 kV)	6.2E-02(3)	1.1E-01(4)	5.9E-02(3)	1.1E-01(4)
Difference (%)	58.5	39.8	56.1	39.2
(90 kV)	9.3E-02(3)	1.4E-01(3)	8.8E-02(3)	1.4E-01(4)
Difference (%)	50.1	31.6	49.5	32.1
(100 kV)	1.3E-01(2)	1.8E-01(3)	1.3E-01(3)	1.8E-01(3)
Difference (%)	42.1	25.4	42.5	25.8
(110 kV)	1.8E-01(2)	2.1E-01(3)	1.7E-01(2)	2.1E-01(3)
Difference (%)	33.7	20.6	32.7	20.4

individuals (> 165 cm).

Table 8 – Comparison of E values for physician with other studies and this one.

Physician			
Study	DAP Gy.cm^2	E μSv	E this study μSv
Seo *et al.* (2016)	47.06 ^{M}	175	6.1
	2.5 ^{L}	127	0.3
	277.43 ^{H}	197	35.8

^{M}Mean
^{L}Lowest
^{H}Highest

Table 9 – Comparison of E values for assistant physician with other studies and this one.

Assistant physician			
Study	DAP Gy.cm^2	E μSv	E this study μSv
Seo *et al.* (2016)	47.06^M	69	4.5
	2.5^L	21	0.2
	277.43^H	116	26.3

^{M}Mean
^{L}Lowest
^{H}Highest

Seo *et al.* (2016) performed a study covering 126 ERCP procedures performed by 3 endoscopists (5 years of experience). The endoscopists wore lead apron (0.35 mm Pb), lead collar (0.35 mm Pb), lead eyewear (0.75 mm Pb) and stayed behind ceiling mounted lead glass shield. The patient BMI varied from 16.03 to 31.19 kg/m^2. Their results revealed an mean endoscopist dose of 175 μSv, while the assistant received 69 μSv.

Despite the differences between the effective dose values of this study and the ones presented in Tables 8 and 9 our results are in agreement with Sulieman *et al.* (2011) who found a physician E values from 0.01 to 11.8 μSv, for the assistant physician the range was 0.2 to 1.2 μSv. In the referred study the physician wore a 0.25 mm lead equivalent apron while the assistant physician wore a 0.5 mm Pb apron, neither one wore lead glass eyewear nor thyroid collar. Huda *et al.* (2016) found effective dose values of 10 μSv to the physician and 14 μSv to the assistant physician, both wore a 0.25 mm Pb lead apron. The patient was a pregnant woman with a BMI of 22.5 kg/m^2. In our study the staff were equipped with 0.5 mm Pb apron, thyroid collar and eyewear which provide more protection than in both studies.

The protective equipment play a fundamental role on the exposure to ionizing radiation. Haussen *et al.* (2016) reported that ceiling mounted lead glass shield may lead to a reduction of 290% in Entrance Skin Dose (ESD) to the operator, 110 % head, 1290% for the thyroid and a total reduction at the chest level with no weight stress on endoscopist body. Overall, the device reduced the accumulated dose 4 fold when compared to a regular lead apron. It is also important to emphasize the better protection given by a lead apron that covers the whole body and not only the front body parts. During ERCP procedures, the staff must turn their body constantly, thus exposing several parts of their body to the scattered radiation.

The effectiveness of a lead free radiation shield drape placed around the image intensifier in a over-couch x-ray system was evaluated by Muniraj *et al.* (2015). The results show a reduction of 90% on the effective doses for endoscopist and nurse. In a similar approach, Morishima *et al.* (2018) found that a lead shield curtain hanging from ceiling around the x-ray beam can reduce the staff effective dose between 41.0 to 76.5%. In a third study using curtain around the tube, the authors found reductions of 87.5%, 84.7%,

71.1%, and 68.0% in the mean radiation dose to for endoscopists, first assistants, second assistants, and nurses, respectively. The mean E doses without the curtain to the physician was 340.9 ± 313.9 μSv and 27.5±48.5 μSv to the first assistant. No significant patient dose increase was found, and the heavy curtain (8 kg) did not damage the x-ray system (MINAMI *et al.*, 2014).

The position of staff in the surgical room is another key factor regarding the radiation exposure (MARSHALL; FAULKNER, 1992). The closer to the x-ray tube and patient the higher the absorbed dose. As observed in Table 7 the assistant physician CC[E] values are higher than the physician CC[E], since the assistant is closer to the x-ray tube in this study. The differences vary from 65.7% (70 kV and FOV size of 15 × 15 cm^2) to 23.5% (110 kV and FOV size of 38 × 38 cm^2). These differences are consequences of the more intensified radiation scattering as the tube voltage increased and the larger irradiated area.

Another feasible practice to reduce the exposure is to use single-frame fluoroscopy, it was found that this technique can reduce the effective dose by 50% compared with the values found in literature, keeping the ERCP procedure success rate in 92%, which is acceptable (CHURRANGO *et al.*, 2015).

Despite the existence of many radiation protection equipment and techniques, the incorrect use, or the no usage at all, is a constant concern. Some studies have shown flaws in radiation protection practices since the staff did not know the correct way to use the equipment, did not have access to all necessary equipment or consider the equipment to be bothersome (SHIN *et al.*, 2013). A 2011 survey on the radiation protection with Korean endoscopists showed that 75% do not monitor their radiation exposure. In addition, just 14% wore lead eyewear, 52.5% the thyroid protection and 69% never attached the personal dosimeter (SON *et al.*, 2011). In fact, the protective equipment is heavy and may cause injuries (REES; DUNCAN, 2018; ALEXANDRE *et al.*, 2017). However, efforts must be done to ensure a safe work environment for the staff involved in ERCP procedures. Concerning the endoscopist, a study have described the ERCP procedure with the endoscopist in sitting position, which reduces the weight stress in the spine (ECKARDT *et al.*, 2010).

5.4 Evaluation of eye lens exposure

The H_T for the eye lens is the quantity to be under control in the clinical practice due to its relationship to cataractogenesis (SEALS *et al.*, 2016). There is a debate on the existence of a threshold dose to radiation induced cataract, some studies have shown potentially cataract leading cell damages below the recommended limits (JACOB *et al.*, 2012). In 2011, the ICRP reduced the exposure limits from 2 Gy to 0.5 Gy due to the evidences of abnormal cells and lens opacity resulted from exposures below 1 Gy. The

occupational eye lens doses were also reduced from 150 to 20 mSv/year averaged in 5 years, with no year exceeding 50 mSv (STEWART *et al.*, 2012).

In Tables 10 and 11 are presented the H_T to the eye lens for the physician and assistant physician calculated from the CC[H_T] values of this study and the DAP values from previous studies. As observed, there is a great difference between the values found in the literature. These differences are consequence of different clinical practices, equipment, case complexity among other factors.

The effects of staff distance and orientation in relation to the tube, eyewear protection and staff height on the eye exposure to ionizing radiation are known key factors in the eye lens occupational dose. In fact, a 10 cm increase in height is related to a 2 fold reduction on eye dose (PRINCIPI *et al.*, 2016).This finding may play a role on the differences found between the results of the present work and the literature since we simulated individuals with the same height, but the studies analysed information about different professionals. Concerning the head orientation in relation to x-ray tube, we simulated a scenario in which both professionals keep the head high facing straight forward. In the clinical practice, the staff have to change their head position constantly which strongly affect the doses levels (PRINCIPI *et al.*, 2016). Moreover, in some studies, the eye dose is estimated based on the dosimeter placed on the thorax/thyroid, not at the eye level or in the eye itself as the MCNPX allowed to do. This methodology can lead to a wide range of the conversion factors used to adjust the measured value to eye lens dose (CARINOU *et al.*, 2015; MARTIN, 2011).

Table 10 – Comparison of H_T mean values for female and male physician with other studies and this one.

FASH3			
Study	DAP Gy.cm^2	H_T (μSv)	H_T (μSv) this study
O'Connor *et al.* (2013)	14.5	10 (10-30)^A	0.96
	5.4	90 (90-100)^B	0.36
Muniraj *et al.* (2015)	7.02	210 (130-290)*	0.64
Angsuwatcharakon *et al.* (2018)	23.2	19.2 (IQR=207)^C	1.54
	22.3	30.7 (IQR=24.5)	1.49
MASH3			
O'Connor *et al.* (2013)	14.5	10 (10-30)^A	
	5.4	90 (90-100)^B	0.70
Muniraj *et al.* (2015)	7.02	210 (130-290)*	0.91
Angsuwatcharakon *et al.* (2018)	23.2	19.2 (IQR=207)^C	3.01
	22.3	30.7 (IQR=24.5)	2.9

^{A}Hospital A (Fixed undercouch X-ray tube, ceiling-mounted lead glass screen, tableside lead shielding, no eyewear)
^{B}Hospital B (Mobile overcouch X-ray tube, no ceiling-mounted lead glass screen, tableside lead shielding, no eyewear)
^{C}Patient in prone position/patient in left lateral decubitus (LLD) position. No lead eyewear in both situations
Dosimeter positioned outside the eyewear
IQR = Interquartile range

Table 11 – Comparison of H_T mean values for female and male physician assistant with other studies and this one.

Study	DAP Gy.cm^2	H_T (μSv)	H_T (μSv) this study
FASH3			
O'Connor *et al.* (2013)	14.5	10 ^{A}	1.77
	5.4	20 ^{B}	0.66
Angsuwatcharakon *et al.* (2018)	23.2	9.6 (IQR=13.5)^C	2.84
	22.3	15.4 (IQR=19.2)	2.73
MASH3			
O'Connor *et al.* (2013)	14.5	10 ^{A}	3.29
	5.4	20 ^{B}	1.22
Angsuwatcharakon *et al.* (2018)	23.2	9.6 (IQR=13.5)^C	5.27
	22.3	15.4 (IQR=19.2)	5.06

^{A}Hospital A (Fixed undercouch X-ray tube, ceiling-mounted lead glass screen, tableside lead shielding, no eyewear) ^{B}Hospital B (Mobile overcouch X-ray tube, no ceiling-mounted lead glass screen, tableside lead shielding, no eyewear) ^{C}Patient in prone position/patient in left lateral decubitus (LLD) position. No lead eyewear in both situations IQR = Interquartile range

The estimated H_T values also largely vary from the values found by Muniraj *et al.* (2015) in a sham controlled study on the protective effects of a lead drape placed around the x-ray image intensifier (under-couch x-ray tube). They found, at the eyewear level a dose of 210 μSv with the sham drape and 20 μSv with the lead drape, for the physician. Our results are lower, however, in their study the doses were measured by a dosimeter attached to the side of the eyewear, i.e, our measurements take account of the attenuated effect of the eyewear. Considering an eyewear dose reduction factor between 7.9 and 10.0 (ROOIJEN *et al.*, 2014), our estimated H_T value is consistent with the range of 130 to 290 μSv found by the authors.

O'Connor *et al.* (2013) evaluated the occupational eye lens exposure in two hospitals in Ireland. The ERCP procedures in hospital A were performed in a room with under-couch x-ray system, suspended lead glass shield, lead drape around the x-ray system and table side lead shields. In hospital B the procedures performed in a room equipped with a c-arm operated in over-couch position with no lead shields. In both hospitals the staff wore lead apron (0.25-0.5 mmPb) and thyroid protection (0.5 mmPb), but not lead eyewear. The authors concluded that the eye lens dose due to the use of an over-couch x-ray system, without suspended lead glass protection, can be 9 fold higher than when an under-couch system, with suspended protection is used. Regarding our physician eye lens estimates, the H_T values are 90 and 99% lower compared with the under-couch and over-couch system, respectively. For the physician assistant, the differences are slightly lower. These divergences are explained by the different radiation protection strategies between our studies, we considered the eyewear protection, while the cited study did not include this type of protection. Taking in account dose reduction factors due to eyewear protection from previous works (ROOIJEN *et al.*, 2014; MAGEE *et al.*, 2014), our H_T

values lies in the range found by O'Connor *et al.* (2013).

Angsuwatcharakon *et al.* (2018) performed a randomized study on the effect of patient position in the staff eye lens dose. They found that the left lateral decubitus patient position (LLD) is linked to a higher dose to both primary and secondary endoscopists than the prone position. Regarding the physician, our values are approximately 90% lower for both positions whereas for the assistant physician, the differences vary from 45 to 82.3%. Our lower results may be explained by the use of lead eyewear by the staff in the simulations in contrary to Angsuwatcharakon *et al.* (2018) study in which no eyewear were used. It is also important to highlight that in our simulations, the patient lays in the prone position only. Our values are in agreement considering the dose reduction provided by the eyewear (ROOIJEN *et al.*, 2014).

Although our results diverge from the referenced studies, their are in agreement with Huda *et al.* (2016) who found eye lenses doses ranging from 4 μSv to 28 μSv in a study with a pregnant patient.

Experimental and computational studies assessed the efficiency of lead glass eyewear on the reduction of the H_T for the eye lens. Rooijen *et al.* (2014) found a clear dependence of the eyewear protection on angle of exposure, for frontal exposure the reduction factor ranges between 7.9 and 10.0 during phantom studies. The protection is highly reduced for side exposure and in clinical practice. In our simulation, the assistant physician is positioned in front of the x-ray tube and the main physician is mainly exposed to lateral scattered radiation. Another study found a reduction range factor of 1.1 to 3.4 depending on eyewear design and staff position (DOMIENIK *et al.*, 2016). Magee *et al.* (2014) reported dose reduction factors varying from 5.2 to 7.6 for frontal exposure and between 1.4 and 5.2 for orientations commonly found in the clinical routine. In a MCNPX code based study on eye lens dose reduction techniques and devices, Koukorava *et al.* (2014) concluded that lead glass eyewear can reduce the eye dose by 74% (left) and 21% (right). They also found that staff position and head orientation, patient to image detector distance and beam projection have more effect on the eye and whole body dose than beam quality and lead thickness. Once again, eyewear with air gaps showed lower protection.

In order to assess the staff eye lens exposure to ionizing radiation, Zagorska *et al.* (2015) employed TL dosimeters to measure the dose equivalent to the eye. Forty nine therapeutic procedures were recorded. The mean dose to the eye was found to vary between 34.9 μSv and 93.3 μSv. The authors found that if the eyes are not protected, the annual dose limit can be exceeded. The highest doses were measured for individual at the closest position relative do the x-ray system, and in this case, the anesthesiologist (30-40 cm) and gastroenterologist (50-80 cm). The researchers also emphasized the importance of lateral eyewear protection in order to efficiently reduce the eye exposure.

Another study on protective devices for eye lens reported a reduction ratio of 1.7 and

2.2 comparing exposure scenarios with and with ceiling suspended shield (CARINOU *et al.*, 2011). The eyes must be protected with lead eyewear, the ones with lateral protection further minimise the exposure and the use of ceiling suspended shield offers a reduction up to 97% (KOUKORAVA *et al.*, 2011). Various studies have reported techniques and equipment to reduce eye lens doses in ERCP and other IR procedures (CARINOU *et al.*, 2011; MARTIN, 2009; MARTIN, 2011; CARINOU *et al.*, 2015).

Chapter 6

Conclusion

The effects of tube voltage and FOV sizes changes were analysed. For fixed tube voltage, the results showed an increase of patient CC[E] values as the FOV size is risen from 15×15 cm^2 to 17×17 cm^2, after a FOV size of 22×22 cm^2 the CC[E] reduced since the irradiated area starts to reach the table. These findings are in agreement with previous studies. For a fixed FOV, the patient CC[E] values increased as the tube voltage is raised, since the x-ray photons deposit energy in deeper portions in matter

Regarding the staff conversion coefficients, the higher values were found to the assistant physician due to his/her closer distance to the x-ray tube and patient. For a fixed tube voltage, the CC[E] values elevated as the FOV sizes were increased. This finding is explained by the expansion of the scattering area. For a fixed FOV size, the CC[E] values raised as the tube voltage was increased. This happened because the scattered x-rays gained more energy and then, suffered less attenuation from the lead protection wore by the staff. In this way, more energy was deposited in their organs and tissues.

The calculated CC[E] values were coupled with DAP values found in the literature in order do estimated E values. Considering the wide range of E values reported from ERCP procedures, our results are consistent for all individuals studied. The H_T values for the eye lens of the staff are also consistent with the range of values found in the literature.

The scarcity of data on staff exposure for results comparison, reveals a need for further investigations covering different equipment, filtration, FOV size, tube voltage, patient position among other key parameters in ERCP.

Bibliography

AERTS, R.; PENNINCKX, F. The burden of gallstone disease in Europe. **Alimentary Pharmacology & Therapeutics**, Wiley Online Library, v. 18, p. 49–53, 2003. https://doi.org/10.1046/j.0953-0673.2003.01721.x.

ALEXANDRE, D.; PRIETO, M.; BEAUMONT, F.; TAIAR, R.; POLIDORI, G. Wearing lead aprons in surgical operating rooms: ergonomic injuries evidenced by infrared thermography. **Journal of Surgical Research**, Elsevier, v. 209, p. 227–233, 2017. https://doi.org/10.1016/j.jss.2016.10.019.

ALZIMAMI, K.; SULIEMAN, A.; PAROUTOGLOU, G.; POTAMIANOS, S.; VLYCHOU, M.; THEODOROU, K. Optimisation of radiation exposure to gastroenterologists and patients during therapeutic ERCP. **Gastroenterology Research and Practice**, Hindawi, v. 2013, p. 1–7, 2013. http://dx.doi.org/10.1155/2013/587574.

ANGSUWATCHARAKON, P.; JANJEURMAT, W.; KRISANACHINDA, A.; RIDTITID, W.; KONGKAM, P.; RERKNIMITR, R. The difference in ocular lens equivalent dose to ERCP personnel between prone and left lateral decubitus positions: a prospective randomized study. **Endoscopy International Open**, Georg Thieme Verlag KG, v. 6, n. 08, p. E969–E974, 2018. https://doi.org/10.1055/a-0599-5917.

AUXIER, J.; SNYDER, W.; JONES, T. Neutron interactions and penetration in tissue. **Radiation Dosimetry**, v. 1, p. 275–316, 1968.

BAIU, I.; VISSER, B. Endoscopic Retrograde Cholangiopancreatography. **JAMA**, v. 320, n. 19, p. 2050–2050, 11 2018. ISSN 0098-7484. https://doi.org/10.1001/jama.2018.14481.

BARAKAT, M. T.; THOSANI, N. C.; HUANG, R. J.; CHOUDHARY, A.; KOCHAR, R.; KOTHARI, S.; BANERJEE, S. Effects of a brief educational program on optimization of fluoroscopy to minimize radiation exposure during endoscopic retrograde cholangiopancreatography. **Clinical Gastroenterology and Hepatology**, Elsevier, v. 16, n. 4, p. 550–557, 2018. https://doi.org/10.1016/j.cgh.2017.08.008.

BASTIONI, M.; FLERACKERS, M.; CAPCO, J. **Make human: Open Source Tool for Making 3d Characters**. 2007.

BEIR VII. **Health risks from exposure to low levels of ionizing radiation: phase 2**. [S.l.]: National Academies Press, 2006. v. 7.

BELINATO, W.; SILVA, R. M.; PERINI, A. P.; NEVES, L. P.; SANTOS, C. J.; SOUZA, D. N.; SANTOS, W. S. Monte Carlo dosimetric evaluation in PET exams for patients with different BMI and heights. **Radiation Physics and Chemistry**, Elsevier, v. 151, p. 36–41, 2018. https://doi.org/10.1016/j.radphyschem.2018.05.011.

BOR, D.; SANCAK, T.; OLGAR, T.; ELCIM, Y.; ADANALI, A.; SANLIDILEK, U.; AKYAR, S. Comparison of effective doses obtained from dose–area product and air kerma measurements in interventional radiology. **The British Journal of Radiology**, British Institute of Radiology, v. 77, n. 916, p. 315–322, 2004. https://doi.org/10.1259/bjr/29942833.

BULS, N.; PAGES, J.; MANA, F.; OSTEAUX, M. Patient and staff exposure during endoscopic retrograde cholangiopancreatography. **The British Journal of Radiology**, British Institute of Radiology, v. 75, n. 893, p. 435–443, 2002. https://doi.org/10.1259/bjr.75.893.750435.

CARINOU, E.; BRODECKI, M.; DOMIENIK, J.; DONADILLE, L.; KOUKORAVA, C.; KRIM, S.; NIKODEMOVA, D.; RUIZ-LOPEZ, N.; SANS-MERCÉ, M.; STRUELENS, L. *et al.* Recommendations to reduce extremity and eye lens doses in interventional radiology and cardiology. **Radiation Measurements**, Elsevier, v. 46, n. 11, p. 1324–1329, 2011. https://doi.org/10.1016/j.radmeas.2011.05.027.

CARINOU, E.; FERRARI, P.; BJELAC, O. C.; GINGAUME, M.; MERCE, M. S.; O'CONNOR, U. Eye lens monitoring for interventional radiology personnel: dosemeters, calibration and practical aspects of Hp (3) monitoring. a 2015 review. **Journal of Radiological Protection**, IOP Publishing, v. 35, n. 3, p. R17–R34, 2015. https://doi.org/10.1088/0952-4746/35/3/R17.

CASSOLA, V.; LIMA, V. de M.; KRAMER, R.; KHOURY, H. FASH and MASH: female and male adult human phantoms based on polygon mesh surfaces: I. development of the anatomy. **Physics in Medicine & Biology**, IOP Publishing, v. 55, n. 1, p. 133–162, 2009. https://doi.org/10.1088/0031-9155/55/1/009.

CHERRY, R. N. **Chapter 48 - Radiation: Ionizing**. Geneva: International Labour Office, 1998.

CHURRANGO, G.; DEUTSCH, J. K.; DINNEEN, H. S.; CHURRANGO, J.; SAMIULLAH, S.; AHLAWAT, S. K. Minimizing radiation exposure during ERCP by avoiding live or continuous fluoroscopy. **Journal of Clinical Gastroenterology**, Wolters Kluwer, v. 49, n. 10, p. e96–e100, 2015. https://doi.org/10.1097/MCG.0000000000000385.

COMPTON, A. H. A quantum theory of the scattering of x-rays by light elements. **Physical Review**, APS, v. 21, n. 5, p. 483–502, 1923. https://doi.org/10.1103/PhysRev.21.483.

CRANLEY, K. Catalogue of diagnostic x-ray spectra and other data. **The Institute of Physics and Engineering in Medicine Report**, 1997.

CUSHMAN, D.; MATTIE, R.; CURTIS, B.; FLIS, A.; MCCORMICK, Z. L. The effect of body mass index on fluoroscopic time and radiation dose during lumbar transforaminal epidural steroid injections. **The Spine Journal**, Elsevier, v. 16, n. 7, p. 876–883, 2016. https://doi.org/10.1016/j.spinee.2016.03.041.

DOMIENIK, J.; BISSINGER, A.; GRABOWICZ, W.; KRĘCKI, R.; MAKOWSKI, M.; MASIAREK, K.; PLEWKA, M.; LUBIŃSKI, A.; PERUGA, J. *et al.* The impact of various protective tools on the dose reduction in the eye lens in an interventional cardiology—clinical study. **Journal of Radiological Protection**, IOP Publishing, v. 36, n. 2, p. 309–318, 2016. https://doi.org/10.1088/0952-4746/36/2/309.

ECKARDT, A. J.; VELTZKE-SCHLIEKER, W.; HINTZE, R. E.; WIEDENMANN, B.; ADLER, A. ERCP in the sitting position—an alternative technique with potential benefits (with video). **Surgical Laparoscopy, Endoscopy & Percutaneous Techniques**, Ovid Technologies (Wolters Kluwer Health), v. 20, n. 4, p. 247–249, 2010. https://doi.org/10.1097/sle.0b013e3181ec886e.

EINSTEIN, A. Über einen die Erzeugung und Verwandlung des Lichtes betreffenden heuristischen Gesichtspunkt. **Annalen der Physik**, Wiley Online Library, v. 322, n. 6, p. 132–148, 1905. https://doi.org/10.1002/andp.19053220607.

FERREIRA, T.; RASBAND, W. ImageJ user guide. **ImageJ/Fiji**, v. 1, p. 155–161, 2012.

FISHER, H.; SNYDER, W. Distribution of dose in the body from a source of gamma rays distributed uniformly in an organ. In: ELSEVIER. **Proceedings of the First International Congress of Radiation Protection**. 1968. p. 1473–1486. https://doi.org/10.1016/B978-1-4832-8312-8.50220-4.

GARDUMI, A.; FARAH, J.; DESBRéE, A. Creation of ORNL NURBS-based phantoms: evaluation of the voxel effect on absorbed doses from radiopharmaceuticals. **Radiation Protection Dosimetry**, v. 153, n. 3, p. 273–281, 2012. https://doi.org/10.1093/rpd/ncs103.

GIBBS, S. J.; JR, A. P.; CHEN, T.-S.; MALCOLM, A. W.; JR, A. E. J. Patient risk from interproximal radiography. **Oral Surgery, Oral Medicine, Oral Pathology**, Elsevier, v. 58, n. 3, p. 347–354, 1984a. https://doi.org/10.1016/0030-4220(84)90066-5.

GIBBS, S. J.; PUJOL, A.; CHEN, T.; MALCOLM, A. Computer-simulation of patient dose from dental radiography. In: AMER ASSOC DENTAL RESEARCH 1619 DUKE ST, ALEXANDRIA, VA 22314. **Journal of Dental Research**. [S.l.], 1984b. v. 63, p. 209–209.

HADJICONSTANTI, A. C.; MESSARIS, G. A.; THOMOPOULOS, K. C.; PANAYIOTAKIS, G. S. Patient dose during therapeutic endoscopic retrograde cholangiopancreatography procedure. **Radiation Protection Dosimetry**, Oxford University Press, v. 173, n. 4, p. 380–382, 2016. https://doi.org/10.1093/rpd/ncw023.

HAN, M. C.; KIM, C. H.; JEONG, J. H.; YEOM, Y. S.; KIM, S.; WILSON, P. P. H.; APOSTOLAKIS, J. DagSolid: a new Geant4 solid class for fast simulation in polygon-mesh geometry. **Physics in Medicine and Biology**, IOP Publishing, v. 58, n. 13, p. 4595–4609, 2013. https://doi.org/10.1088/0031-9155/58/13/4595.

HAUSSEN, D. C.; BOM, I. M. J. V. D.; NOGUEIRA, R. G. A prospective case control comparison of the zerogravity system versus a standard lead apron as radiation protection strategy in neuroendovascular procedures. **Journal of Neurointerventional Surgery**, British Medical Journal Publishing Group, v. 8, n. 10, p. 1052–1055, 2016. https://doi.org/10.1136/neurintsurg-2015-012038.

HERON, J. L. Estimation of effective dose to the patient during medical x-ray examinations from measurements of the dose-area product. **Physics in Medicine & Biology**, IOP Publishing, v. 37, n. 11, p. 2117–2126, 1992. https://doi.org/10.1088/0031-9155/37/11/008.

HESS, R. **The Essential Blender: Guide to 3D Creation with the Open Source Suite Blender**. San Francisco, CA: No Starch Press, 2007. ISBN 978-1-59327-166-4.

HEYD, R. L.; KOPECKY, K. K.; SHERMAN, S.; LEHMAN, G. A.; STOCKBERGER, S. M. Radiation exposure to patients and personnel during interventional ERCP at a teaching institution. **Gastrointestinal Endoscopy**, Elsevier, v. 44, n. 3, p. 287–292, 1996. https://doi.org/10.1016/S0016-5107(96)70166-9.

HSI, R. S.; ZAMORA, D. A.; KANAL, K. M.; HARPER, J. D. Severe obesity is associated with 3-fold higher radiation dose rate during ureteroscopy. **Urology**, Elsevier, v. 82, n. 4, p. 780–785, 2013. https://doi.org/10.1016/j.urology.2013.06.030.

HUDA, A.; GARZÓN, W.; FILHO, G.; VIEIRA, B.; KRAMER, R.; XU, X.; GAO, Y.; KHOURY, H. Evaluation of staff, patient and foetal radiation doses due to endoscopic retrograde cholangiopancreatography (ERCP) procedures in a pregnant patient. **Radiation Protection Dosimetry**, Oxford University Press, v. 168, n. 3, p. 401–407, 2016. https://doi.org/10.1093/rpd/ncv354.

ICRP 103. The 2007 recommendations of the International Commission on Radiological Protection. **Ann ICRP**, v. 37, p. 2–4, 2007.

JACOB, S.; MICHEL, M.; BRÉZIN, A.; LAURIER, D.; BERNIER, M. Ionizing radiation as a risk factor for cataract: what about low-dose effects. **Journal of Clinical & Experimental Ophthalmology**, v. 1, p. 1–7, 2012. https://doi.org/10.4172/2155-9570.S1-005.

JORGENSEN, J. E.; RUBENSTEIN, J. H.; GOODSITT, M. M.; ELTA, G. H. Radiation doses to ERCP patients are significantly lower with experienced endoscopists. **Gastrointestinal Endoscopy**, Elsevier, v. 72, n. 1, p. 58–65, 2010. https://doi.org/10.1016/j.gie.2009.12.060.

KIM, C. H.; JEONG, J. H.; BOLCH, W. E.; CHO, K.-W.; HWANG, S. B. A polygon-surface reference Korean male phantom (PSRK-Man) and its direct implementation in Geant4 Monte Carlo simulation. **Physics in Medicine and Biology**, IOP Publishing, v. 56, n. 10, p. 3137–3161, 2011. https://doi.org/10.1088/0031-9155/56/10/016.

KOUKORAVA, C.; CARINOU, E.; FERRARI, P.; KRIM, S.; STRUELENS, L. Study of the parameters affecting operator doses in interventional radiology using Monte Carlo simulations. **Radiation Measurements**, Elsevier, v. 46, n. 11, p. 1216–1222, 2011. https://doi.org/10.1016/j.radmeas.2011.06.057.

KOUKORAVA, C.; FARAH, J.; STRUELENS, L.; CLAIRAND, I.; DONADILLE, L.; VANHAVERE, F.; DIMITRIOU, P. Efficiency of radiation protection equipment in interventional radiology: a systematic Monte Carlo study of eye lens and whole body doses. **Journal of Radiological Protection**, IOP Publishing, v. 34, n. 3, p. 509–528, 2014. https://doi.org/10.1088/0952-4746/34/3/509.

KRAMER, R. The calculation of dose from external photon exposures using reference human phantoms and Monte Carlo methods. **Part I: the male (ADAM) and female (EVA) adult mathematical phantoms**, GSF-Bericht, 1982.

KRAMER, R.; CASSOLA, V.; KHOURY, H.; VIEIRA, J.; LIMA, V. de M.; BROWN, K. R. FASH and MASH: female and male adult human phantoms based on polygon mesh surfaces: II. dosimetric calculations. **Physics in Medicine & Biology**, IOP Publishing, v. 55, n. 1, p. 163–189, 2009. https://doi.org/10.1088/0031-9155/55/1/010.

KRAMER, R.; KHOURY, H.; VIEIRA, J.; LOUREIRO, E.; LIMA, V.; LIMA, F.; HOFF, G. All about FAX: a female adult voxel phantom for Monte Carlo calculation in radiation protection dosimetry. **Physics in Medicine & Biology**, IOP Publishing, v. 49, n. 23, p. 5203–5216, 2004. https://doi.org/10.1088/0031-9155/49/23/001.

KRAMER, R.; VIEIRA, J.; KHOURY, H.; LIMA, F.; FUELLE, D. All about MAX: a male adult voxel phantom for Monte Carlo calculations in radiation protection dosimetry. **Physics in Medicine & Biology**, IOP Publishing, v. 48, n. 10, p. 1239–1262, 2003. https://doi.org/10.1088/0031-9155/48/10/301.

KRAMER, R.; VIEIRA, J.; KHOURY, H.; LIMA, F. de A. MAX meets ADAM: a dosimetric comparison between a voxel-based and a mathematical model for external exposure to photons. **Physics in Medicine & Biology**, IOP Publishing, v. 49, n. 6, p. 887–910, 2004. https://doi.org/10.1088/0031-9155/49/6/002.

KRUIT, A. S.; VLEGGAAR, F. P.; ERPECUM, K. J. van; TIMMERMAN, A. M.; SIERSEMA, P. D.; OLDENBURG, B. No reduction of radiation dose following the introduction of dose–area product measurement in endoscopic retrograde cholangiopancreatography. **European Journal of Gastroenterology & Hepatology**, Wolters Kluwer, v. 27, n. 12, p. 1454–1458, 2015. https://doi.org/10.1097/MEG.0000000000000128.

LARKIN, C. J.; WORKMAN, A.; WRIGHT, R. E.; THAM, T. C. Radiation doses to patients during ERCP. **Gastrointestinal Endoscopy**, Elsevier, v. 53, n. 2, p. 161–164, 2001. https://doi.org/10.1067/mge.2001.111389.

LIAO, C.; THOSANI, N.; KOTHARI, S.; FRIEDLAND, S.; CHEN, A.; BANERJEE, S. Radiation exposure to patients during ERCP is significantly higher with low-volume endoscopists. **Gastrointestinal Endoscopy**, Elsevier, v. 81, n. 2, p. 391–398, 2015. https://doi.org/10.1016/j.gie.2014.08.001.

LORENZO-ZÚÑIGA, V.; ÁLVAREZ, M. A.; VEGA, V. M. de; SEOANE, A.; BORY, F.; BOIX, J. Predictive factors of radiation dose in ERCP: a prospective study in 2 tertiary centers. **Surgical Laparoscopy Endoscopy & Percutaneous Techniques**, LWW, v. 23, n. 3, p. 266–270, 2013. https://doi.org/10.1097/SLE.0b013e31828b8860.

MAGEE, J. S.; MARTIN, C. J.; SANDBLOM, V.; CARTER, M. J.; ALMÉN, A.; CEDERBLAD, Å.; JONASSON, P.; LUNDH, C. Derivation and application of dose reduction factors for protective eyewear worn in interventional radiology and cardiology. **Journal of Radiological Protection**, IOP Publishing, v. 34, n. 4, p. 811–823, 2014. https://doi.org/10.1088/0952-4746/34/4/811.

MARSHALL, N.; FAULKNER, K. The dependence of the scattered radiation dose to personnel on technique factors in diagnostic radiology. **The British Journal of Radiology**, The British Institute of Radiology, v. 65, n. 769, p. 44–49, 1992. https://doi.org/10.1259/0007-1285-65-769-44.

MARTIN, C. A review of radiology staff doses and dose monitoring requirements. **Radiation Protection Dosimetry**, Oxford University Press, v. 136, n. 3, p. 140–157, 2009. https://doi.org/10.1093/rpd/ncp168.

MARTIN, C. Personal dosimetry for interventional operators: when and how should monitoring be done? **The British Journal of Radiology**, The British Institute of Radiology. 36 Portland Place, London, W1B 1AT, v. 84, n. 1003, p. 639–648, 2011. https://doi.org/10.1259/bjr/24828606.

McCUNE, W. S.; SHORB, P. E.; MOSCOVITZ, H. Endoscopic cannulation of the ampulla of Vater: a preliminary report. **Annals of Surgery**, Lippincott, Williams, and Wilkins, v. 167, n. 5, p. 752–756, 1968. https://dx.doi.org/10.1097%2F00000658-196805000-00013.

MILLER, D. L. Review of air kerma-area product, effective dose and dose conversion coefficients for non-cardiac interventional fluoroscopy procedures. **Medical Physics**, Wiley, v. 47, n. 3, p. 975–982, jan. 2020. https://doi.org/10.1002/mp.13990.

MIN, P. Binvox 3D mesh voxelizer. 2005? https://www.patrickmin.com/binvox/.

MINAMI, T.; SASAKI, T.; SERIKAWA, M.; KAMIGAKI, M.; YUKUTAKE, M.; ISHIGAKI, T.; ISHII, Y.; MOURI, T.; YOSHIMI, S.; SHIMIZU, A. *et al.* Occupational radiation exposure during endoscopic retrograde cholangiopancreatography and usefulness of radiation protective curtains. **Gastroenterology Research and Practice**, Hindawi, v. 2014, p. 1–5, 2014. https://doi.org/10.1155/2014/926876.

MITCHELL, R. M.; GRIMM, I. S. ERCP radiology basics. **Techniques in Gastrointestinal Endoscopy**, Elsevier, v. 5, n. 1, p. 11–16, 2003. https://doi.org/10.1053/tgie.2003.50008.

MORISHIMA, Y.; CHIDA, K.; MEGURO, T. Effectiveness of additional lead shielding to protect staff from scattering radiation during endoscopic retrograde cholangiopancreatography procedures. **Journal of Radiation Research**, Oxford University Press, v. 59, n. 2, p. 225–232, 2018. https://doi.org/10.1093/jrr/rrx039.

MUNIRAJ, T.; ASLANIAN, H. R.; LAINE, L.; FARRELL, J.; CIARLEGLIO, M. M.; DENG, Y.; HO, H.; JAMIDAR, P. A. A double-blind, randomized, sham-controlled trial of the effect of a radiation-attenuating drape on radiation exposure to endoscopy staff during ERCP. **American Journal of Gastroenterology**, LWW, v. 110, n. 5, p. 690–696, 2015. https://doi.org/10.1038/ajg.2015.85.

NAGAOKA, T.; WATANABE, S.; SAKURAI, K.; KUNIEDA, E.; WATANABE, S.; TAKI, M.; YAMANAKA, Y. Development of realistic high-resolution whole-body voxel models of Japanese adult males and females of average height and weight, and application of models to radio-frequency electromagnetic-field dosimetry. **Physics in Medicine & Biology**, IOP Publishing, v. 49, n. 1, p. 1–15, 2003. https://doi.org/10.1088/0031-9155/49/1/001.

NEVES, L. P.; FRANCO, A. B.; FRANÇA, M.; SOARES, M. R.; BELINATO, W.; SANTOS, W. S.; CALDAS, L. V.; PERINI, A. P. Computational dosimetry in a pediatric i-CAT procedure using virtual anthropomorphic phantoms. **Radiation Physics and Chemistry**, Elsevier, p. 1–5, 2019. https://doi.org/10.1016/j.radphyschem.2019.03.040.

O'CONNOR, U.; GALLAGHER, A.; MALONE, L.; O'REILLY, G. Occupational radiation dose to eyes from endoscopic retrograde cholangiopancreatography procedures in light of the revised eye lens dose limit from the International Commission on Radiological Protection. **The British Journal of Radiology**, The British Institute of Radiology, v. 86, n. 1022, p. 20120289, 2013. https://doi.org/10.1259/bjr.20120289.

PELOWITZ, D. B. MCNPX USER'S MANUAL version 2.7. 0-la-cp-11-00438. **Los Alamos National Laboratory**, 2011.

PERCUOCO, R. Plain radiographic imaging. In: **Clinical Imaging**. 3rd. ed. Elsevier, 2014. p. 1–43. ISBN 978-0-323-08495-6. https://doi.org/10.1016/C2009-0-42800-9.

PEREIRA, M. A.; SILVEIRA, L. M.; NANNINI, F.; NEVES, L. P.; PERINI, A. P.; SANTOS, C. J.; BELINATO, W.; SANTOS, W. S. Dosimetric evaluation of individuals to ^{238}U series, ^{232}Th series and ^{40}K radionuclides present in Brazilian ornamental rocks using computational simulation. **Ecotoxicology and Environmental Safety**, Elsevier, v. 173, p. 401–410, 2019. https://doi.org/10.1016/j.ecoenv.2019.02.038.

PERINI, A. P.; SANTOS, W. S.; NEVES, L. P.; BELINATO, W.; CALDAS, L. V. Estimation of conversion coefficients for absorbed and effective doses for pediatric CT examinations in two different PET/CT scanners. **Radiation Physics and Chemistry**, Elsevier, v. 155, p. 9–16, 2019. https://doi.org/10.1016/j.radphyschem.2018.07.009.

PLANCK, M. **Original Papers in Quantum Physics**. London: Taylor & Francis Group, 1972. v. 1.

PRINCIPI, S.; FARAH, J.; FERRARI, P.; CARINOU, E.; CLAIRAND, I.; GINJAUME, M. The influence of operator position, height and body orientation on eye lens dose in interventional radiology and cardiology: Monte Carlo simulations versus realistic clinical measurements. **Physica Medica**, Elsevier BV, v. 32, n. 9, p. 1111–1117, 2016. https://doi.org/10.1016/j.ejmp.2016.08.010.

REED, A. L. Medical Physics Calculations with MCNP: a Primer. 2007. Boston, MA: Los Alamos National Laboratory, X-3 MCC, LA-UR-07-4133.

REES, C. R.; DUNCAN, B. W. Get the lead off our backs! **Techniques in Vascular and Interventional Radiology**, Elsevier, v. 21, n. 1, p. 7–15, 2018. https://doi.org/10.1053/j.tvir.2017.12.003.

RIGATELLI, G.; PANIN, S.; FIORREVANTI, R.; OLIVA, L.; DARIO, A.; TIBERIO, L.; BEDENDO, E.; PERTOLDI, D.; CHAMBERS, C. Impact of operators' height on individual radiation exposure measurements during catheter-based cardiovascular interventions. **Journal of Interventional Cardiology**, Wiley Online Library, v. 29, n. 1, p. 83–88, 2016. https://doi.org/10.1111/joic.12263.

ROOIJEN, B. D. van; HAAN, M. W. de; DAS, M.; ARNOLDUSSEN, C. W.; GRAAF, R. D.; ZWAM, W. H. van; BACKES, W. H.; JEUKENS, C. R. Efficacy of radiation safety

glasses in interventional radiology. **Cardiovascular and Interventional Radiology**, Springer, v. 37, n. 5, p. 1149–1155, 2014. https://doi.org/10.1007/s00270-013-0766-0.

SAMARA, E. T.; STRATAKIS, J.; MELONO, J. M. E.; MOUZAS, I. A.; PERISINAKIS, K.; DAMILAKIS, J. Therapeutic ERCP and pregnancy: is the radiation risk for the conceptus trivial? **Gastrointestinal Endoscopy**, Elsevier, v. 69, n. 4, p. 824–831, 2009. https://doi.org/10.1016/j.gie.2008.05.068.

SANDLER, R. S.; EVERHART, J. E.; DONOWITZ, M.; ADAMS, E.; CRONIN, K.; GOODMAN, C.; GEMMEN, E.; SHAH, S.; AVDIC, A.; RUBIN, R. The burden of selected digestive diseases in the United States. **Gastroenterology**, Elsevier, v. 122, n. 5, p. 1500–1511, 2002. https://doi.org/10.1053/gast.2002.32978.

SANTOS, W. S.; BELINATO, W.; PERINI, A. P.; CALDAS, L. V.; GALEANO, D. C.; SANTOS, C. J.; NEVES, L. P. Occupational exposures during abdominal fluoroscopically guided interventional procedures for different patient sizes—a Monte Carlo approach. **Physica Medica**, Elsevier, v. 45, p. 35–43, 2018. https://doi.org/10.1016/j.ejmp.2017.11.016.

SAUKKO, E.; GRÖNROOS, J. M.; SALMINEN, P.; HENNER, A.; NIEMINEN, M. T. Patient radiation dose and fluoroscopy time during ERCP: a single-center, retrospective study of influencing factors. **Scandinavian Journal of Gastroenterology**, Taylor & Francis, v. 53, n. 4, p. 495–504, 2018. https://doi.org/10.1080/00365521.2018.1445774.

SAUKKO, E.; HENNER, A.; AHONEN, S.-M. Radiation exposure to patients during endoscopic retrograde cholangiopancreatography: A multicentre study in Finland. **Radiography**, Elsevier, v. 21, n. 2, p. 131–135, 2015. https://doi.org/10.1016/j.radi.2014.08.001.

SCHUELER, B. A.; VRIEZE, T. J.; BJARNASON, H.; STANSON, A. W. An investigation of operator exposure in interventional radiology. **Radiographics**, Radiological Society of North America, v. 26, n. 5, p. 1533–1541, 2006. https://doi.org/10.1148/rg.265055127.

SEALS, K. F.; LEE, E. W.; CAGNON, C. H.; AL-HAKIM, R. A.; KEE, S. T. Radiation-induced cataractogenesis: a critical literature review for the interventional radiologist. **Cardiovascular and Interventional Radiology**, Springer, v. 39, n. 2, p. 151–160, 2016. https://doi.org/10.1007/s00270-015-1207-z.

SEO, D.; KIM, K. H.; KIM, J.-S.; HAN, S.; PARK, K.; KIM, J. Evaluation of radiation doses in patient and medical staff during endoscopic retrograde cholangiopancreatography procedures. **Radiation Protection Dosimetry**, Oxford University Press, v. 168, n. 4, p. 516–522, 2016. https://doi.org/10.1093/rpd/ncv373.

SHAFFER, E. A. Epidemiology of gallbladder stone disease. **Best Practice & Research Clinical Gastroenterology**, Elsevier, v. 20, n. 6, p. 981–996, 2006. https://doi.org/10.1016/j.bpg.2006.05.004.

SHIN, J. M.; LEE, T. H.; PARK, S.-H.; KANG, S. G.; LEE, Y. S.; PARK, S. J.; KU, M. G.; LEE, S.-H.; CHUNG, I.-K.; CHOI, H. J. *et al.* A survey of the radiation exposure protection of health care providers during endoscopic retrograde cholangiopancreatography in Korea. **Gut and Liver**, Editorial Office of Gut and Liver, v. 7, n. 1, p. 100–105, 2013. https://doi.org/10.5009/gnl.2013.7.1.100.

SILVA, R. M.; BELINATO, W.; SANTOS, W. S.; SOUZA, L. F.; PERINI, A. P.; NEVES, L. P.; SOUZA, D. N. Low cost electron irradiator using ^{90}Sr+ ^{90}Y sources. **Radiation Physics and Chemistry**, Elsevier, v. 167, p. 108235, 2020. https://doi.org/10.1016/j.radphyschem.2019.03.039.

SNYDER, W. S. Calculations for maximum permissible exposure to thermal neutrons. **Nucleonics (US) Ceased Publication**, v. 6, 1950.

SOARES, M. R.; SANTOS, W. S.; NEVES, L. P.; PERINI, A. P.; BATISTA, W. O.; MAIA, A. F.; BELINATO, W.; CALDAS, L. V. The use of personal protection equipment for the absorbed doses of eye lens and thyroid gland in CBCT exams using Monte Carlo. **Radiation Physics and Chemistry**, Elsevier, v. 167, p. 108347, 2020. https://doi.org/10.1016/j.radphyschem.2019.108347.

SON, B. K.; LEE, K. T.; KIM, J. S.; LEE, S. O. Lack of radiation protection for endoscopists performing endoscopic retrograde cholangiopancreatography. **The Korean Journal of Gastroenterology**, The Korean Society of Gastroenterology (KAMJE), v. 58, n. 2, p. 93–99, 2011. https://doi.org/10.4166/kjg.2011.58.2.93.

SOUZA, L. W. G.; SOUZA, S. P.; SILVA, M. F.; SILVA, A. F.; TOBIAS, I. P.; PERINI, A. P.; SANTOS, W. S.; NEVES, L. P. Levantamento do número de procedimentos de colangiopancretografia retrógrada endoscópica realizados no Brasil entre 2008 e 2018. In: . Zenodo, 2019. XII SIMPÓSIO DE ENGENHARIA BIOMÉDICA - IX SIMPÓSIO DE INSTRUMENTAÇÃO E IMAGENS MÉDICAS. https://doi.org/10.5281/zenodo.3459827.

STABIN, M.; WATSON, E.; CRISTY, M.; RYMAN, J.; ECKERMAN, K.; DAVIS, J.; MARSHALL, D.; GEHLEN, M. Mathematical models and specific absorbed fractions of photon energy in the nonpregnant adult female and at the end of each trimester of pregnancy. 5 1995. https://doi.org/10.2172/91944.

STEWART, F.; AKLEYEV, A.; HAUER-JENSEN, M.; HENDRY, J.; KLEIMAN, N.; MACVITTIE, T.; ALEMAN, B.; EDGAR, A.; MABUCHI, K.; MUIRHEAD, C. *et al.* ICRP publication 118: ICRP statement on tissue reactions and early and late effects of radiation in normal tissues and organs–threshold doses for tissue reactions in a radiation protection context. **Annals of the ICRP**, Elsevier, v. 41, n. 1-2, p. 1–322, 2012.

SULIEMAN, A.; ELZAKI, M.; ALKHORAYEF, M.; BABIKIR, E.; ABUZAID, M.; DALTON, A.; BRADLEY, D. Assessment of patient dose and radiogenic risks during endoscopic retrograde cholangiopancreatography. **Applied Radiation and Isotopes**, Elsevier, v. 117, p. 65–69, 2016. http://dx.doi.org/10.1016/j.apradiso.2016.03.010.

SULIEMAN, A.; ELZAKI, M.; KHALIL, M. Occupational exposure to staff during endoscopic retrograde cholangiopancreatography in Sudan. **Radiation Protection Dosimetry**, Oxford University Press, v. 144, n. 1-4, p. 530–533, 2010. https://doi.org/10.1093/rpd/ncq353.

SULIEMAN, A.; PAROUTOGLOU, G.; KAPSORITAKIS, A.; KAPATENAKIS, A.; POTAMIANOS, S.; VLYCHOU, M.; THEODOROU, K. Reduction of radiation doses to patients and staff during endoscopic retrograde cholangiopancreatography. **Saudi Journal of Gastroenterology**, Wolters Kluwer–Medknow Publications, v. 17, n. 1, p. 23–29, 2011. https://doi.org/10.4103/1319-3767.74456.

TAPIOVAARA, M.; SIISKONEN, T. **PCXMC, A Monte Carlo program for calculating patient doses in medical x-ray examinations**. Helsinki: Radiation and Nuclear Safety Authority (STUK), 2008. ISBN 978-952-478-397-2.

VALDIVIESO, V.; COVARRUBIAS, C.; SIEGEL, F.; CRUZ, F. Pregnancy and cholelithiasis: pathogenesis and natural course of gallstones diagnosed in early puerperium. **Hepatology**, Wiley Online Library, v. 17, n. 1, p. 1–4, 1993. https://doi.org/10.1002/hep.1840170102.

VALENTIN, J. Basic anatomical and physiological data for use in radiological protection: reference values: Icrp publication 89. **Annals of the ICRP**, Elsevier, v. 32, n. 3-4, p. 1–277, 2002.

VEIT, R.; ZANKL, M.; PETOUSSI, N.; MANNWEILER, E.; WILLIAMS, G.; DREXLER, G. Tomographic anthropomorphic models, part I: Construction technique and description of models of an 8 week old baby and a 7 year old child. **GSF-Report**, v. 3, p. 89, 1989.

XU, X. G. An exponential growth of computational phantom research in radiation protection, imaging, and radiotherapy: a review of the fifty-year history. **Physics in Medicine & Biology**, IOP Publishing, v. 59, n. 18, p. R233–302, 2014. https://doi.org/10.1088/0031-9155/59/18/R233.

XU, X. G. Innovations in computer technologies have impacted radiation dosimetry through anatomically realistic phantoms and fast Monte Carlo simulations. **Health Physics**, Ovid Technologies (Wolters Kluwer Health), v. 116, n. 2, p. 263–275, 2019. https://doi.org/10.1097/hp.0000000000001007.

YEOM, Y. S.; JEONG, J. H.; HAN, M. C.; KIM, C. H. Tetrahedral-mesh-based computational human phantom for fast Monte Carlo dose calculations. **Physics in Medicine and Biology**, v. 59, n. 12, p. 3173–3185, 2014. https://doi.org/10.1088/0031-9155/59/12/3173.

ZAGORSKA, A.; ROMANOVA, K.; HRISTOVA-POPOVA, J.; VASSILEVA, J.; KATZAROV, K. Eye lens exposure to medical staff during endoscopic retrograde cholangiopancreatography. **Physica Medica**, v. 31, n. 7, p. 781 – 784, 2015. ISSN 1120-1797. https://doi.org/10.1016/j.ejmp.2015.03.011.

ZANKL, M.; VEIT, R.; WILLIAMS, G.; SCHNEIDER, K.; FENDEL, H.; PETOUSSI, N.; DREXLER, G. The construction of computer tomographic phantoms and their application in radiology and radiation protection. **Radiation and Environmental Biophysics**, Springer, v. 27, n. 2, p. 153–164, 1988. https://doi.org/10.1007/BF01214605.

ZHANG, B.; MA, J.; LIU, L.; CHENG, J. CNMAN: a Chinese adult male voxel phantom constructed from color photographs of a visible anatomical data set. **Radiation Protection Dosimetry**, Oxford University Press, v. 124, n. 2, p. 130–136, 2007. https://doi.org/10.1093/rpd/ncm184.

Appendix

APPENDIX A

CC[E] and CC[H_T] estimates for patient.

Table 12 – Tube voltage effect on CC[H_T] and CC[E] (mSv/Gy.cm^2) for the FASH3 (patient) for FOV of 15 × 15 cm^2. The Type A uncertainties are presented in parentheses (*in* %).

Organ/Tissue	70 kV	80 kV	90 kV	100 kV	110 kV
Bone marrow	1.2E-01 (0.0)	1.4E-01 (0.0)	1.6E-01 (0.0)	1.7E-01 (0.0)	1.9E-01 (0.0)
Colon	1.0E-01 (0.0)	1.3E-01 (0.0)	1.6E-01 (0.0)	1.8E-01 (0.0)	2.0E-01 (0.0)
Lung	1.8E-01 (0.0)	2.2E-01 (0.0)	2.5E-01 (0.0)	2.7E-01 (0.0)	3.0E-01 (0.0)
Stomach	3.2E-01 (0.0)	4.1E-01 (0.0)	4.9E-01 (0.0)	5.7E-01 (0.0)	6.4E-01 (0.0)
Breast	5.7E-02 (0.0)	7.6E-02 (0.0)	9.5E-02 (0.0)	1.1E-01 (0.0)	1.3E-01 (0.0)
Remainder tissues*	8.4E-03 (0.0)	9.5E-03 (0.0)	1.1E-02 (0.0)	1.1E-02 (0.0)	1.2E-02 (0.0)
Gonads	5.5E-03 (0.6)	8.7E-03 (0.5)	1.2E-02 (0.4)	1.5E-02 (0.4)	1.8E-02 (0.4)
Bladder	2.7E-03 (0.5)	4.5E-03 (0.4)	6.4E-03 (0.4)	8.4E-03 (0.3)	1.0E-02 (0.3)
Oesophagus	8.3E-02 (0.1)	1.1E-01 (0.1)	1.4E-01 (0.1)	1.7E-01 (0.1)	2.0E-01 (0.1)
Liver	5.7E-01 (0.0)	6.9E-01 (0.0)	8.1E-01 (0.0)	9.2E-01 (0.0)	1.0E+00 (0.0)
Thyroid	6.6E-03 (0.5)	9.5E-03 (0.4)	1.2E-02 (0.4)	1.5E-02 (0.4)	1.8E-02 (0.3)
Bone surface	6.1E-02 (0.0)	7.1E-02 (0.0)	8.0E-02 (0.0)	8.8E-02 (0.0)	9.4E-02 (0.0)
Brain	1.6E-04 (0.8)	2.5E-04 (0.6)	3.7E-04 (0.5)	4.9E-04 (0.5)	6.1E-04 (0.4)
Salivary glands	6.2E-04 (0.5)	9.2E-04 (0.4)	1.2E-03 (0.3)	1.5E-03 (0.3)	1.8E-03 (0.3)
Skin	8.5E-02 (0.0)	9.1E-02 (0.0)	9.6E-02 (0.0)	1.0E-01 (0.0)	1.0E-01 (0.0)
Eyes	8.1E-06 (6.9)	1.3E-05 (5.4)	2.2E-05 (4.4)	2.6E-05 (3.9)	3.2E-05 (3.6)
CC[E] (mSv/Gy.cm^2)	1.2E-01 (0.1)	1.5E-01 (0.1)	1.8E-01 (0.1)	2.1E-01 (0.1)	2.3E-01 (0.1)

*Adrenals, extratoracic region, gall bladder, kidneys, lymphatic nodes, muscle, oral mucosa, pancreas,prostate, small intestine, spleen, thymus and heart..

Table 13 – Tube voltage effect on CC[H_T] and CC[E] (mSv/Gy.cm^2) for the FASH3 (patient) for FOV of 17 × 17 cm^2. The Type A uncertainties are presented in parentheses (*in* %).

Organ/Tissue	**70 kV**	**80 kV**	**90 kV**	**100 kV**	**110 kV**
Bone marrow	1.1E-01 (0.0)	1.3E-01 (0.0)	1.5E-01 (0.0)	1.7E-01 (0.0)	1.8E-01 (0.0)
Colon	1.1E-01 (0.0)	1.4E-01 (0.0)	1.7E-01 (0.0)	1.9E-01 (0.0)	2.2E-01 (0.0)
Lung	2.2E-01 (0.0)	2.6E-01 (0.0)	2.9E-01 (0.0)	3.2E-01 (0.0)	3.5E-01 (0.0)
Stomach	3.1E-01 (0.0)	3.9E-01 (0.0)	4.7E-01 (0.0)	5.5E-01 (0.0)	6.1E-01 (0.0)
Breast	6.5E-02 (0.0)	8.6E-02 (0.0)	1.1E-01 (0.0)	1.3E-01 (0.0)	1.4E-01 (0.0)
Remainder tissues*	8.5E-03 (0.0)	9.7E-03 (0.0)	1.1E-02 (0.0)	1.2E-02 (0.0)	1.2E-02 (0.0)
Gonads	6.5E-03 (0.6)	1.0E-02 (0.5)	1.4E-02 (0.4)	1.8E-02 (0.4)	2.1E-02 (0.3)
Bladder	3.2E-03 (0.5)	5.2E-03 (0.4)	7.4E-03 (0.3)	9.5E-03 (0.3)	1.2E-02 (0.3)
Oesophagus	8.4E-02 (0.1)	1.1E-01 (0.1)	1.4E-01 (0.1)	1.7E-01 (0.1)	2.0E-01 (0.1)
Liver	4.7E-01 (0.0)	5.8E-01 (0.0)	6.8E-01 (0.0)	7.7E-01 (0.0)	8.5E-01 (0.0)
Thyroid	7.3E-03 (0.5)	1.0E-02 (0.4)	1.4E-02 (0.4)	1.7E-02 (0.3)	1.9E-02 (0.3)
Bone surface	5.8E-02 (0.0)	6.8E-02 (0.0)	7.6E-02 (0.0)	8.3E-02 (0.0)	8.9E-02 (0.0)
Brain	1.7E-04 (0.7)	2.7E-04 (0.6)	3.9E-04 (0.5)	5.2E-04 (0.5)	6.4E-04 (0.4)
Salivary glands	6.8E-04 (0.4)	1.0E-03 (0.4)	1.3E-03 (0.3)	1.7E-03 (0.3)	2.0E-03 (0.3)
Skin	8.7E-02 (0.0)	9.3E-02 (0.0)	9.8E-02 (0.0)	1.0E-01 (0.0)	1.1E-01 (0.0)
Eyes	1.2E-05 (6.2)	1.5E-05 (5.0)	2.3E-05 (4.2)	3.0E-05 (3.7)	3.5E-05 (3.4)
CC[E] (mSv/Gy.cm^2)	1.2E-01 (0.1)	1.8E-01 (0.1)	1.8E-01 (0.0)	2.1E-01 (0.1)	2.3E-01 (0.1)

*Adrenals, extratoracic region, gall bladder, kidneys, lymphatic nodes, muscle, oral mucosa, pancreas,prostate, small intestine, spleen, thymus and heart..

Table 14 – Tube voltage effect on CC[H_T] and CC[E] (mSv/Gy.cm^2) for the FASH3 (patient) for FOV of 22 × 22 cm^2. The Type A uncertainties are presented in parentheses (*in* %).

Organ/Tissue	**70 kV**	**80 kV**	**90 kV**	**100 kV**	**110 kV**
Bone marrow	1.0E-01 (0.0)	1.2E-01 (0.0)	1.4E-01 (0.0)	1.5E-01 (0.0)	1.7E-01 (0.0)
Colon	1.3E-01 (0.0)	1.6E-01 (0.0)	1.9E-01 (0.0)	2.2E-01 (0.0)	2.4E-01 (0.0)
Lung	2.6E-01 (0.0)	3.0E-01 (0.0)	3.4E-01 (0.0)	3.7E-01 (0.0)	4.0E-01 (0.0)
Stomach	2.2E-01 (0.0)	2.8E-01 (0.0)	3.4E-01 (0.0)	3.9E-01 (0.0)	4.4E-01 (0.0)
Breast	7.3E-02 (0.0)	9.4E-02 (0.0)	1.2E-01 (0.0)	1.3E-01 (0.0)	1.5E-01 (0.0)
Remainder tissues*	7.8E-03 (0.0)	8.9E-03 (0.0)	9.9E-03 (0.0)	1.1E-02 (0.0)	1.1E-02 (0.0)
Gonads	9.8E-03 (0.5)	1.5E-02 (0.4)	2.0E-02 (0.3)	2.5E-02 (0.3)	3.0E-02 (0.3)
Bladder	4.6E-03 (0.4)	7.4E-03 (0.3)	1.0E-02 (0.3)	1.3E-02 (0.3)	1.6E-02 (0.2)
Oesophagus	8.0E-02 (0.1)	1.1E-01 (0.1)	1.3E-01 (0.1)	1.6E-01 (0.1)	1.8E-01 (0.1)
Liver	2.8E-01 (0.0)	3.5E-01 (0.0)	4.1E-01 (0.0)	4.7E-01 (0.0)	5.2E-01 (0.0)
Thyroid	9.5E-03 (0.4)	1.3E-02 (0.4)	1.7E-02 (0.3)	2.0E-02 (0.3)	2.3E-02 (0.3)
Bone surface	5.0E-02 (0.0)	5.9E-02 (0.0)	6.7E-02 (0.0)	7.3E-02 (0.0)	7.8E-02 (0.0)
Brain	2.0E-04 (0.7)	3.2E-04 (0.6)	4.6E-04 (0.5)	6.1E-04 (0.4)	7.5E-04 (0.4)
Salivary glands	8.5E-04 (0.4)	1.2E-03 (0.3)	1.6E-03 (0.3)	2.0E-03 (0.3)	2.3E-03 (0.2)
Skin	9.2E-02 (0.0)	9.8E-02 (0.0)	1.0E-01 (0.0)	1.1E-01 (0.0)	1.1E-01 (0.0)
Eyes	1.3E-05 (5.6)	2.0E-05 (4.4)	2.7E-05 (3.7)	3.5E-05 (3.4)	4.4E-05 (3.0)
CC[E] (mSv/Gy.cm^2)	1.1E-01 (0.1)	1.4E-01 (0.1)	1.6E-01 (0.1)	1.8E-01 (0.1)	2.0E-01 (0.1)

*Adrenals, extratoracic region, gall bladder, kidneys, lymphatic nodes, muscle, oral mucosa, pancreas,prostate, small intestine, spleen, thymus and heart..

Table 15 – Tube voltage effect on CC[H_T] and CC[E] (mSv/Gy.cm^2) for the FASH3 (patient) for FOV of 25 × 25 cm^2. The Type A uncertainties are presented in parentheses (*in* %).

Organ/Tissue	**70 kV**	**80 kV**	**90 kV**	**100 kV**	**110 kV**
Bone marrow	1.0E-01 (0.0)	1.2E-01 (0.0)	1.4E-01 (0.0)	1.6E-01 (0.0)	1.7E-01 (0.0)
Colon	1.2E-01 (0.0)	1.5E-01 (0.0)	1.8E-01 (0.0)	2.1E-01 (0.0)	2.3E-01 (0.0)
Lung	2.5E-01 (0.0)	2.9E-01 (0.0)	3.3E-01 (0.0)	3.6E-01 (0.0)	3.9E-01 (0.0)
Stomach	1.9E-01 (0.0)	2.5E-01 (0.0)	3.0E-01 (0.0)	3.4E-01 (0.0)	3.8E-01 (0.0)
Breast	6.6E-02 (0.0)	8.5E-02 (0.0)	1.0E-01 (0.0)	1.2E-01 (0.0)	1.4E-01 (0.0)
Remainder tissues*	7.6E-03 (0.0)	8.7E-03 (0.0)	9.6E-03 (0.0)	1.0E-02 (0.0)	1.1E-02 (0.0)
Gonads	1.1E-02 (0.4)	1.6E-02 (0.4)	2.2E-02 (0.3)	2.7E-02 (0.3)	3.3E-02 (0.3)
Bladder	5.2E-03 (0.4)	8.2E-03 (0.3)	1.1E-02 (0.3)	1.5E-02 (0.2)	1.8E-02 (0.2)
Oesophagus	7.7E-02 (0.1)	1.0E-01 (0.1)	1.3E-01 (0.1)	1.5E-01 (0.1)	1.8E-01 (0.1)
Liver	2.4E-01 (0.0)	3.0E-01 (0.0)	3.6E-01 (0.0)	4.0E-01 (0.0)	4.5E-01 (0.0)
Thyroid	1.0E-02 (0.4)	1.4E-02 (0.4)	1.8E-02 (0.3)	2.2E-02 (0.3)	2.5E-02 (0.3)
Bone surface	5.0E-02 (0.0)	5.9E-02 (0.0)	6.6E-02 (0.0)	7.2E-02 (0.0)	7.7E-02 (0.0)
Brain	2.1E-04 (0.7)	3.4E-04 (0.5)	4.9E-04 (0.5)	6.3E-04 (0.4)	7.9E-04 (0.4)
Salivary glands	8.9E-04 (0.4)	1.3E-03 (0.3)	1.7E-03 (0.3)	2.0E-03 (0.3)	2.4E-03 (0.2)
Skin	9.2E-02 (0.0)	9.8E-02 (0.0)	1.0E-01 (0.0)	1.1E-01 (0.0)	1.1E-01 (0.0)
Eyes	1.3E-05 (5.2)	2.1E-05 (4.3)	2.7E-05 (3.8)	3.6E-05 (3.3)	4.6E-05 (3.0)
CC[E] (mSv/Gy.cm^2)	1.1E-01 (0.1)	1.3E-01 (0.1)	1.5E-01 (0.1)	1.7E-01 (0.1)	1.9E-01 (0.1)

*Adrenals, extratoracic region, gall bladder, kidneys, lymphatic nodes, muscle, oral mucosa, pancreas,prostate, small intestine, spleen, thymus and heart..

Table 16 – Tube voltage effect on CC[H_T] and CC[E] (mSv/Gy.cm^2) for the FASH3 (patient) for FOV of 31 × 31 cm^2. The Type A uncertainties are presented in parentheses (*in* %).

Organ/Tissue	**70 kV**	**80 kV**	**90 kV**	**100 kV**	**110 kV**
Bone marrow	1.0E-01 (0.0)	1.2E-01 (0.0)	1.4E-01 (0.0)	1.6E-01 (0.0)	1.7E-01 (0.0)
Colon	9.6E-02 (0.0)	1.2E-01 (0.0)	1.4E-01 (0.0)	1.7E-01 (0.0)	1.9E-01 (0.0)
Lung	2.2E-01 (0.0)	2.5E-01 (0.0)	2.9E-01 (0.0)	3.2E-01 (0.0)	3.4E-01 (0.0)
Stomach	1.3E-01 (0.0)	1.7E-01 (0.0)	2.1E-01 (0.0)	2.4E-01 (0.0)	2.7E-01 (0.0)
Breast	4.8E-02 (0.0)	6.2E-02 (0.0)	7.6E-02 (0.0)	8.9E-02 (0.0)	1.0E-01 (0.0)
Remainder tissues*	7.0E-03 (0.0)	8.0E-03 (0.0)	8.9E-03 (0.0)	9.7E-03 (0.0)	1.0E-02 (0.0)
Gonads	1.6E-02 (0.4)	2.3E-02 (0.3)	3.1E-02 (0.3)	3.9E-02 (0.2)	4.5E-02 (0.2)
Bladder	7.5E-03 (0.3)	1.2E-02 (0.3)	1.6E-02 (0.2)	2.0E-02 (0.2)	2.4E-02 (0.2)
Oesophagus	7.0E-02 (0.1)	9.4E-02 (0.1)	1.2E-01 (0.1)	1.4E-01 (0.1)	1.6E-01 (0.1)
Liver	1.7E-01 (0.0)	2.0E-01 (0.0)	2.4E-01 (0.0)	2.8E-01 (0.0)	3.1E-01 (0.0)
Thyroid	1.2E-02 (0.4)	1.7E-02 (0.3)	2.1E-02 (0.3)	2.5E-02 (0.3)	2.9E-02 (0.3)
Bone surface	4.9E-02 (0.0)	5.8E-02 (0.0)	6.5E-02 (0.0)	7.1E-02 (0.0)	7.5E-02 (0.0)
Brain	2.4E-04 (0.6)	3.9E-04 (0.5)	5.6E-04 (0.4)	7.3E-04 (0.4)	9.0E-04 (0.4)
Salivary glands	9.8E-04 (0.4)	1.4E-03 (0.3)	1.8E-03 (0.3)	2.2E-03 (0.2)	2.6E-03 (0.2)
Skin	9.4E-02 (0.0)	1.0E-01 (0.0)	1.1E-01 (0.0)	1.1E-01 (0.0)	1.1E-01 (0.0)
Eyes	1.4E-05 (5.3)	2.4E-05 (4.0)	3.0E-05 (3.6)	3.8E-05 (3.6)	4.6E-05 (2.9)
CC[E] (mSv/Gy.cm^2)	8.6E-02 (0.1)	1.1E-01 (0.1)	1.2E-01 (0.1)	1.4E-01 (0.1)	1.6E-01 (0.1)

*Adrenals, extratoracic region, gall bladder, kidneys, lymphatic nodes, muscle, oral mucosa, pancreas,prostate, small intestine, spleen, thymus and heart..

Table 17 – Tube voltage effect on CC[H_T] and CC[E] (mSv/Gy.cm^2) for the FASH3 (patient) for FOV of 38 × 38 cm^2. The Type A uncertainties are presented in parentheses (*in* %).

Organ/Tissue	**70 kV**	**80 kV**	**90 kV**	**100 kV**	**110 kV**
Bone marrow	1.0E-01 (0.0)	1.2E-01 (0.0)	1.4E-01 (0.0)	1.5E-01 (0.0)	1.6E-01 (0.0)
Colon	8.0E-02 (0.0)	1.0E-01 (0.0)	1.2E-01 (0.0)	1.4E-01 (0.0)	1.6E-01 (0.0)
Lung	1.7E-01 (0.0)	2.0E-01 (0.0)	2.3E-01 (0.0)	2.6E-01 (0.0)	2.8E-01 (0.0)
Stomach	9.1E-02 (0.1)	1.2E-01 (0.0)	1.4E-01 (0.0)	1.6E-01 (0.0)	1.8E-01 (0.0)
Breast	3.4E-02 (0.1)	4.5E-02 (0.0)	5.5E-02 (0.0)	6.5E-02 (0.0)	7.3E-02 (0.0)
Remainder tissues*	6.5E-03 (0.0)	7.4E-03 (0.0)	8.3E-03 (0.0)	9.0E-03 (0.0)	9.6E-03 (0.0)
Gonads	4.7E-02 (0.2)	6.2E-02 (0.2)	7.7E-02 (0.2)	9.1E-02 (0.1)	1.0E-01 (0.1)
Bladder	1.6E-02 (0.2)	2.3E-02 (0.2)	3.0E-02 (0.2)	3.6E-02 (0.2)	4.2E-02 (0.1)
Oesophagus	6.2E-02 (0.1)	8.3E-02 (0.1)	1.0E-01 (0.1)	1.2E-01 (0.1)	1.4E-01 (0.1)
Liver	1.1E-01 (0.0)	1.4E-01 (0.0)	1.7E-01 (0.0)	1.9E-01 (0.0)	2.1E-01 (0.0)
Thyroid	1.5E-02 (0.3)	2.0E-02 (0.3)	2.5E-02 (0.3)	3.0E-02 (0.2)	3.4E-02 (0.2)
Bone surface	4.7E-02 (0.0)	5.5E-02 (0.0)	6.2E-02 (0.0)	6.7E-02 (0.0)	7.1E-02 (0.0)
Brain	3.4E-04 (0.5)	5.3E-04 (0.4)	7.5E-04 (0.4)	9.7E-04 (0.3)	1.2E-03 (0.3)
Salivary glands	1.1E-03 (0.3)	1.6E-03 (0.3)	2.1E-03 (0.3)	2.5E-03 (0.2)	2.9E-03 (0.2)
Skin	9.2E-02 (0.0)	9.7E-02 (0.0)	1.0E-01 (0.0)	1.1E-01 (0.0)	1.1E-01 (0.0)
Eyes	1.7E-05 (4.7)	2.5E-05 (3.9)	3.4E-05 (3.3)	4.5E-05 (2.9)	5.1E-05 (2.7)
CC[E] (mSv/Gy.cm^2)	7.2E-02 (0.1)	8.9E-02 (0.1)	1.0E-01 (0.1)	1.2E-01 (0.1)	1.3E-01 (0.1)

*Adrenals, extratoracic region, gall bladder, kidneys, lymphatic nodes, muscle, oral mucosa, pancreas,prostate, small intestine, spleen, thymus and heart..

Table 18 – Tube voltage effect on CC[H_T] and CC[E] (mSv/Gy.cm^2) for the MASH3 (patient) for FOV of 15 × 15 cm^2. The Type A uncertainties are presented in parentheses (*in* %).

Organ/Tissue	**70 kV**	**80 kV**	**90 kV**	**100 kV**	**110 kV**
Bone marrow	7.1E-02 (0.0)	8.8E-02 (0.0)	1.0E-01 (0.0)	1.2E-01 (0.0)	1.3E-01 (0.0)
Colon	9.0E-02 (0.0)	1.2E-01 (0.0)	1.5E-01 (0.0)	1.8E-01 (0.0)	2.0E-01 (0.0)
Lung	1.4E-02 (0.1)	2.0E-02 (0.1)	2.6E-02 (0.0)	3.2E-02 (0.0)	3.7E-02 (0.0)
Stomach	1.4E-01 (0.0)	1.9E-01 (0.0)	2.4E-01 (0.0)	2.8E-01 (0.0)	3.3E-01 (0.0)
Breast	3.2E-03 (0.5)	5.2E-03 (0.4)	7.4E-03 (0.3)	9.7E-03 (0.3)	1.2E-02 (0.3)
Remainder tissues*	7.9E-03 (0.0)	9.1E-03 (0.0)	1.0E-02 (0.0)	1.1E-02 (0.0)	1.2E-02 (0.0)
Gonads	5.8E-04 (1.3)	1.0E-03 (1.0)	1.5E-03 (0.9)	2.0E-03 (0.8)	2.6E-03 (0.7)
Bladder	7.9E-03 (0.3)	1.3E-02 (0.2)	1.8E-02 (0.2)	2.3E-02 (0.2)	2.8E-02 (0.1)
Oesophagus	1.4E-02 (0.2)	2.1E-02 (0.2)	2.8E-02 (0.2)	3.5E-02 (0.1)	4.2E-02 (0.1)
Liver	1.3E-01 (0.0)	1.8E-01 (0.0)	2.2E-01 (0.0)	2.6E-01 (0.0)	3.0E-01 (0.0)
Thyroid	1.4E-03 (1.1)	2.3E-03 (0.8)	3.2E-03 (0.7)	4.1E-03 (0.7)	5.0E-03 (0.6)
Bone surface	3.9E-02 (0.0)	4.7E-02 (0.0)	5.5E-02 (0.0)	6.2E-02 (0.0)	6.7E-02 (0.0)
Brain	5.0E-05 (1.3)	7.6E-05 (1.1)	1.1E-04 (1.0)	1.4E-04 (0.9)	1.7E-04 (0.8)
Salivary glands	1.0E-04 (1.1)	1.6E-04 (0.8)	2.3E-04 (0.7)	3.1E-04 (0.6)	3.8E-04 (0.6)
Skin	1.0E-01 (0.0)	1.1E-01 (0.0)	1.1E-01 (0.0)	1.2E-01 (0.0)	1.2E-01 (0.0)
Eyes	2.5E-06 (14.2)	4.0E-06 (10.8)	7.2E-06 (8.4)	1.0E-05 (7.7)	1.1E-05 (7.0)
CC[E] (mSv/Gy.cm^2)	4.7E-02 (0.1)	6.2E-02 (0.1)	7.7E-02 (0.1)	9.1E-02 (0.1)	1.0E-01 (0.1)

*Adrenals, extratoracic region, gall bladder, kidneys, lymphatic nodes, muscle, oral mucosa, pancreas,prostate, small intestine, spleen, thymus and heart..

Table 19 – Tube voltage effect on CC[H_T] and CC[E] (mSv/Gy.cm^2) for the MASH3 (patient) for FOV of 17 × 17 cm^2. The Type A uncertainties are presented in parentheses (*in* %).

Organ/Tissue	70 kV	80 kV	90 kV	100 kV	110 kV
Bone marrow	7.4E-02 (0.0)	9.2E-02 (0.0)	1.1E-01 (0.0)	1.2E-01 (0.0)	1.3E-01 (0.0)
Colon	1.0E-01 (0.0)	1.3E-01 (0.0)	1.6E-01 (0.0)	1.9E-01 (0.0)	2.2E-01 (0.0)
Lung	1.7E-02 (0.1)	2.4E-02 (0.0)	3.0E-02 (0.0)	3.7E-02 (0.0)	4.3E-02 (0.0)
Stomach	1.3E-01 (0.0)	1.8E-01 (0.0)	2.3E-01 (0.0)	2.7E-01 (0.0)	3.1E-01 (0.0)
Breast	3.7E-03 (0.5)	5.9E-03 (0.4)	8.3E-03 (0.3)	1.1E-02 (0.3)	1.3E-02 (0.3)
Remainder tissues*	7.9E-03 (0.0)	9.1E-03 (0.0)	1.0E-02 (0.0)	1.1E-02 (0.0)	1.2E-02 (0.0)
Gonads	6.3E-04 (1.3)	1.1E-03 (1.0)	1.6E-03 (0.8)	2.2E-03 (0.7)	2.7E-03 (0.7)
Bladder	8.9E-03 (0.2)	1.4E-02 (0.2)	2.0E-02 (0.2)	2.5E-02 (0.2)	3.1E-02 (0.1)
Oesophagus	1.6E-02 (0.2)	2.4E-02 (0.2)	3.2E-02 (0.1)	4.0E-02 (0.1)	4.7E-02 (0.1)
Liver	1.4E-01 (0.0)	1.8E-01 (0.0)	2.2E-01 (0.0)	2.6E-01 (0.0)	3.0E-01 (0.0)
Thyroid	1.7E-03 (0.9)	2.7E-03 (0.8)	3.8E-03 (0.7)	4.9E-03 (0.6)	5.8E-03 (0.6)
Bone surface	3.9E-02 (0.0)	4.7E-02 (0.0)	5.5E-02 (0.0)	6.1E-02 (0.0)	6.7E-02 (0.0)
Brain	5.4E-05 (1.3)	8.1E-05 (1.1)	1.2E-04 (0.9)	1.5E-04 (0.8)	1.9E-04 (0.8)
Salivary glands	1.1E-04 (1.0)	1.9E-04 (0.8)	2.7E-04 (0.7)	3.5E-04 (0.6)	4.3E-04 (0.5)
Skin	1.0E-01 (0.0)	1.1E-01 (0.0)	1.1E-01 (0.0)	1.2E-01 (0.0)	1.2E-01 (0.0)
Eyes	3.2E-06 (12.8)	5.6E-06 (9.9)	8.8E-06 (7.6)	1.1E-05 (7.0)	1.4E-05 (6.2)
CC[E] (mSv/Gy.cm^2)	4.9E-02 (0.1)	6.4E-02 (0.1)	9.3E-02 (0.1)	9.7E-02 (0.1)	1.1E-01 (0.1)

*Adrenals, extratoracic region, gall bladder, kidneys, lymphatic nodes, muscle, oral mucosa, pancreas,prostate, small intestine, spleen, thymus and heart..

Table 20 – Tube voltage effect on CC[H_T] and CC[E] (mSv/Gy.cm^2) for the MASH3 (patient) for FOV of 22 × 22 cm^2. The Type A uncertainties are presented in parentheses (*in* %).

Organ/Tissue	70 kV	80 kV	90 kV	100 kV	110 kV
Bone marrow	7.9E-02 (0.0)	9.7E-02 (0.0)	1.1E-01 (0.0)	1.3E-01 (0.0)	1.4E-01 (0.0)
Colon	9.5E-02 (0.0)	1.3E-01 (0.0)	1.6E-01 (0.0)	1.8E-01 (0.0)	2.1E-01 (0.0)
Lung	3.7E-02 (0.0)	4.8E-02 (0.0)	5.8E-02 (0.0)	6.8E-02 (0.0)	7.7E-02 (0.0)
Stomach	9.7E-02 (0.1)	1.3E-01 (0.0)	1.7E-01 (0.0)	2.0E-01 (0.0)	2.3E-01 (0.0)
Breast	1.0E-02 (0.3)	1.5E-02 (0.2)	2.0E-02 (0.2)	2.4E-02 (0.2)	2.9E-02 (0.2)
Remainder tissues*	7.7E-03 (0.0)	8.8E-03 (0.0)	9.9E-03 (0.0)	1.1E-02 (0.0)	1.2E-02 (0.0)
Gonads	8.5E-04 (1.1)	1.5E-03 (0.9)	2.1E-03 (0.7)	2.9E-03 (0.6)	3.6E-03 (0.6)
Bladder	1.3E-02 (0.2)	2.0E-02 (0.2)	2.8E-02 (0.1)	3.5E-02 (0.1)	4.2E-02 (0.1)
Oesophagus	2.6E-02 (0.1)	3.7E-02 (0.1)	4.8E-02 (0.1)	5.8E-02 (0.1)	6.8E-02 (0.1)
Liver	1.1E-01 (0.0)	1.5E-01 (0.0)	1.8E-01 (0.0)	2.2E-01 (0.0)	2.5E-01 (0.0)
Thyroid	2.9E-03 (0.7)	4.3E-03 (0.6)	5.9E-03 (0.5)	7.3E-03 (0.5)	8.7E-03 (0.5)
Bone surface	4.0E-02 (0.0)	4.8E-02 (0.0)	5.5E-02 (0.0)	6.2E-02 (0.0)	6.7E-02 (0.0)
Brain	6.2E-05 (1.2)	9.9E-05 (1.0)	1.4E-04 (0.8)	1.8E-04 (0.7)	2.3E-04 (0.7)
Salivary glands	1.7E-04 (0.8)	2.7E-04 (0.6)	3.8E-04 (0.5)	4.9E-04 (0.5)	5.9E-04 (0.5)
Skin	1.0E-01 (0.0)	1.1E-01 (0.0)	1.1E-01 (0.0)	1.2E-01 (0.0)	1.2E-01 (0.0)
Eyes	3.9E-06 (11.2)	7.7E-06 (7.6)	1.2E-05 (6.7)	1.5E-05 (5.9)	1.9E-05 (5.2)
CC[E] (mSv/Gy.cm^2)	4.7E-02 (0.1)	6.1E-02 (0.1)	7.6E-02 (0.1)	8.9E-02 (0.1)	1.0E-01 (0.1)

*Adrenals, extratoracic region, gall bladder, kidneys, lymphatic nodes, muscle, oral mucosa, pancreas,prostate, small intestine, spleen, thymus and heart..

Table 21 – Tube voltage effect on CC[H_T] and CC[E] (mSv/Gy.cm^2) for the MASH3 (patient) for FOV of 25 × 25 cm^2. The Type A uncertainties are presented in parentheses (*in* %).

Organ/Tissue	70 kV	80 kV	90 kV	100 kV	110 kV
Bone marrow	7.8E-02 (0.0)	9.5E-02 (0.0)	1.1E-01 (0.0)	1.3E-01 (0.0)	1.4E-01 (0.0)
Colon	9.0E-02 (0.0)	1.2E-01 (0.0)	1.5E-01 (0.0)	1.8E-01 (0.0)	2.0E-01 (0.0)
Lung	4.6E-02 (0.0)	5.9E-02 (0.0)	7.1E-02 (0.0)	8.3E-02 (0.0)	9.3E-02 (0.0)
Stomach	8.7E-02 (0.1)	1.2E-01 (0.0)	1.5E-01 (0.0)	1.8E-01 (0.0)	2.0E-01 (0.0)
Breast	1.7E-02 (0.2)	2.3E-02 (0.2)	3.0E-02 (0.2)	3.6E-02 (0.1)	4.2E-02 (0.1)
Remainder tissues*	7.4E-03 (0.0)	8.6E-03 (0.0)	9.6E-03 (0.0)	1.1E-02 (0.0)	1.1E-02 (0.0)
Gonads	9.7E-04 (1.0)	1.6E-03 (0.8)	2.4E-03 (0.7)	3.2E-03 (0.6)	3.9E-03 (0.5)
Bladder	1.5E-02 (0.2)	2.3E-02 (0.2)	3.2E-02 (0.1)	4.0E-02 (0.1)	4.7E-02 (0.1)
Oesophagus	2.8E-02 (0.1)	4.0E-02 (0.1)	5.1E-02 (0.1)	6.2E-02 (0.1)	7.2E-02 (0.1)
Liver	1.0E-01 (0.0)	1.3E-01 (0.0)	1.7E-01 (0.0)	1.9E-01 (0.0)	2.2E-01 (0.0)
Thyroid	3.2E-03 (0.7)	4.8E-03 (0.6)	6.4E-03 (0.5)	8.1E-03 (0.5)	9.5E-03 (0.4)
Bone surface	3.9E-02 (0.0)	4.7E-02 (0.0)	5.4E-02 (0.0)	6.0E-02 (0.0)	6.5E-02 (0.0)
Brain	6.7E-05 (1.1)	1.0E-04 (0.9)	1.5E-04 (0.8)	2.0E-04 (0.7)	2.5E-04 (0.7)
Salivary glands	1.9E-04 (0.7)	3.0E-04 (0.6)	4.1E-04 (0.5)	5.3E-04 (0.5)	6.5E-04 (0.4)
Skin	1.0E-01 (0.0)	1.1E-01 (0.0)	1.1E-01 (0.0)	1.2E-01 (0.0)	1.2E-01 (0.0)
Eyes	5.3E-06 (10.)	8.6E-06 (7.5)	1.4E-05 (6.8)	1.8E-05 (5.4)	2.4E-05 (4.9)
CC[E] (mSv/Gy.cm^2)	4.6E-02 (0.1)	6.1E-02 (0.1)	7.5E-02 (0.1)	8.7E-02 (0.1)	9.9E-02 (0.1)

*Adrenals, extratoracic region, gall bladder, kidneys, lymphatic nodes, muscle, oral mucosa, pancreas,prostate, small intestine, spleen, thymus and heart..

Table 22 – Tube voltage effect on CC[H_T] and CC[E] (mSv/Gy.cm^2) for the MASH3 (patient) for FOV of 31 × 31 cm^2. The Type A uncertainties are presented in parentheses (*in* %).

Organ/Tissue	70 kV	80 kV	90 kV	100 kV	110 kV
Bone marrow	6.9E-02 (0.0)	8.5E-02 (0.0)	9.9E-02 (0.0)	1.1E-01 (0.0)	1.2E-01 (0.0)
Colon	7.8E-02 (0.0)	1.0E-01 (0.0)	1.3E-01 (0.0)	1.5E-01 (0.0)	1.7E-01 (0.0)
Lung	6.2E-02 (0.0)	7.8E-02 (0.0)	9.3E-02 (0.0)	1.1E-01 (0.0)	1.2E-01 (0.0)
Stomach	6.2E-02 (0.1)	8.4E-02 (0.1)	1.1E-01 (0.1)	1.3E-01 (0.0)	1.5E-01 (0.0)
Breast	2.0E-02 (0.2)	2.7E-02 (0.2)	3.4E-02 (0.1)	4.1E-02 (0.1)	4.8E-02 (0.1)
Remainder tissues*	6.6E-03 (0.0)	7.6E-03 (0.0)	8.5E-03 (0.0)	9.3E-03 (0.0)	1.0E-02 (0.0)
Gonads	1.6E-03 (0.8)	2.6E-03 (0.6)	3.6E-03 (0.6)	4.7E-03 (0.5)	5.7E-03 (0.5)
Bladder	3.1E-02 (0.1)	4.4E-02 (0.1)	5.7E-02 (0.1)	6.9E-02 (0.1)	8.0E-02 (0.1)
Oesophagus	3.3E-02 (0.1)	4.5E-02 (0.1)	5.8E-02 (0.1)	6.9E-02 (0.1)	8.0E-02 (0.1)
Liver	7.1E-02 (0.0)	9.5E-02 (0.0)	1.2E-01 (0.0)	1.4E-01 (0.0)	1.6E-01 (0.0)
Thyroid	4.1E-03 (0.6)	5.9E-03 (0.5)	7.9E-03 (0.5)	9.7E-03 (0.4)	1.1E-02 (0.4)
Bone surface	3.4E-02 (0.0)	4.1E-02 (0.0)	4.7E-02 (0.0)	5.3E-02 (0.0)	5.7E-02 (0.0)
Brain	7.7E-05 (1.0)	1.2E-04 (0.9)	1.8E-04 (0.7)	2.3E-04 (0.7)	2.9E-04 (0.6)
Salivary glands	2.5E-04 (0.6)	3.7E-04 (0.5)	5.1E-04 (0.5)	6.4E-04 (0.4)	7.7E-04 (0.4)
Skin	1.1E-01 (0.0)	1.1E-01 (0.0)	1.2E-01 (0.0)	1.2E-01 (0.0)	1.2E-01 (0.0)
Eyes	7.4E-06 (8.1)	1.1E-05 (7.1)	1.8E-05 (5.3)	2.2E-05 (4.9)	2.8E-05 (4.3)
CC[E] (mSv/Gy.cm^2)	4.3E-02 (0.1)	5.6E-02 (0.1)	6.8E-02 (0.1)	7.9E-02 (0.1)	8.9E-02 (0.1)

*Adrenals, extratoracic region, gall bladder, kidneys, lymphatic nodes, muscle, oral mucosa, pancreas,prostate, small intestine, spleen, thymus and heart..

Table 23 – Tube voltage effect on CC[H_T] and CC[E] (mSv/Gy.cm^2) for the MASH3 (patient) for FOV of 38 × 38 cm^2. The Type A uncertainties are presented in parentheses (*in* %).

Organ/Tissue	**70 kV**	**80 kV**	**90 kV**	**100 kV**	**110 kV**
Bone marrow	6.5E-02 (0.0)	8.0E-02 (0.0)	9.3E-02 (0.0)	1.0E-01 (0.0)	1.1E-01 (0.0)
Colon	6.7E-02 (0.0)	8.7E-02 (0.0)	1.1E-01 (0.0)	1.2E-01 (0.0)	1.4E-01 (0.0)
Lung	6.9E-02 (0.0)	8.5E-02 (0.0)	1.0E-01 (0.0)	1.1E-01 (0.0)	1.3E-01 (0.0)
Stomach	4.3E-02 (0.1)	6.0E-02 (0.1)	7.6E-02 (0.1)	9.0E-02 (0.1)	1.0E-01 (0.1)
Breast	1.6E-02 (0.2)	2.2E-02 (0.2)	2.7E-02 (0.2)	3.3E-02 (0.2)	3.8E-02 (0.1)
Remainder tissues*	6.0E-03 (0.0)	6.9E-03 (0.0)	7.8E-03 (0.0)	8.5E-03 (0.0)	9.1E-03 (0.0)
Gonads	2.9E-03 (0.6)	4.3E-03 (0.5)	6.0E-03 (0.4)	7.5E-03 (0.4)	9.0E-03 (0.4)
Bladder	5.5E-02 (0.1)	7.4E-02 (0.1)	9.2E-02 (0.1)	1.1E-01 (0.1)	1.2E-01 (0.1)
Oesophagus	3.5E-02 (0.1)	4.8E-02 (0.1)	6.0E-02 (0.1)	7.2E-02 (0.1)	8.2E-02 (0.1)
Liver	5.1E-02 (0.0)	6.8E-02 (0.0)	8.4E-02 (0.0)	1.0E-01 (0.0)	1.1E-01 (0.0)
Thyroid	5.2E-03 (0.5)	7.5E-03 (0.5)	9.8E-03 (0.4)	1.2E-02 (0.4)	1.4E-02 (0.4)
Bone surface	3.1E-02 (0.0)	3.7E-02 (0.0)	4.3E-02 (0.0)	4.8E-02 (0.0)	5.1E-02 (0.0)
Brain	9.2E-05 (0.9)	1.5E-04 (0.8)	2.1E-04 (0.7)	2.8E-04 (0.6)	3.5E-04 (0.5)
Salivary glands	3.1E-04 (0.6)	4.6E-04 (0.5)	6.2E-04 (0.4)	7.8E-04 (0.4)	9.2E-04 (0.4)
Skin	1.0E-01 (0.0)	1.1E-01 (0.0)	1.1E-01 (0.0)	1.2E-01 (0.0)	1.2E-01 (0.0)
Eyes	1.1E-05 (6.8)	1.7E-05 (5.4)	2.2E-05 (4.8)	2.9E-05 (4.2)	3.5E-05 (3.8)
CC[E] (mSv/Gy.cm^2)	3.9E-02 (0.1)	5.0E-02 (0.1)	6.1E-02 (0.1)	7.1E-02 (0.1)	8.0E-02 (0.1)

*Adrenals, extratoracic region, gall bladder, kidneys, lymphatic nodes, muscle, oral mucosa, pancreas,prostate, small intestine, spleen, thymus and heart..

APPENDIX **B**

CC[E] and CC[H_T] estimates for physician.

Table 24 – Tube voltage effect on CC[H_T] and CC[E] (μSv/Gy.cm^2) for the FASH3 (physician) for FOV of 15 × 15 cm^2. The Type A uncertainties are presented in parentheses (*in* %).

Organ/Tissue	70 kV	80 kV	90 kV	100 kV	110 kV
Bone marrow	7.8E-02 (0.4)	1.1E-01 (0.3)	1.5E-01 (0.3)	1.9E-01 (0.3)	2.3E-01 (0.2)
Colon	6.4E-03 (3.7)	1.7E-02 (2.2)	3.8E-02 (1.5)	6.8E-02 (1.2)	9.9E-02 (1.0)
Lung	3.0E-02 (1.3)	4.6E-02 (1.0)	6.7E-02 (0.9)	9.7E-02 (0.7)	1.3E-01 (0.6)
Stomach	6.2E-03 (5.6)	2.0E-02 (3.2)	4.4E-02 (2.3)	7.8E-02 (1.7)	1.2E-01 (1.4)
Breast	2.6E-02 (2.3)	4.6E-02 (1.7)	7.4E-02 (1.3)	1.1E-01 (1.1)	1.6E-01 (0.9)
Remainder tissues*	2.4E-03 (0.3)	3.3E-03 (0.3)	4.4E-03 (0.2)	5.7E-03 (0.2)	7.1E-03 (0.2)
Gonads	2.4E-03 (27.1)	8.9E-03 (14.1)	1.6E-02 (10.3)	3.6E-02 (7.3)	5.4E-02 (6.1)
Bladder	1.7E-03 (19.8)	6.3E-03 (11.8)	1.4E-02 (7.4)	2.7E-02 (5.3)	3.7E-02 (4.6)
Oesophagus	2.5E-02 (5.3)	3.8E-02 (4.0)	5.5E-02 (3.3)	8.0E-02 (2.9)	1.2E-01 (2.3)
Liver	1.1E-02 (2.8)	2.6E-02 (1.8)	5.3E-02 (1.4)	8.8E-02 (1.1)	1.4E-01 (0.9)
Thyroid	7.1E-02 (5.2)	1.0E-01 (4.2)	1.3E-01 (3.7)	1.7E-01 (3.2)	2.3E-01 (2.9)
Bone surface	0.0E+00 (0.0)	0.0E+00 (0.0)	0.0E+00 (0.0)	0.0E+00 (0.0)	0.0E+00 (0.0)
Brain	3.0E-01 (0.6)	4.5E-01 (0.5)	6.1E-01 (0.4)	7.7E-01 (0.4)	9.1E-01 (0.4)
Salivary glands	3.9E-01 (0.7)	4.7E-01 (0.6)	5.2E-01 (0.6)	5.9E-01 (0.6)	6.4E-01 (0.5)
Skin	1.9E-01 (0.2)	2.3E-01 (0.2)	2.7E-01 (0.2)	3.1E-01 (0.2)	3.5E-01 (0.1)
Eyes	8.1E-02 (2.1)	9.9E-02 (1.9)	1.2E-01 (1.7)	1.4E-01 (1.6)	1.6E-01 (1.6)
CC[E] (μSv/Gy.cm^2)	3.1E-02 (2.5)	4.8E-02 (1.4)	7.1E-02 (1.0)	9.9E-02 (0.7)	1.3E-01 (0.6)

*Adrenals, extratoracic region, gall bladder, kidneys, lymphatic nodes, muscle, oral mucosa, pancreas,prostate, small intestine, spleen, thymus and heart..

Table 25 – Tube voltage effect on CC[H_T] and CC[E] (μSv/Gy.cm^2) for the FASH3 (physician) for FOV of 17 × 17 cm^2. The Type A uncertainties are presented in parentheses (*in* %).

Organ/Tissue	70 kV	80 kV	90 kV	100 kV	110 kV
Bone marrow	7.9E-02 (0.4)	1.1E-01 (0.3)	1.5E-01 (0.3)	1.9E-01 (0.3)	2.3E-01 (0.2)
Colon	7.5E-03 (3.3)	2.0E-02 (2.0)	4.2E-02 (1.4)	7.4E-02 (1.1)	1.1E-01 (0.9)
Lung	3.1E-02 (1.2)	4.6E-02 (1.0)	6.8E-02 (0.8)	9.7E-02 (0.7)	1.3E-01 (0.6)
Stomach	7.3E-03 (5.3)	2.1E-02 (3.2)	4.8E-02 (2.2)	8.3E-02 (1.7)	1.3E-01 (1.4)
Breast	2.8E-02 (2.2)	4.6E-02 (1.7)	7.1E-02 (1.3)	1.1E-01 (1.1)	1.6E-01 (0.9)
Remainder tissues*	2.5E-03 (0.3)	3.4E-03 (0.3)	4.6E-03 (0.2)	5.9E-03 (0.2)	7.4E-03 (0.2)
Gonads	3.5E-03 (23.9)	9.0E-03 (13.3)	2.1E-02 (8.9)	3.7E-02 (6.9)	5.9E-02 (5.7)
Bladder	1.9E-03 (18.0)	6.6E-03 (9.8)	1.5E-02 (6.5)	2.7E-02 (5.1)	4.3E-02 (4.2)
Oesophagus	2.5E-02 (5.1)	4.0E-02 (4.1)	5.9E-02 (3.2)	8.4E-02 (2.7)	1.1E-01 (2.4)
Liver	1.2E-02 (2.6)	2.9E-02 (1.8)	5.7E-02 (1.3)	9.7E-02 (1.0)	1.4E-01 (0.8)
Thyroid	6.7E-02 (5.2)	9.9E-02 (4.5)	1.2E-01 (3.7)	1.7E-01 (3.3)	2.4E-01 (2.8)
Bone surface	0.0E+00 (0.0)	0.0E+00 (0.0)	0.0E+00 (0.0)	0.0E+00 (0.0)	0.0E+00 (0.0)
Brain	3.0E-01 (0.6)	4.5E-01 (0.5)	6.1E-01 (0.4)	7.6E-01 (0.4)	9.1E-01 (0.4)
Salivary glands	3.8E-01 (0.7)	4.5E-01 (0.6)	5.1E-01 (0.6)	5.6E-01 (0.6)	6.1E-01 (0.5)
Skin	2.0E-01 (0.2)	2.4E-01 (0.2)	2.8E-01 (0.2)	3.2E-01 (0.2)	3.6E-01 (0.1)
Eyes	8.6E-02 (2.1)	1.0E-01 (1.9)	1.2E-01 (1.7)	1.4E-01 (1.6)	1.6E-01 (1.5)
CC[E] (μSv/Gy.cm^2)	3.2E-02 (2.2)	4.9E-02 (1.3)	7.2E-02 (0.9)	1.0E-01 (0.7)	1.4E-01 (0.6)

*Adrenals, extratoracic region, gall bladder, kidneys, lymphatic nodes, muscle, oral mucosa, pancreas,prostate, small intestine, spleen, thymus and heart..

Table 26 – Tube voltage effect on CC[H_T] and CC[E] (μSv/Gy.cm^2) for the FASH3 (physician) for FOV of 22 × 22 cm^2. The Type A uncertainties are presented in parentheses (*in* %).

Organ/Tissue	70 kV	80 kV	90 kV	100 kV	110 kV
Bone marrow	8.2E-02 (0.4)	1.2E-01 (0.3)	1.6E-01 (0.3)	2.0E-01 (0.3)	2.4E-01 (0.2)
Colon	9.8E-03 (2.9)	2.7E-02 (1.8)	5.5E-02 (1.3)	9.6E-02 (1.0)	1.4E-01 (0.8)
Lung	3.2E-02 (1.2)	4.8E-02 (1.0)	7.2E-02 (0.8)	1.0E-01 (0.7)	1.4E-01 (0.6)
Stomach	9.2E-03 (4.6)	2.8E-02 (2.8)	6.3E-02 (1.9)	1.1E-01 (1.5)	1.6E-01 (1.2)
Breast	2.9E-02 (2.2)	5.2E-02 (1.6)	8.2E-02 (1.2)	1.3E-01 (1.0)	1.8E-01 (0.8)
Remainder tissues*	2.8E-03 (0.3)	3.9E-03 (0.2)	5.2E-03 (0.2)	6.8E-03 (0.2)	8.4E-03 (0.2)
Gonads	2.9E-03 (24.0)	1.1E-02 (12.1)	2.8E-02 (7.7)	5.0E-02 (6.1)	7.9E-02 (4.9)
Bladder	3.6E-03 (13.1)	1.0E-02 (8.1)	2.2E-02 (6.0)	4.4E-02 (4.2)	6.5E-02 (3.6)
Oesophagus	2.3E-02 (5.1)	3.7E-02 (3.9)	5.8E-02 (3.2)	8.7E-02 (2.7)	1.2E-01 (2.2)
Liver	1.6E-02 (2.3)	3.7E-02 (1.5)	7.3E-02 (1.1)	1.2E-01 (0.9)	1.8E-01 (0.8)
Thyroid	6.9E-02 (5.1)	9.7E-02 (4.4)	1.3E-01 (3.8)	1.7E-01 (3.3)	2.2E-01 (2.9)
Bone surface	0.0E+00 (0.0)	0.0E+00 (0.0)	0.0E+00 (0.0)	0.0E+00 (0.0)	0.0E+00 (0.0)
Brain	2.9E-01 (0.6)	4.4E-01 (0.5)	5.9E-01 (0.4)	7.3E-01 (0.4)	8.6E-01 (0.4)
Salivary glands	3.4E-01 (0.7)	4.1E-01 (0.6)	4.7E-01 (0.6)	5.1E-01 (0.6)	5.6E-01 (0.6)
Skin	2.0E-01 (0.2)	2.5E-01 (0.2)	2.9E-01 (0.2)	3.3E-01 (0.1)	3.7E-01 (0.1)
Eyes	8.7E-02 (2.1)	1.1E-01 (1.8)	1.2E-01 (1.7)	1.4E-01 (1.6)	1.6E-01 (1.6)
CC[E] (μSv/Gy.cm^2)	3.3E-02 (2.1)	5.2E-02 (1.1)	7.9E-02 (0.8)	1.1E-01 (0.6)	1.5E-01 (0.5)

*Adrenals, extratoracic region, gall bladder, kidneys, lymphatic nodes, muscle, oral mucosa, pancreas,prostate, small intestine, spleen, thymus and heart..

Table 27 – Tube voltage effect on CC[H_T] and CC[E] (μSv/Gy.cm^2) for the FASH3 (physician) for FOV of 25 × 25 cm^2. The Type A uncertainties are presented in parentheses (*in* %).

Organ/Tissue	70 kV	80 kV	90 kV	100 kV	110 kV
Bone marrow	8.4E-02 (0.3)	1.2E-01 (0.3)	1.6E-01 (0.3)	2.0E-01 (0.3)	2.5E-01 (0.2)
Colon	1.1E-02 (2.7)	2.8E-02 (1.2)	6.1E-02 (1.2)	1.1E-01 (0.9)	1.5E-01 (0.8)
Lung	3.2E-02 (1.2)	4.9E-02 (0.8)	7.4E-02 (0.8)	1.0E-01 (0.7)	1.4E-01 (0.6)
Stomach	9.9E-03 (4.5)	3.0E-02 (1.9)	6.4E-02 (1.9)	1.1E-01 (1.4)	1.7E-01 (1.2)
Breast	3.0E-02 (2.1)	5.3E-02 (1.2)	8.7E-02 (1.2)	1.3E-01 (1.0)	1.9E-01 (0.8)
Remainder tissues*	2.9E-03 (0.3)	4.0E-03 (0.2)	5.4E-03 (0.2)	7.1E-03 (0.2)	8.8E-03 (0.2)
Gonads	4.8E-03 (19.9)	1.5E-02 (7.1)	3.5E-02 (7.1)	6.4E-02 (5.5)	8.9E-02 (4.6)
Bladder	3.7E-03 (12.8)	1.2E-02 (5.1)	2.6E-02 (5.1)	4.8E-02 (4.0)	6.8E-02 (3.5)
Oesophagus	2.5E-02 (5.1)	4.0E-02 (3.2)	6.0E-02 (3.2)	9.2E-02 (2.7)	1.2E-01 (2.2)
Liver	1.6E-02 (2.2)	3.9E-02 (1.1)	7.9E-02 (1.1)	1.3E-01 (0.9)	1.9E-01 (0.7)
Thyroid	7.4E-02 (5.0)	8.5E-02 (3.8)	1.3E-01 (3.8)	1.7E-01 (3.2)	2.1E-01 (2.8)
Bone surface	0.0E+00 (0.0)	0.0E+00 (0.0)	0.0E+00 (0.0)	0.0E+00 (0.0)	0.0E+00 (0.0)
Brain	2.9E-01 (0.6)	4.3E-01 (0.4)	5.8E-01 (0.4)	7.2E-01 (0.4)	8.6E-01 (0.4)
Salivary glands	3.4E-01 (0.7)	3.9E-01 (0.6)	4.5E-01 (0.6)	5.0E-01 (0.6)	5.5E-01 (0.6)
Skin	2.1E-01 (0.2)	2.5E-01 (0.2)	3.0E-01 (0.2)	3.4E-01 (0.1)	3.8E-01 (0.1)
Eyes	8.7E-02 (2.0)	1.1E-01 (0.6)	1.3E-01 (1.7)	1.5E-01 (1.7)	1.6E-01 (1.5)
CC[E] (μSv/Gy.cm^2)	3.4E-02 (1.8)	5.3E-02 (1.1)	8.2E-02 (0.7)	1.2E-01 (0.6)	1.6E-01 (0.5)

*Adrenals, extratoracic region, gall bladder, kidneys, lymphatic nodes, muscle, oral mucosa, pancreas,prostate, small intestine, spleen, thymus and heart..

Table 28 – Tube voltage effect on CC[H_T] and CC[E] (μSv/Gy.cm^2) for the FASH3 (physician) for FOV of 31 × 31 cm^2. The Type A uncertainties are presented in parentheses (*in* %).

Organ/Tissue	70 kV	80 kV	90 kV	100 kV	110 kV
Bone marrow	8.5E-02 (0.3)	1.2E-01 (0.3)	1.6E-01 (0.3)	2.0E-01 (0.3)	2.5E-01 (0.2)
Colon	1.2E-02 (2.6)	3.1E-02 (1.6)	6.3E-02 (1.2)	1.1E-01 (0.9)	1.6E-01 (0.8)
Lung	3.3E-02 (1.2)	5.1E-02 (1.0)	7.6E-02 (0.8)	1.1E-01 (0.7)	1.5E-01 (0.6)
Stomach	1.0E-02 (4.5)	3.2E-02 (2.6)	6.7E-02 (1.8)	1.2E-01 (1.4)	1.8E-01 (1.2)
Breast	3.2E-02 (2.1)	5.4E-02 (1.5)	9.0E-02 (1.2)	1.4E-01 (0.9)	2.0E-01 (0.8)
Remainder tissues*	3.1E-03 (0.3)	4.3E-03 (0.2)	5.8E-03 (0.2)	7.5E-03 (0.2)	9.3E-03 (0.2)
Gonads	3.6E-03 (21.1)	1.9E-02 (9.5)	3.9E-02 (6.8)	6.7E-02 (5.3)	9.7E-02 (4.4)
Bladder	4.5E-03 (11.6)	1.6E-02 (6.7)	3.0E-02 (5.0)	5.7E-02 (3.6)	8.2E-02 (3.1)
Oesophagus	2.3E-02 (5.1)	3.9E-02 (3.9)	6.1E-02 (3.2)	8.7E-02 (2.6)	1.2E-01 (2.2)
Liver	1.8E-02 (2.1)	4.2E-02 (1.4)	8.0E-02 (1.1)	1.4E-01 (0.8)	2.0E-01 (0.7)
Thyroid	7.0E-02 (5.2)	9.5E-02 (4.3)	1.4E-01 (3.6)	1.7E-01 (3.1)	2.3E-01 (2.7)
Bone surface	0.0E+00 (0.0)	0.0E+00 (0.0)	0.0E+00 (0.0)	0.0E+00 (0.0)	0.0E+00 (0.0)
Brain	2.9E-01 (0.6)	4.3E-01 (0.5)	5.7E-01 (0.4)	7.1E-01 (0.4)	8.4E-01 (0.4)
Salivary glands	3.4E-01 (0.7)	3.9E-01 (0.6)	4.5E-01 (0.6)	5.0E-01 (0.6)	5.4E-01 (0.6)
Skin	2.2E-01 (0.2)	2.6E-01 (0.2)	3.0E-01 (0.2)	3.5E-01 (0.1)	3.9E-01 (0.1)
Eyes	9.1E-02 (1.9)	1.1E-01 (1.8)	1.3E-01 (1.7)	1.4E-01 (1.6)	1.6E-01 (1.6)
CC[E] (μSv/Gy.cm^2)	1.4E-02 (1.9)	5.5E-02 (0.9)	8.4E-02 (0.7)	1.2E-01 (0.5)	1.6E-01 (0.5)

*Adrenals, extratoracic region, gall bladder, kidneys, lymphatic nodes, muscle, oral mucosa, pancreas,prostate, small intestine, spleen, thymus and heart..

Table 29 – Tube voltage effect on CC[H_T] and CC[E] (μSv/Gy.cm^2) for the FASH3 (physician) for FOV of 38 × 38 cm^2. The Type A uncertainties are presented in parentheses (*in* %).

Organ/Tissue	70 kV	80 kV	90 kV	100 kV	110 kV
Bone marrow	8.4E-02 (0.3)	1.2E-01 (0.3)	1.6E-01 (0.3)	2.0E-01 (0.3)	2.4E-01 (0.2)
Colon	1.2E-02 (2.7)	3.1E-02 (1.7)	6.0E-02 (1.2)	1.0E-01 (0.9)	1.5E-01 (0.8)
Lung	3.5E-02 (1.1)	5.4E-02 (0.9)	7.8E-02 (0.8)	1.1E-01 (0.7)	1.5E-01 (0.6)
Stomach	1.0E-02 (4.4)	3.1E-02 (2.6)	6.4E-02 (1.8)	1.1E-01 (1.4)	1.7E-01 (1.2)
Breast	3.1E-02 (2.0)	5.6E-02 (1.5)	9.1E-02 (1.2)	1.4E-01 (0.9)	2.0E-01 (0.8)
Remainder tissues*	3.5E-03 (0.2)	4.7E-03 (0.2)	6.2E-03 (0.2)	8.0E-03 (0.2)	9.8E-03 (0.2)
Gonads	4.2E-03 (18.1)	1.7E-02 (9.7)	3.5E-02 (7.0)	6.1E-02 (5.7)	9.5E-02 (4.4)
Bladder	4.3E-03 (12.0)	1.4E-02 (7.2)	3.1E-02 (5.1)	5.6E-02 (3.7)	8.2E-02 (3.1)
Oesophagus	2.7E-02 (4.6)	4.1E-02 (4.0)	6.1E-02 (3.1)	9.1E-02 (2.6)	1.3E-01 (2.2)
Liver	1.9E-02 (2.0)	4.5E-02 (1.4)	8.1E-02 (1.1)	1.3E-01 (0.8)	1.9E-01 (0.7)
Thyroid	7.4E-02 (4.9)	9.2E-02 (4.4)	1.4E-01 (3.7)	1.8E-01 (3.3)	2.2E-01 (2.9)
Bone surface	0.0E+00 (0.0)	0.0E+00 (0.0)	0.0E+00 (0.0)	0.0E+00 (0.0)	0.0E+00 (0.0)
Brain	2.8E-01 (0.6)	4.1E-01 (0.5)	5.5E-01 (0.4)	6.9E-01 (0.4)	8.0E-01 (0.4)
Salivary glands	3.4E-01 (0.7)	3.9E-01 (0.6)	4.5E-01 (0.6)	5.0E-01 (0.6)	5.4E-01 (0.6)
Skin	2.2E-01 (0.2)	2.7E-01 (0.2)	3.1E-01 (0.1)	3.5E-01 (0.1)	4.0E-01 (0.1)
Eyes	8.5E-02 (2.1)	1.0E-01 (1.8)	1.2E-01 (1.7)	1.4E-01 (1.7)	1.5E-01 (1.6)
CC[E] (μSv/Gy.cm^2)	3.5E-02 (1.7)	5.5E-02 (1.0)	8.3E-02 (0.7)	1.2E-01 (0.6)	1.6E-01 (0.5)

*Adrenals, extratoracic region, gall bladder, kidneys, lymphatic nodes, muscle, oral mucosa, pancreas,prostate, small intestine, spleen, thymus and heart..

Table 30 – Tube voltage effect on CC[H_T] and CC[E] (μSv/Gy.cm^2) for the MASH3 (physician) for FOV of 15 × 15 cm^2. The Type A uncertainties are presented in parentheses (*in* %).

Organ/Tissue	70 kV	80 kV	90 kV	100 kV	110 kV
Bone marrow	2.1E-01 (0.2)	2.8E-01 (0.2)	3.6E-01 (0.2)	4.4E-01 (0.2)	5.2E-01 (0.2)
Colon	6.3E-03 (3.7)	1.8E-02 (2.2)	3.6E-02 (1.6)	6.4E-02 (1.2)	1.0E-01 (1.0)
Lung	1.7E-02 (1.6)	3.2E-02 (1.2)	5.4E-02 (0.9)	8.4E-02 (0.7)	1.2E-01 (0.6)
Stomach	5.7E-03 (5.8)	1.8E-02 (3.5)	3.9E-02 (2.4)	6.9E-02 (1.8)	1.1E-01 (1.5)
Breast	2.3E-02 (6.5)	5.3E-02 (4.4)	9.1E-02 (3.0)	1.6E-01 (2.3)	2.4E-01 (1.8)
Remainder tissues*	3.2E-03 (0.2)	4.4E-03 (0.2)	5.9E-03 (0.2)	7.7E-03 (0.2)	9.7E-03 (0.2)
Gonads	2.6E-03 (17.2)	9.5E-03 (9.4)	2.7E-02 (6.1)	4.3E-02 (4.7)	5.8E-02 (3.9)
Bladder	2.5E-03 (11.1)	9.8E-03 (6.6)	2.2E-02 (4.6)	4.2E-02 (3.4)	6.6E-02 (2.8)
Oesophagus	1.5E-02 (6.3)	2.2E-02 (4.9)	4.2E-02 (3.8)	6.8E-02 (3.0)	1.0E-01 (2.4)
Liver	1.1E-02 (2.5)	2.6E-02 (1.7)	5.3E-02 (1.2)	9.1E-02 (1.0)	1.4E-01 (0.8)
Thyroid	3.9E-02 (6.2)	6.1E-02 (5.0)	1.0E-01 (4.0)	1.4E-01 (3.3)	2.0E-01 (2.7)
Bone surface	0.0E+00 (0.0)	0.0E+00 (0.0)	0.0E+00 (0.0)	0.0E+00 (0.0)	0.0E+00 (0.0)
Brain	2.2E-01 (0.6)	3.4E-01 (0.5)	4.6E-01 (0.5)	5.7E-01 (0.4)	6.8E-01 (0.4)
Salivary glands	7.0E-02 (1.4)	8.6E-02 (1.3)	1.1E-01 (1.2)	1.2E-01 (1.1)	1.5E-01 (1.0)
Skin	1.5E-01 (0.2)	1.9E-01 (0.2)	2.3E-01 (0.2)	2.7E-01 (0.1)	3.1E-01 (0.1)
Eyes	1.8E-01 (1.8)	2.2E-01 (1.6)	2.5E-01 (1.5)	2.9E-01 (1.4)	3.3E-01 (1.3)
CC[E] (μSv/Gy.cm^2)	3.9E-02(1.9)	6.0E-02 (1.1)	8.9E-02 (0.8)	1.3E-01 (0.6)	1.7E-02 (0.5)

*Adrenals, extratoracic region, gall bladder, kidneys, lymphatic nodes, muscle, oral mucosa, pancreas,prostate, small intestine, spleen, thymus and heart..

Table 31 – Tube voltage effect on CC[H_T] and CC[E] (μSv/Gy.cm^2) for the MASH3 (physician) for FOV of 17 × 17 cm^2. The Type A uncertainties are presented in parentheses (*in* %).

Organ/Tissue	**70 kV**	**80 kV**	**90 kV**	**100 kV**	**110 kV**
Bone marrow	2.1E-01 (0.2)	2.9E-01 (0.2)	3.7E-01 (0.2)	4.4E-01 (0.2)	5.2E-01 (0.2)
Colon	7.2E-03 (3.3)	1.9E-02 (2.1)	4.0E-02 (1.5)	7.0E-02 (1.1)	1.1E-01 (0.9)
Lung	1.7E-02 (1.5)	3.1E-02 (1.2)	5.3E-02 (0.9)	8.6E-02 (0.7)	1.3E-01 (0.6)
Stomach	6.4E-03 (5.6)	2.0E-02 (3.4)	3.9E-02 (2.3)	7.4E-02 (1.7)	1.2E-01 (1.4)
Breast	2.5E-02 (6.4)	4.9E-02 (4.2)	9.4E-02 (3.0)	1.6E-01 (2.3)	2.4E-01 (1.8)
Remainder tissues*	3.3E-03 (0.2)	4.6E-03 (0.2)	6.2E-03 (0.2)	8.0E-03 (0.2)	1.0E-02 (0.2)
Gonads	3.9E-03 (12.8)	1.1E-02 (8.2)	2.8E-02 (5.5)	4.5E-02 (4.4)	7.0E-02 (3.6)
Bladder	3.1E-03 (11.4)	1.2E-02 (6.2)	2.3E-02 (4.4)	4.6E-02 (3.1)	7.1E-02 (2.8)
Oesophagus	1.4E-02 (6.6)	2.6E-02 (4.7)	4.3E-02 (3.6)	6.8E-02 (2.8)	9.9E-02 (2.3)
Liver	1.1E-02 (2.5)	2.8E-02 (1.6)	5.5E-02 (1.2)	9.4E-02 (0.9)	1.4E-01 (0.8)
Thyroid	3.8E-02 (6.5)	6.5E-02 (5.0)	9.4E-02 (4.1)	1.5E-01 (3.2)	2.1E-01 (2.6)
Bone surface	0.0E+00 (0.0)	0.0E+00 (0.0)	0.0E+00 (0.0)	0.0E+00 (0.0)	0.0E+00 (0.0)
Brain	2.2E-01 (0.6)	3.4E-01 (0.5)	4.5E-01 (0.5)	5.7E-01 (0.4)	6.7E-01 (0.4)
Salivary glands	7.3E-02 (1.3)	8.7E-02 (1.2)	1.1E-01 (1.1)	1.3E-01 (1.1)	1.5E-01 (1.0)
Skin	1.6E-01 (0.2)	2.0E-01 (0.2)	2.4E-01 (0.2)	2.8E-01 (0.1)	3.2E-01 (0.1)
Eyes	1.8E-01 (1.8)	2.2E-01 (1.6)	2.5E-01 (1.5)	2.9E-01 (1.4)	3.3E-01 (1.3)
CC[E] (μSv/Gy.cm^2)	4.0E-02 (1.6)	6.1E-02 (1.0)	9.1E-02 (0.7)	1.3E-01 (0.6)	1.7E-01 (0.5)

*Adrenals, extratoracic region, gall bladder, kidneys, lymphatic nodes, muscle, oral mucosa, pancreas,prostate, small intestine, spleen, thymus and heart..

Table 32 – Tube voltage effect on CC[H_T] and CC[E] (μSv/Gy.cm^2) for the MASH3 (physician) for FOV of 22 × 22 cm^2. The Type A uncertainties are presented in parentheses (*in* %).

Organ/Tissue	**70 kV**	**80 kV**	**90 kV**	**100 kV**	**110 kV**
Bone marrow	2.2E-01 (0.2)	3.0E-01 (0.2)	3.9E-01 (0.2)	4.7E-01 (0.2)	5.5E-01 (0.2)
Colon	9.2E-03 (3.0)	2.5E-02 (1.8)	5.3E-02 (1.3)	9.2E-02 (1.0)	1.4E-01 (0.8)
Lung	1.8E-02 (1.5)	3.3E-02 (1.1)	5.7E-02 (0.9)	8.9E-02 (0.7)	1.3E-01 (0.6)
Stomach	7.6E-03 (5.2)	2.4E-02 (3.0)	5.0E-02 (2.1)	9.1E-02 (1.5)	1.4E-01 (1.3)
Breast	2.5E-02 (6.4)	5.5E-02 (4.1)	1.0E-01 (3.0)	1.6E-01 (2.3)	2.4E-01 (1.8)
Remainder tissues*	3.8E-03 (0.2)	5.3E-03 (0.2)	7.1E-03 (0.2)	9.2E-03 (0.2)	1.1E-02 (0.2)
Gonads	6.4E-03 (10.7)	2.1E-02 (6.5)	4.5E-02 (4.3)	7.5E-02 (3.4)	1.0E-01 (3.0)
Bladder	4.4E-03 (10.0)	1.6E-02 (5.3)	3.2E-02 (3.7)	6.3E-02 (2.7)	9.1E-02 (2.3)
Oesophagus	1.4E-02 (6.1)	2.6E-02 (4.7)	4.4E-02 (3.6)	6.6E-02 (2.8)	1.0E-01 (2.4)
Liver	1.4E-02 (2.2)	3.3E-02 (1.5)	6.6E-02 (1.1)	1.1E-01 (0.9)	1.7E-01 (0.7)
Thyroid	3.5E-02 (6.5)	6.4E-02 (5.1)	9.6E-02 (3.9)	1.4E-01 (3.3)	2.0E-01 (2.7)
Bone surface	0.0E+00 (0.0)	0.0E+00 (0.0)	0.0E+00 (0.0)	0.0E+00 (0.0)	0.0E+00 (0.0)
Brain	2.2E-01 (0.6)	3.3E-01 (0.5)	4.4E-01 (0.5)	5.5E-01 (0.4)	6.4E-01 (0.4)
Salivary glands	7.7E-02 (1.3)	9.4E-02 (1.2)	1.1E-01 (1.1)	1.3E-01 (1.0)	1.5E-01 (1.0)
Skin	1.8E-01 (0.2)	2.3E-01 (0.2)	2.7E-01 (0.1)	3.1E-01 (0.1)	3.6E-01 (0.1)
Eyes	1.7E-01 (1.8)	2.1E-01 (1.7)	2.5E-01 (1.5)	2.8E-01 (1.4)	3.0E-01 (1.4)
CC[E] (μSv/Gy.cm^2)	4.2E-02 (1.5)	6.7E-02 (0.9)	1.0E-01 (0.6)	1.4E-01 (0.5)	1.9E-01 (0.4)

*Adrenals, extratoracic region, gall bladder, kidneys, lymphatic nodes, muscle, oral mucosa, pancreas,prostate, small intestine, spleen, thymus and heart..

Table 33 – Tube voltage effect on CC[H_T] and CC[E] (μSv/Gy.cm^2) for the MASH3 (physician) for FOV of 25 × 25 cm^2. The Type A uncertainties are presented in parentheses (*in* %).

Organ/Tissue	70 kV	80 kV	90 kV	100 kV	110 kV
Bone marrow	2.3E-01 (0.2)	3.1E-01 (0.2)	4.0E-01 (0.2)	4.8E-01 (0.2)	5.6E-01 (0.2)
Colon	1.0E-02 (2.8)	2.8E-02 (1.7)	5.8E-02 (1.2)	1.0E-01 (0.9)	1.5E-01 (0.8)
Lung	1.8E-02 (1.5)	3.3E-02 (1.1)	5.7E-02 (0.9)	8.9E-02 (0.7)	1.3E-01 (0.6)
Stomach	8.3E-03 (4.9)	2.7E-02 (2.8)	5.3E-02 (2.0)	9.9E-02 (1.5)	1.5E-01 (1.2)
Breast	2.3E-02 (6.8)	5.2E-02 (4.2)	9.4E-02 (3.0)	1.6E-01 (2.3)	2.4E-01 (1.9)
Remainder tissues*	4.1E-03 (0.2)	5.6E-03 (0.2)	7.5E-03 (0.2)	9.7E-03 (0.2)	1.2E-02 (0.2)
Gonads	7.8E-03 (12.2)	2.4E-02 (5.5)	5.1E-02 (4.0)	9.1E-02 (3.2)	1.2E-01 (2.7)
Bladder	5.2E-03 (8.5)	1.6E-02 (5.4)	3.6E-02 (3.4)	6.9E-02 (2.7)	9.9E-02 (2.1)
Oesophagus	1.4E-02 (6.8)	2.7E-02 (4.6)	4.6E-02 (3.4)	7.4E-02 (2.8)	1.0E-01 (2.4)
Liver	1.5E-02 (2.2)	3.5E-02 (1.4)	6.8E-02 (1.1)	1.2E-01 (0.8)	1.8E-01 (0.7)
Thyroid	3.9E-02 (6.2)	5.8E-02 (5.0)	9.3E-02 (4.0)	1.4E-01 (3.3)	2.0E-01 (2.8)
Bone surface	0.0E+00 (0.0)	0.0E+00 (0.0)	0.0E+00 (0.0)	0.0E+00 (0.0)	0.0E+00 (0.0)
Brain	2.1E-01 (0.6)	3.2E-01 (0.5)	4.3E-01 (0.5)	5.3E-01 (0.4)	6.3E-01 (0.4)
Salivary glands	7.7E-02 (1.3)	9.5E-02 (1.2)	1.2E-01 (1.1)	1.3E-01 (1.0)	1.5E-01 (0.9)
Skin	2.0E-01 (0.2)	2.4E-01 (0.1)	2.9E-01 (0.1)	3.3E-01 (0.1)	3.8E-01 (0.1)
Eyes	1.6E-01 (1.9)	2.0E-01 (1.7)	2.4E-01 (1.5)	2.6E-01 (1.5)	3.0E-01 (1.4)
CC[E] (μSv/Gy.cm^2)	4.4E-02 (1.5)	6.9E-02 (0.9)	1.0E-01 (0.6)	1.5E-01 (0.5)	1.9E-01 (0.4)

*Adrenals, extratoracic region, gall bladder, kidneys, lymphatic nodes, muscle, oral mucosa, pancreas,prostate, small intestine, spleen, thymus and heart..

Table 34 – Tube voltage effect on CC[H_T] and CC[E] (μSv/Gy.cm^2) for the MASH3 (physician) for FOV of 31 × 31 cm^2. The Type A uncertainties are presented in parentheses (*in* %).

Organ/Tissue	70 kV	80 kV	90 kV	100 kV	110 kV
Bone marrow	2.2E-01 (0.2)	3.0E-01 (0.2)	3.8E-01 (0.2)	4.6E-01 (0.2)	5.4E-01 (0.2)
Colon	1.1E-02 (2.7)	2.9E-02 (1.7)	5.9E-02 (1.2)	1.0E-01 (0.9)	1.5E-01 (0.8)
Lung	1.9E-02 (1.5)	3.4E-02 (1.1)	5.7E-02 (0.9)	8.7E-02 (0.7)	1.3E-01 (0.6)
Stomach	8.4E-03 (4.7)	2.7E-02 (2.8)	5.7E-02 (1.9)	1.0E-01 (1.5)	1.6E-01 (1.2)
Breast	2.8E-02 (6.2)	5.5E-02 (4.3)	9.1E-02 (3.1)	1.5E-01 (2.3)	2.2E-01 (1.9)
Remainder tissues*	4.2E-03 (0.2)	5.8E-03 (0.2)	7.7E-03 (0.2)	9.9E-03 (0.2)	1.2E-02 (0.2)
Gonads	8.5E-03 (9.5)	2.8E-02 (5.2)	6.0E-02 (3.7)	9.5E-02 (3.0)	1.4E-01 (2.5)
Bladder	5.1E-03 (8.1)	1.7E-02 (5.0)	4.0E-02 (3.4)	7.2E-02 (2.5)	1.1E-01 (2.1)
Oesophagus	1.5E-02 (6.2)	2.6E-02 (4.9)	4.3E-02 (3.8)	6.6E-02 (2.9)	9.7E-02 (2.4)
Liver	1.5E-02 (2.1)	3.6E-02 (1.4)	7.2E-02 (1.0)	1.2E-01 (0.8)	1.8E-01 (0.7)
Thyroid	3.6E-02 (6.3)	5.9E-02 (5.1)	9.4E-02 (4.2)	1.3E-01 (3.4)	1.9E-01 (2.9)
Bone surface	0.0E+00 (0.0)	0.0E+00 (0.0)	0.0E+00 (0.0)	0.0E+00 (0.0)	0.0E+00 (0.0)
Brain	1.9E-01 (0.7)	2.9E-01 (0.6)	3.9E-01 (0.5)	4.8E-01 (0.5)	5.7E-01 (0.4)
Salivary glands	7.8E-02 (1.3)	9.6E-02 (1.2)	1.1E-01 (1.1)	1.3E-01 (1.0)	1.5E-01 (1.0)
Skin	2.0E-01 (0.2)	2.4E-01 (0.1)	2.9E-01 (0.1)	3.4E-01 (0.1)	3.8E-01 (0.1)
Eyes	1.5E-01 (2.0)	1.8E-01 (1.8)	2.1E-01 (1.7)	2.4E-01 (1.6)	2.5E-01 (1.5)
CC[E] (μSv/Gy.cm^2)	4.4E-02 (1.4)	6.8E-02 (0.9)	1.0E-01 (0.6)	1.4E-01 (0.5)	1.9E-01 (0.4)

*Adrenals, extratoracic region, gall bladder, kidneys, lymphatic nodes, muscle, oral mucosa, pancreas,prostate, small intestine, spleen, thymus and heart..

Table 35 – Tube voltage effect on CC[H_T] and CC[E] (μSv/Gy.cm^2) for the MASH3 (physician) for FOV of 38 × 38 cm^2. The Type A uncertainties are presented in parentheses (*in* %).

Organ/Tissue	**70 kV**	**80 kV**	**90 kV**	**100 kV**	**110 kV**
Bone marrow	2.1E-01 (0.2)	2.8E-01 (0.2)	3.5E-01 (0.2)	4.3E-01 (0.2)	5.0E-01 (0.2)
Colon	9.9E-03 (2.8)	2.6E-02 (1.7)	5.4E-02 (1.2)	9.4E-02 (1.0)	1.4E-01 (0.8)
Lung	2.0E-02 (1.4)	3.3E-02 (1.1)	5.6E-02 (0.9)	8.4E-02 (0.7)	1.2E-01 (0.6)
Stomach	7.8E-03 (4.9)	2.3E-02 (2.9)	5.2E-02 (2.0)	9.6E-02 (1.5)	1.4E-01 (1.2)
Breast	2.3E-02 (7.1)	4.9E-02 (4.5)	8.4E-02 (3.2)	1.4E-01 (2.4)	2.0E-01 (2.0)
Remainder tissues*	4.2E-03 (0.2)	5.7E-03 (0.2)	7.5E-03 (0.2)	9.7E-03 (0.2)	1.2E-02 (0.2)
Gonads	8.5E-03 (9.8)	2.6E-02 (5.3)	5.4E-02 (4.0)	9.2E-02 (3.0)	1.3E-01 (2.6)
Bladder	4.2E-03 (8.9)	1.5E-02 (5.0)	3.6E-02 (3.5)	6.3E-02 (2.7)	9.1E-02 (2.2)
Oesophagus	1.6E-02 (6.3)	2.5E-02 (4.9)	4.0E-02 (3.6)	6.1E-02 (3.0)	9.0E-02 (2.4)
Liver	1.6E-02 (2.1)	3.6E-02 (1.4)	6.8E-02 (1.1)	1.2E-01 (0.8)	1.7E-01 (0.7)
Thyroid	4.2E-02 (6.7)	5.3E-02 (5.3)	7.9E-02 (4.5)	1.2E-01 (3.5)	1.6E-01 (3.0)
Bone surface	0.0E+00 (0.0)	0.0E+00 (0.0)	0.0E+00 (0.0)	0.0E+00 (0.0)	0.0E+00 (0.0)
Brain	1.7E-01 (0.7)	2.6E-01 (0.6)	3.5E-01 (0.5)	4.4E-01 (0.5)	5.1E-01 (0.4)
Salivary glands	8.2E-02 (1.3)	9.9E-02 (1.2)	1.1E-01 (1.1)	1.3E-01 (1.0)	1.5E-01 (0.9)
Skin	1.9E-01 (0.2)	2.3E-01 (0.1)	2.8E-01 (0.1)	3.2E-01 (0.1)	3.6E-01 (0.1)
Eyes	1.3E-01 (2.1)	1.5E-01 (1.9)	1.8E-01 (1.7)	2.0E-01 (1.7)	2.2E-01 (1.6)
CC[E] (μSv/Gy.cm^2)	4.1E-02 (1.4)	6.3E-02 (0.9)	9.4E-02 (0.6)	1.3E-01 (0.5)	1.7E-01 (0.4)

*Adrenals, extratoracic region, gall bladder, kidneys, lymphatic nodes, muscle, oral mucosa, pancreas,prostate, small intestine, spleen, thymus and heart..

APPENDIX C

CC[E] and CC[H_T] estimates for assistant physician.

Table 36 – Tube voltage effect on CC[H_T] and CC[E] (μSv/Gy.cm^2) for the FASH3 (assistant physician) for FOV of 15 × 15 cm^2. The Type A uncertainties are presented in parentheses (*in* %).

Organ/Tissue	70 kV	80 kV	90 kV	100 kV	110 kV
Bone marrow	2.4E-01 (0.2)	3.4E-01 (0.2)	4.1E-01 (0.2)	4.9E-01 (0.2)	5.7E-01 (0.2)
Colon	2.1E-02 (2.2)	4.2E-02 (1.7)	5.6E-02 (1.4)	7.9E-02 (1.2)	1.0E-01 (1.0)
Lung	5.6E-02 (0.9)	9.0E-02 (0.8)	1.1E-01 (0.7)	1.4E-01 (0.6)	1.7E-01 (0.6)
Stomach	1.7E-02 (3.9)	3.4E-02 (3.0)	5.1E-02 (2.3)	7.6E-02 (1.9)	1.0E-01 (1.7)
Breast	2.3E-02 (2.5)	3.8E-02 (2.0)	5.0E-02 (1.7)	6.6E-02 (1.5)	8.4E-02 (1.3)
Remainder tissues*	4.9E-03 (0.2)	7.1E-03 (0.2)	8.3E-03 (0.2)	1.0E-02 (0.2)	1.2E-02 (0.2)
Gonads	2.1E-03 (28.5)	8.2E-03 (14.5)	1.9E-02 (10.9)	2.5E-02 (9.8)	3.1E-02 (8.0)
Bladder	1.3E-03 (24.5)	6.6E-03 (12.7)	8.5E-03 (9.3)	1.6E-02 (7.2)	2.3E-02 (6.3)
Oesophagus	2.1E-02 (5.1)	4.1E-02 (4.3)	4.8E-02 (3.8)	6.6E-02 (3.2)	8.6E-02 (2.9)
Liver	4.9E-03 (4.0)	9.7E-03 (3.0)	1.6E-02 (2.4)	2.5E-02 (2.0)	3.8E-02 (1.6)
Thyroid	5.0E-02 (5.9)	7.5E-02 (4.9)	9.7E-02 (4.4)	1.2E-01 (4.0)	1.6E-01 (3.5)
Bone surface	9.1E-02 (0.2)	1.3E-01 (0.2)	1.5E-01 (0.2)	1.8E-01 (0.2)	2.0E-01 (0.2)
Brain	3.0E-01 (0.6)	4.4E-01 (0.5)	5.6E-01 (0.4)	6.8E-01 (0.4)	8.0E-01 (0.4)
Salivary glands	2.9E-01 (0.7)	3.4E-01 (0.6)	3.9E-01 (0.6)	4.3E-01 (0.6)	4.7E-01 (0.5)
Skin	2.0E-01 (0.2)	2.6E-01 (0.2)	2.9E-01 (0.1)	3.3E-01 (0.1)	3.7E-01 (0.1)
Eyes	4.6E-02 (2.8)	5.8E-02 (2.6)	6.8E-02 (2.4)	7.4E-02 (2.3)	8.3E-02 (2.2)
CC[E] (μSv/Gy.cm^2)	5.60E-02 (3.0)	8.4E-2 (3.0)	1.E-01 (1.5)	1.3E-01 (1.0)	1.6E-01 (1.0)

*Adrenals, extratoracic region, gall bladder, kidneys, lymphatic nodes, muscle, oral mucosa, pancreas,prostate, small intestine, spleen, thymus and heart..

Table 37 – Tube voltage effect on CC[H_T] and CC[E] (μSv/Gy.cm^2) for the FASH3 (assistant physician) for FOV of 17 × 17 cm^2. The Type A uncertainties are presented in parentheses (*in* %).

Organ/Tissue	70 kV	80 kV	90 kV	100 kV	110 kV
Bone marrow	2.5E-01(0.2)	3.4E-01 (0.2)	4.3E-01 (0.2)	5.2E-01 (0.2)	5.9E-01 (0.2)
Colon	2.5E-02(2.0)	4.2E-02 (1.5)	6.4E-02 (1.3)	8.9E-02 (1.1)	1.2E-01 (1.0)
Lung	6.2E-02(0.9)	9.0E-02 (0.7)	1.2E-01 (0.6)	1.5E-01 (0.6)	1.8E-01 (0.5)
Stomach	1.8E-02(3.8)	3.4E-02 (2.8)	5.6E-02 (2.1)	8.1E-02 (1.8)	1.1E-01 (1.6)
Breast	2.4E-02(2.4)	3.8E-02 (1.9)	5.2E-02 (1.6)	7.1E-02 (1.4)	9.0E-02 (1.3)
Remainder tissues*	5.3E-03(0.2)	7.1E-03 (0.2)	9.1E-03 (0.2)	1.1E-02 (0.2)	1.3E-02 (0.2)
Gonads	4.9E-03(24.3)	8.2E-03 (15.7)	1.4E-02 (11.7)	2.7E-02 (8.5)	3.1E-02 (8.1)
Bladder	1.5E-03(22.5)	6.6E-03 (10.8)	1.0E-02 (8.6)	1.8E-02 (6.5)	2.4E-02 (5.7)
Oesophagus	2.3E-02(5.0)	4.1E-02 (4.2)	5.3E-02 (3.5)	6.8E-02 (3.1)	9.5E-02 (2.8)
Liver	5.1E-03(3.8)	9.7E-03 (2.9)	1.8E-02 (2.3)	2.9E-02 (1.8)	4.1E-02 (1.6)
Thyroid	5.3E-02(5.8)	7.5E-02 (5.0)	1.0E-01 (4.3)	1.3E-01 (3.8)	1.6E-01 (3.4)
Bone surface	9.6E-02(0.2)	1.3E-01 (0.2)	1.6E-01 (0.2)	1.9E-01 (0.2)	2.1E-01 (0.2)
Brain	3.0E-01(0.6)	4.4E-01 (0.5)	5.7E-01 (0.4)	7.0E-01 (0.4)	8.1E-01 (0.4)
Salivary glands	2.9E-01(0.7)	3.4E-01 (0.6)	4.0E-01 (0.6)	4.4E-01 (0.6)	4.8E-01 (0.5)
Skin	2.1E-01(0.2)	2.6E-01 (0.2)	3.1E-01 (0.1)	3.5E-01 (0.1)	3.9E-01 (0.1)
Eyes	4.7E-02(2.8)	5.8E-02 (2.6)	6.8E-02 (2.4)	7.5E-02 (2.3)	8.2E-02 (2.2)
CC[E] (μSv/Gy.cm^2)	5.6E-02 (1.0)	8.4E-02 (1.0)	1.1E-01 (1.4)	1.4E-01 (1.0)	1.7E-01 (1.0)

*Adrenals, extratoracic region, gall bladder, kidneys, lymphatic nodes, muscle, oral mucosa, pancreas,prostate, small intestine, spleen, thymus and heart.

Table 38 – Tube voltage effect on CC[H_T] and CC[E] (μSv/Gy.cm^2) for the FASH3 (assistant physician) for FOV of 22 × 22 cm^2. The Type A uncertainties are presented in parentheses (*in* %).

Organ/Tissue	70 kV	80 kV	90 kV	100 kV	110 kV
Bone marrow	2.9E-01 (0.2)	3.9E-01 (0.2)	4.8E-01 (0.2)	5.8E-01 (0.2)	6.6E-01 (0.2)
Colon	4.5E-02 (1.5)	7.0E-02 (1.2)	1.0E-01 (1.0)	1.4E-01 (0.9)	1.7E-01 (0.8)
Lung	8.0E-02 (0.7)	1.1E-01 (0.6)	1.5E-01 (0.6)	1.9E-01 (0.5)	2.3E-01 (0.5)
Stomach	2.7E-02 (2.9)	5.1E-02 (2.2)	8.2E-02 (1.8)	1.2E-01 (1.5)	1.6E-01 (1.3)
Breast	2.9E-02 (2.2)	4.4E-02 (1.8)	6.3E-02 (1.5)	8.4E-02 (1.3)	1.1E-01 (1.1)
Remainder tissues*	6.9E-03 (0.2)	9.1E-03 (0.2)	1.1E-02 (0.2)	1.4E-02 (0.2)	1.6E-02 (0.2)
Gonads	5.2E-03 (19.7)	1.5E-02 (12.0)	2.1E-02 (8.9)	3.8E-02 (7.6)	5.8E-02 (6.2)
Bladder	3.4E-03 (16.4)	7.8E-03 (10.1)	1.5E-02 (7.6)	2.5E-02 (5.7)	3.6E-02 (4.7)
Oesophagus	2.6E-02 (5.0)	4.3E-02 (3.9)	6.1E-02 (3.4)	8.2E-02 (2.8)	1.1E-01 (2.5)
Liver	6.7E-03 (3.4)	1.4E-02 (2.4)	2.4E-02 (1.9)	3.8E-02 (1.6)	5.4E-02 (1.4)
Thyroid	5.7E-02 (5.7)	7.7E-02 (4.9)	1.1E-01 (4.2)	1.4E-01 (3.9)	1.8E-01 (3.3)
Bone surface	1.1E-01 (0.2)	1.5E-01 (0.2)	1.8E-01 (0.2)	2.1E-01 (0.2)	2.4E-01 (0.2)
Brain	3.1E-01 (0.5)	4.6E-01 (0.5)	5.9E-01 (0.4)	7.2E-01 (0.4)	8.3E-01 (0.4)
Salivary glands	3.0E-01 (0.6)	3.6E-01 (0.6)	4.1E-01 (0.6)	4.5E-01 (0.6)	4.9E-01 (0.5)
Skin	2.6E-01 (0.2)	3.1E-01 (0.1)	3.6E-01 (0.1)	4.1E-01 (0.1)	4.6E-01 (0.1)
Eyes	4.6E-02 (2.7)	5.6E-02 (2.7)	6.9E-02 (2.4)	7.4E-02 (2.2)	8.4E-02 (2.2)
CC[E] (mSv/Gy.cm^2)	7.1E-02 (2.0)	1.0E-01 (1.0)	1.3E-01 (1.0)	1.7E-01 (1.0)	2.0E-01 (1.0)

*Adrenals, extratoracic region, gall bladder, kidneys, lymphatic nodes, muscle, oral mucosa, pancreas,prostate, small intestine, spleen, thymus and heart.

Table 39 – Tube voltage effect on CC[H_T] and CC[E] (μSv/Gy.cm^2) for the FASH3 (assistant physician) for FOV of 25 × 25 cm^2. The Type A uncertainties are presented in parentheses (*in* %).

Organ/Tissue	70 kV	80 kV	90 kV	100 kV	110 kV
Bone marrow	3.0E-01 (0.2)	4.0E-01 (0.2)	5.0E-01 (0.2)	6.0E-01 (0.2)	6.8E-01 (0.2)
Colon	5.3E-02 (1.3)	8.2E-02 (1.1)	1.2E-01 (1.0)	1.5E-01 (0.8)	1.9E-01 (0.8)
Lung	8.9E-02 (0.7)	1.2E-01 (0.6)	1.6E-01 (0.5)	2.0E-01 (0.5)	2.4E-01 (0.5)
Stomach	3.0E-02 (2.8)	5.7E-02 (2.1)	9.0E-02 (1.7)	1.3E-01 (1.5)	1.7E-01 (1.3)
Breast	3.0E-02 (2.2)	4.5E-02 (1.8)	6.6E-02 (1.5)	9.1E-02 (1.2)	1.2E-01 (1.1)
Remainder tissues*	7.4E-03 (0.2)	9.8E-03 (0.2)	1.2E-02 (0.2)	1.5E-02 (0.2)	1.7E-02 (0.1)
Gonads	6.0E-03 (17.1)	1.6E-02 (12.0)	2.4E-02 (8.9)	3.5E-02 (7.2)	5.7E-02 (5.9)
Bladder	3.7E-03 (15.3)	9.9E-03 (8.9)	1.6E-02 (6.9)	3.0E-02 (5.2)	4.5E-02 (4.6)
Oesophagus	2.9E-02 (4.6)	4.5E-02 (3.7)	6.5E-02 (3.2)	8.8E-02 (2.7)	1.1E-01 (2.4)
Liver	7.5E-03 (3.2)	1.6E-02 (2.4)	2.6E-02 (1.8)	4.2E-02 (1.5)	5.9E-02 (1.3)
Thyroid	6.0E-02 (5.8)	7.9E-02 (4.8)	1.1E-01 (4.2)	1.5E-01 (3.6)	1.7E-01 (3.3)
Bone surface	1.1E-01 (0.2)	1.5E-01 (0.2)	1.9E-01 (0.2)	2.2E-01 (0.2)	2.5E-01 (0.2)
Brain	3.2E-01 (0.5)	4.5E-01 (0.5)	5.9E-01 (0.4)	7.2E-01 (0.4)	8.4E-01 (0.4)
Salivary glands	3.1E-01 (0.6)	3.6E-01 (0.6)	4.1E-01 (0.6)	4.6E-01 (0.6)	4.9E-01 (0.5)
Skin	2.7E-01 (0.1)	3.3E-01 (0.1)	3.8E-01 (0.1)	4.3E-01 (0.1)	4.8E-01 (0.1)
Eyes	4.6E-02 (2.8)	6.0E-02 (2.6)	6.6E-02 (2.5)	7.9E-02 (2.2)	8.4E-02 (2.3)
CC[E] (μSv/Gy.cm^2)	7.6E-02 (1.6)	1.1E-01 (1.1)	1.4E-01 (0.9)	1.8E-01 (0.7)	2.1E-01 (0.6)

*Adrenals, extratoracic region, gall bladder, kidneys, lymphatic nodes, muscle, oral mucosa, pancreas,prostate, small intestine, spleen, thymus and heart.

Table 40 – Tube voltage effect on CC[H_T] and CC[E] (μSv/Gy.cm^2) for the FASH3 (assistant physician) for FOV of 31 × 31 cm^2. The Type A uncertainties are presented in parentheses (*in* %).

Organ/Tissue	70 kV	80 kV	90 kV	100 kV	110 kV
Bone marrow	3.2E-01 (0.2)	4.2E-01 (0.2)	5.2E-01 (0.2)	6.2E-01 (0.2)	7.1E-01 (0.2)
Colon	7.0E-02 (1.2)	1.0E-01 (1.0)	1.4E-01 (0.9)	1.8E-01 (0.8)	2.2E-01 (0.7)
Lung	1.0E-01 (0.7)	1.4E-01 (0.6)	1.8E-01 (0.5)	2.3E-01 (0.5)	2.7E-01 (0.4)
Stomach	4.0E-02 (2.4)	6.6E-02 (2.0)	1.1E-01 (1.6)	1.5E-01 (1.4)	1.9E-01 (1.2)
Breast	3.2E-02 (2.0)	4.9E-02 (1.7)	6.9E-02 (1.4)	9.7E-02 (1.2)	1.3E-01 (1.0)
Remainder tissues*	8.2E-03 (0.2)	1.1E-02 (0.2)	1.3E-02 (0.2)	1.6E-02 (0.1)	1.8E-02 (0.1)
Gonads	8.0E-03 (16.9)	2.1E-02 (10.1)	3.2E-02 (7.7)	4.1E-02 (7.0)	6.6E-02 (5.7)
Bladder	3.8E-03 (12.8)	1.0E-02 (8.8)	1.9E-02 (6.6)	3.3E-02 (5.0)	4.5E-02 (4.2)
Oesophagus	3.2E-02 (4.6)	5.1E-02 (3.6)	7.3E-02 (3.0)	9.7E-02 (2.7)	1.2E-01 (2.3)
Liver	8.7E-03 (3.0)	1.7E-02 (2.2)	3.0E-02 (1.8)	4.7E-02 (1.4)	6.7E-02 (1.2)
Thyroid	6.2E-02 (5.4)	9.1E-02 (4.5)	1.1E-01 (4.2)	1.5E-01 (3.5)	1.8E-01 (3.3)
Bone surface	1.2E-01 (0.2)	1.6E-01 (0.2)	1.9E-01 (0.2)	2.3E-01 (0.2)	2.6E-01 (0.1)
Brain	3.2E-01 (0.5)	4.6E-01 (0.5)	5.9E-01 (0.4)	7.2E-01 (0.4)	8.4E-01 (0.4)
Salivary glands	3.2E-01 (0.6)	3.7E-01 (0.6)	4.1E-01 (0.6)	4.6E-01 (0.5)	5.0E-01 (0.5)
Skin	2.9E-01 (0.1)	3.5E-01 (0.1)	4.1E-01 (0.1)	4.6E-01 (0.1)	5.1E-01 (0.1)
Eyes	4.9E-02 (2.8)	6.0E-02 (2.6)	7.1E-02 (2.3)	8.0E-02 (2.2)	8.4E-02 (2.1)
CC[E] (μSv/Gy.cm^2)	8.4E-02 (1.7)	1.2E-01 (1.0)	1.5E-01 (1.0)	1.9E-01 (1.0)	2.3E-01 (1.0)

*Adrenals, extratoracic region, gall bladder, kidneys, lymphatic nodes, muscle, oral mucosa, pancreas,prostate, small intestine, spleen, thymus and heart.

Table 41 – Tube voltage effect on CC[H_T] and CC[E] (μSv/Gy.cm^2) for the FASH3 (assistant physician) for FOV of 38 × 38 cm^2. The Type A uncertainties are presented in parentheses (*in* %).

Organ/Tissue	70 kV	80 kV	90 kV	100 kV	110 kV
Bone marrow	3.2E-01 (0.2)	4.3E-01 (0.2)	5.3E-01 (0.2)	6.2E-01 (0.2)	7.1E-01 (0.1)
Colon	7.3E-02 (1.1)	1.1E-01 (1.0)	1.5E-01 (0.8)	1.9E-01 (0.7)	2.4E-01 (0.7)
Lung	1.1E-01 (0.6)	1.5E-01 (0.6)	1.9E-01 (0.5)	2.4E-01 (0.5)	2.8E-01 (0.4)
Stomach	4.4E-02 (2.3)	7.6E-02 (1.8)	1.1E-01 (1.5)	1.7E-01 (1.2)	2.1E-01 (1.1)
Breast	3.4E-02 (2.0)	5.3E-02 (1.6)	8.0E-02 (1.3)	1.1E-01 (1.1)	1.4E-01 (1.0)
Remainder tissues*	8.7E-03 (0.2)	1.1E-02 (0.2)	1.4E-02 (0.2)	1.6E-02 (0.1)	1.9E-02 (0.1)
Gonads	9.0E-03 (14.6)	1.8E-02 (10.0)	3.2E-02 (8.1)	4.7E-02 (6.4)	7.0E-02 (5.6)
Bladder	4.8E-03 (12.6)	9.9E-03 (8.4)	2.4E-02 (5.8)	3.4E-02 (4.8)	4.8E-02 (4.0)
Oesophagus	3.4E-02 (4.1)	5.1E-02 (3.4)	7.8E-02 (2.9)	1.1E-01 (2.4)	1.3E-01 (2.2)
Liver	9.2E-03 (2.9)	2.0E-02 (2.0)	3.4E-02 (1.6)	5.5E-02 (1.3)	7.6E-02 (1.1)
Thyroid	7.5E-02 (5.0)	9.2E-02 (4.3)	1.1E-01 (3.9)	1.5E-01 (3.4)	2.0E-01 (3.1)
Bone surface	1.2E-01 (0.2)	1.6E-01 (0.2)	2.0E-01 (0.2)	2.3E-01 (0.2)	2.6E-01 (0.1)
Brain	3.1E-01 (0.5)	4.5E-01 (0.5)	5.8E-01 (0.4)	7.1E-01 (0.4)	8.2E-01 (0.4)
Salivary glands	3.1E-01 (0.6)	3.6E-01 (0.6)	4.1E-01 (0.6)	4.6E-01 (0.5)	5.0E-01 (0.5)
Skin	3.1E-01 (0.1)	3.6E-01 (0.1)	4.2E-01 (0.1)	4.7E-01 (0.1)	5.2E-01 (0.1)
Eyes	4.9E-02 (2.7)	6.0E-02 (2.5)	6.7E-02 (2.4)	7.5E-02 (2.3)	8.4E-02 (2.2)
CC[E] (μSv/Gy.cm^2)	8.7E-02 (1.0)	1.2E-01 (1.0)	1.6E-01 (1.0)	2.0E-01 (1.0)	2.4E-01 (1.0)

*Adrenals, extratoracic region, gall bladder, kidneys, lymphatic nodes, muscle, oral mucosa, pancreas,prostate, small intestine, spleen, thymus and heart.

Table 42 – Tube voltage effect on CC[H_T] and CC[E] (μSv/Gy.cm^2) for the MASH3 (assistant physician) for FOV of 15 × 15 cm^2. The Type A uncertainties are presented in parentheses (*in* %).

Organ/Tissue	70 kV	80 kV	90 kV	100 kV	110 kV
Bone marrow	2.7E-01 (0.2)	3.6E-01 (0.2)	4.5E-01 (0.2)	5.4E-01 (0.2)	6.2E-01 (0.1)
Colon	1.5E-02 (2.4)	2.5E-02 (1.9)	3.9E-02 (1.6)	5.5E-02 (1.4)	7.4E-02 (1.2)
Lung	8.2E-02 (0.7)	1.2E-01 (0.6)	1.5E-01 (0.5)	2.0E-01 (0.5)	2.3E-01 (0.4)
Stomach	1.8E-02 (3.6)	3.2E-02 (2.7)	4.9E-02 (2.3)	7.4E-02 (1.8)	1.0E-01 (1.6)
Breast	2.1E-02 (7.0)	3.4E-02 (5.3)	5.5E-02 (4.1)	8.8E-02 (3.8)	1.1E-01 (2.8)
Remainder tissues*	8.3E-03 (0.2)	1.1E-02 (0.2)	1.3E-02 (0.1)	1.5E-02 (0.1)	1.8E-02 (0.1)
Gonads	2.1E-03 (27.3)	4.4E-03 (14.1)	9.2E-03 (10.2)	1.6E-02 (7.5)	2.7E-02 (5.9)
Bladder	1.0E-03 (21.2)	2.9E-03 (10.7)	6.6E-03 (8.1)	1.4E-02 (5.8)	2.2E-02 (4.8)
Oesophagus	2.7E-02 (4.9)	3.9E-02 (3.8)	6.2E-02 (3.1)	8.7E-02 (2.7)	1.1E-01 (2.4)
Liver	5.2E-03 (3.4)	1.1E-02 (2.6)	1.8E-02 (2.1)	2.8E-02 (1.7)	4.0E-02 (1.5)
Thyroid	3.8E-02 (6.5)	5.4E-02 (5.3)	7.8E-02 (4.5)	1.2E-01 (3.7)	1.5E-01 (3.2)
Bone surface	1.0E-01 (0.2)	1.3E-01 (0.2)	1.6E-01 (0.2)	1.9E-01 (0.2)	2.2E-01 (0.1)
Brain	2.8E-01 (0.6)	4.1E-01 (0.5)	5.4E-01 (0.4)	6.7E-01 (0.4)	7.8E-01 (0.4)
Salivary glands	1.7E-01 (0.8)	2.0E-01 (0.7)	2.3E-01 (0.7)	2.5E-01 (0.7)	2.7E-01 (0.7)
Skin	2.4E-01 (0.1)	2.9E-01 (0.1)	3.3E-01 (0.1)	3.7E-01 (0.1)	4.1E-01 (0.1)
Eyes	9.5E-02 (2.5)	1.2E-01 (2.2)	1.5E-01 (2.0)	1.6E-01 (1.9)	1.8E-01 (1.8)
CC[E] (μSv/Gy.cm^2)	6.1E-02 (3.0)	8.4E-02 (1.0)	1.1E-01 (1.0)	1.4E-01 (1.0)	1.7E-01 (1.0)

*Adrenals, extratoracic region, gall bladder, kidneys, lymphatic nodes, muscle, oral mucosa, pancreas,prostate, small intestine, spleen, thymus and heart.

Table 43 – Tube voltage effect on CC[H_T] and CC[E] (μSv/Gy.cm^2) for the MASH3 (assistant physician) for FOV of 17 × 17 cm^2. The Type A uncertainties are presented in parentheses (*in* %).

Organ/Tissue	70 kV	80 kV	90 kV	100 kV	110 kV
Bone marrow	2.7E-01 (0.2)	3.6E-01 (0.2)	4.6E-01 (0.2)	5.4E-01 (0.2)	6.2E-01 (0.1)
Colon	1.7E-02 (2.3)	2.9E-02 (1.8)	4.3E-02 (1.5)	6.0E-02 (1.3)	7.9E-02 (1.1)
Lung	8.4E-02 (0.7)	1.2E-01 (0.6)	1.6E-01 (0.5)	2.0E-01 (0.5)	2.4E-01 (0.4)
Stomach	1.9E-02 (3.4)	3.4E-02 (2.7)	5.4E-02 (2.2)	7.9E-02 (1.9)	1.1E-01 (1.6)
Breast	2.0E-02 (6.9)	3.9E-02 (5.5)	6.0E-02 (4.0)	9.2E-02 (3.5)	1.2E-01 (2.8)
Remainder tissues*	8.4E-03 (0.2)	1.1E-02 (0.2)	1.3E-02 (0.1)	1.6E-02 (0.1)	1.8E-02 (0.1)
Gonads	1.3E-03 (30.5)	4.9E-03 (14.5)	9.6E-03 (9.1)	2.0E-02 (6.5)	2.9E-02 (5.6)
Bladder	9.2E-04 (18.7)	3.9E-03 (10.8)	7.4E-03 (7.7)	1.5E-02 (5.4)	2.6E-02 (4.7)
Oesophagus	2.9E-02 (4.8)	4.1E-02 (3.9)	5.6E-02 (3.3)	8.2E-02 (2.7)	1.1E-01 (2.4)
Liver	5.6E-03 (3.4)	1.1E-02 (2.6)	1.9E-02 (2.0)	2.9E-02 (1.7)	4.1E-02 (1.5)
Thyroid	3.6E-02 (6.4)	5.4E-02 (5.5)	8.1E-02 (4.4)	1.1E-01 (3.9)	1.5E-01 (3.2)
Bone surface	1.0E-01 (0.2)	1.4E-01 (0.2)	1.7E-01 (0.2)	2.0E-01 (0.2)	2.2E-01 (0.1)
Brain	2.8E-01 (0.6)	4.1E-01 (0.5)	5.4E-01 (0.4)	6.7E-01 (0.4)	7.8E-01 (0.4)
Salivary glands	1.7E-01 (0.8)	2.0E-01 (0.7)	2.2E-01 (0.7)	2.4E-01 (0.7)	2.7E-01 (0.7)
Skin	2.4E-01 (0.1)	2.9E-01 (0.1)	3.4E-01 (0.1)	3.8E-01 (0.1)	4.2E-01 (0.1)
Eyes	9.5E-02 (2.4)	1.2E-01 (2.2)	1.4E-01 (2.1)	1.7E-01 (1.9)	1.8E-01 (1.9)
CC[E] (μSv/Gy.cm^2)	6.2E-02 (3.0)	8.7E-02 (1.0)	1.1E-01 (1.0)	1.4E-01 (1.0)	1.7E-01 (1.0)

*Adrenals, extratoracic region, gall bladder, kidneys, lymphatic nodes, muscle, oral mucosa, pancreas,prostate, small intestine, spleen, thymus and heart.

Table 44 – Tube voltage effect on CC[H_T] and CC[E] (μSv/Gy.cm^2) for the MASH3 (assistant physician) for FOV of 22 × 22 cm^2. The Type A uncertainties are presented in parentheses (*in* %).

Organ/Tissue	70 kV	80 kV	90 kV	100 kV	110 kV
Bone marrow	2.9E-01 (0.2)	3.8E-01 (0.2)	4.8E-01 (0.2)	5.7E-01 (0.1)	6.5E-01 (0.1)
Colon	2.6E-02 (1.8)	4.2E-02 (1.5)	6.4E-02 (1.2)	8.8E-02 (1.1)	1.2E-01 (0.9)
Lung	8.9E-02 (0.7)	1.3E-01 (0.6)	1.7E-01 (0.5)	2.1E-01 (0.5)	2.5E-01 (0.4)
Stomach	2.5E-02 (3.0)	4.5E-02 (2.3)	6.9E-02 (1.9)	9.6E-02 (1.6)	1.3E-01 (1.4)
Breast	2.2E-02 (7.1)	3.7E-02 (5.0)	5.8E-02 (4.1)	9.1E-02 (3.5)	1.2E-01 (2.8)
Remainder tissues*	8.8E-03 (0.2)	1.1E-02 (0.1)	1.4E-02 (0.1)	1.7E-02 (0.1)	1.9E-02 (0.1)
Gonads	3.5E-03 (18.7)	9.5E-03 (10.4)	1.9E-02 (7.1)	3.2E-02 (5.5)	4.4E-02 (4.8)
Bladder	2.0E-03 (14.6)	5.7E-03 (8.3)	1.2E-02 (6.5)	2.3E-02 (4.5)	3.2E-02 (3.8)
Oesophagus	2.7E-02 (4.5)	4.5E-02 (3.6)	7.2E-02 (3.0)	9.0E-02 (2.7)	1.2E-01 (2.4)
Liver	6.2E-03 (3.3)	1.3E-02 (2.4)	2.1E-02 (1.9)	3.3E-02 (1.6)	4.7E-02 (1.3)
Thyroid	3.6E-02 (6.5)	5.8E-02 (5.2)	8.2E-02 (4.4)	1.2E-01 (3.9)	1.5E-01 (3.4)
Bone surface	1.1E-01 (0.2)	1.4E-01 (0.2)	1.8E-01 (0.2)	2.1E-01 (0.1)	2.3E-01 (0.1)
Brain	2.7E-01 (0.6)	4.0E-01 (0.5)	5.3E-01 (0.4)	6.5E-01 (0.4)	7.6E-01 (0.4)
Salivary glands	1.6E-01 (0.8)	1.9E-01 (0.8)	2.1E-01 (0.7)	2.3E-01 (0.7)	2.5E-01 (0.7)
Skin	2.6E-01 (0.1)	3.2E-01 (0.1)	3.7E-01 (0.1)	4.2E-01 (0.1)	4.6E-01 (0.1)
Eyes	9.4E-02 (2.5)	1.2E-01 (2.3)	1.4E-01 (2.0)	1.6E-01 (1.9)	1.8E-01 (1.9)
CC[E] (μSv/Gy.cm^2)	6.6E-02 (2.0)	9.4E-02 (1.0)	1.2E-01 (1.0)	1.6E-01 (1.0)	1.9E-01 (1.0)

*Adrenals, extratoracic region, gall bladder, kidneys, lymphatic nodes, muscle, oral mucosa, pancreas,prostate, small intestine, spleen, thymus and heart.

Table 45 – Tube voltage effect on CC[H_T] and CC[E] (μSv/Gy.cm^2) for the MASH3 (assistant physician) for FOV of 25 × 25 cm^2. The Type A uncertainties are presented in parentheses (*in* %).

Organ/Tissue	70 kV	80 kV	90 kV	100 kV	110 kV
Bone marrow	3.0E-01 (0.2)	4.0E-01 (0.2)	4.9E-01 (0.2)	5.8E-01 (0.1)	6.7E-01 (0.1)
Colon	3.2E-02 (1.7)	5.1E-02 (1.3)	7.3E-02 (1.1)	1.0E-01 (1.0)	1.3E-01 (0.9)
Lung	9.0E-02 (0.7)	1.3E-01 (0.6)	1.7E-01 (0.5)	2.1E-01 (0.5)	2.6E-01 (0.4)
Stomach	2.7E-02 (2.9)	5.0E-02 (2.2)	7.5E-02 (1.8)	1.1E-01 (1.5)	1.4E-01 (1.3)
Breast	2.0E-02 (7.2)	4.2E-02 (5.2)	6.3E-02 (3.9)	8.5E-02 (3.3)	1.3E-01 (2.8)
Remainder tissues*	9.1E-03 (0.2)	1.2E-02 (0.1)	1.4E-02 (0.1)	1.7E-02 (0.1)	2.0E-02 (0.1)
Gonads	3.2E-03 (15.5)	8.8E-03 (10.0)	2.0E-02 (6.4)	3.9E-02 (4.7)	5.2E-02 (4.2)
Bladder	1.9E-03 (14.2)	6.3E-03 (8.1)	1.5E-02 (5.4)	2.4E-02 (4.3)	3.8E-02 (3.6)
Oesophagus	2.9E-02 (4.4)	4.6E-02 (3.7)	6.7E-02 (3.1)	8.7E-02 (2.7)	1.2E-01 (2.4)
Liver	6.4E-03 (3.2)	1.3E-02 (2.4)	2.3E-02 (1.8)	3.6E-02 (1.5)	5.2E-02 (1.3)
Thyroid	3.7E-02 (6.3)	5.9E-02 (5.2)	8.3E-02 (4.5)	1.1E-01 (3.8)	1.5E-01 (3.2)
Bone surface	1.1E-01 (0.2)	1.5E-01 (0.2)	1.8E-01 (0.2)	2.1E-01 (0.1)	2.4E-01 (0.1)
Brain	2.8E-01 (0.6)	4.0E-01 (0.5)	5.3E-01 (0.4)	6.4E-01 (0.4)	7.5E-01 (0.4)
Salivary glands	1.5E-01 (0.8)	1.8E-01 (0.8)	2.0E-01 (0.7)	2.3E-01 (0.7)	2.5E-01 (0.7)
Skin	2.7E-01 (0.1)	3.3E-01 (0.1)	3.8E-01 (0.1)	4.3E-01 (0.1)	4.8E-01 (0.1)
Eyes	9.4E-02 (2.5)	1.2E-01 (2.2)	1.3E-01 (2.1)	1.5E-01 (1.9)	1.8E-01 (1.8)
CC[E] (μSv/Gy.cm^2)	6.8E-02 (1.7)	9.7E-02 (1.1)	1.3E-01 (0.8)	1.6E-01 (0.6)	2.0E-01 (0.6)

*Adrenals, extratoracic region, gall bladder, kidneys, lymphatic nodes, muscle, oral mucosa, pancreas,prostate, small intestine, spleen, thymus and heart.

Table 46 – Tube voltage effect on CC[H_T] and CC[E] (μSv/Gy.cm^2) for the MASH3 (assistant physician) for FOV of 31 × 31 cm^2. The Type A uncertainties are presented in parentheses (*in* %).

Organ/Tissue	70 kV	80 kV	90 kV	100 kV	110 kV
Bone marrow	2.9E-01 (0.2)	3.8E-01 (0.2)	4.7E-01 (0.2)	5.6E-01 (0.1)	6.4E-01 (0.1)
Colon	4.2E-02 (1.5)	6.2E-02 (1.2)	8.9E-02 (1.0)	1.2E-01 (0.9)	1.5E-01 (0.8)
Lung	9.3E-02 (0.6)	1.3E-01 (0.6)	1.7E-01 (0.5)	2.1E-01 (0.5)	2.6E-01 (0.4)
Stomach	3.3E-02 (2.6)	5.7E-02 (2.1)	8.8E-02 (1.7)	1.3E-01 (1.4)	1.7E-01 (1.3)
Breast	2.1E-02 (7.0)	3.5E-02 (5.2)	5.8E-02 (4.1)	9.0E-02 (3.3)	1.3E-01 (2.8)
Remainder tissues*	9.1E-03 (0.2)	1.2E-02 (0.1)	1.4E-02 (0.1)	1.7E-02 (0.1)	2.0E-02 (0.1)
Gonads	3.4E-03 (17.8)	1.1E-02 (8.6)	2.6E-02 (6.0)	4.3E-02 (4.5)	6.1E-02 (3.9)
Bladder	2.1E-03 (15.5)	7.0E-03 (7.7)	1.4E-02 (5.5)	2.6E-02 (4.2)	4.0E-02 (3.5)
Oesophagus	2.9E-02 (4.6)	4.7E-02 (3.5)	6.7E-02 (2.9)	9.1E-02 (2.7)	1.2E-01 (2.3)
Liver	7.3E-03 (3.0)	1.5E-02 (2.2)	2.5E-02 (1.7)	3.9E-02 (1.4)	5.6E-02 (1.2)
Thyroid	2.9E-02 (6.9)	5.6E-02 (5.4)	7.8E-02 (4.5)	1.2E-01 (3.7)	1.4E-01 (3.3)
Bone surface	1.1E-01 (0.2)	1.4E-01 (0.2)	1.7E-01 (0.2)	2.0E-01 (0.1)	2.3E-01 (0.1)
Brain	2.5E-01 (0.6)	3.6E-01 (0.5)	4.8E-01 (0.5)	5.8E-01 (0.4)	6.8E-01 (0.4)
Salivary glands	1.4E-01 (0.9)	1.6E-01 (0.8)	1.8E-01 (0.8)	2.0E-01 (0.8)	2.2E-01 (0.7)
Skin	2.8E-01 (0.1)	3.3E-01 (0.1)	3.8E-01 (0.1)	4.3E-01 (0.1)	4.7E-01 (0.1)
Eyes	8.1E-02 (2.6)	1.0E-01 (2.3)	1.2E-01 (2.2)	1.5E-01 (2.1)	1.5E-01 (2.0)
CC[E] (μSv/Gy.cm^2)	6.9E-09 (2.0)	9.7E-02 (1.0)	1.3E-01 (1.0)	1.6E-01 (1.0)	2.0E-01 (1.0)

*Adrenals, extratoracic region, gall bladder, kidneys, lymphatic nodes, muscle, oral mucosa, pancreas,prostate, small intestine, spleen, thymus and heart.

Table 47 – Tube voltage effect on CC[H_T] and CC[E] (μSv/Gy.cm^2) for the MASH3 (assistant physician) for FOV of 38 × 38 cm^2. The Type A uncertainties are presented in parentheses (*in* %).

Organ/Tissue	**70 kV**	**80 kV**	**90 kV**	**100 kV**	**110 kV**
Bone marrow	2.6E-01 (0.2)	3.5E-01 (0.2)	4.3E-01 (0.2)	5.1E-01 (0.2)	5.9E-01 (0.1)
Colon	4.3E-02 (1.4)	6.3E-02 (1.2)	8.9E-02 (1.0)	1.2E-01 (0.9)	1.5E-01 (0.8)
Lung	8.9E-02 (0.7)	1.3E-01 (0.6)	1.6E-01 (0.5)	2.1E-01 (0.5)	2.5E-01 (0.4)
Stomach	3.5E-02 (2.5)	6.2E-02 (1.9)	9.4E-02 (1.6)	1.3E-01 (1.4)	1.7E-01 (1.2)
Breast	2.1E-02 (7.0)	3.5E-02 (5.1)	5.7E-02 (4.1)	8.5E-02 (3.4)	1.2E-01 (2.7)
Remainder tissues*	8.6E-03 (0.2)	1.1E-02 (0.2)	1.4E-02 (0.1)	1.6E-02 (0.1)	1.9E-02 (0.1)
Gonads	4.9E-03 (12.7)	1.1E-02 (8.6)	2.3E-02 (5.8)	4.5E-02 (4.7)	5.7E-02 (4.1)
Bladder	2.1E-03 (14.2)	6.3E-03 (7.7)	1.5E-02 (5.5)	2.6E-02 (4.1)	3.9E-02 (3.5)
Oesophagus	2.9E-02 (4.2)	4.8E-02 (3.6)	6.7E-02 (2.9)	8.9E-02 (2.6)	1.1E-01 (2.4)
Liver	7.2E-03 (2.9)	1.5E-02 (2.2)	2.6E-02 (1.7)	4.1E-02 (1.4)	6.0E-02 (1.2)
Thyroid	3.4E-02 (6.9)	5.4E-02 (5.4)	8.3E-02 (4.3)	1.1E-01 (3.8)	1.5E-01 (3.3)
Bone surface	1.0E-01 (0.2)	1.3E-01 (0.2)	1.6E-01 (0.2)	1.9E-01 (0.1)	2.1E-01 (0.1)
Brain	2.2E-01 (0.6)	3.2E-01 (0.5)	4.3E-01 (0.5)	5.2E-01 (0.4)	6.1E-01 (0.4)
Salivary glands	1.3E-01 (0.9)	1.5E-01 (0.8)	1.7E-01 (0.8)	1.9E-01 (0.8)	2.1E-01 (0.7)
Skin	2.6E-01 (0.1)	3.0E-01 (0.1)	3.5E-01 (0.1)	4.0E-01 (0.1)	4.4E-01 (0.1)
Eyes	7.0E-02 (2.8)	9.1E-02 (2.4)	1.1E-01 (2.4)	1.2E-01 (2.1)	1.4E-01 (2.0)
CC[E] (μSv/Gy.cm^2)	6.6E-02 (2.0)	9.2E-02 (1.0)	1.2E-01 (1.0)	1.6E-01 (1.8)	1.9E-01 (1.0)

*Adrenals, extratoracic region, gall bladder, kidneys, lymphatic nodes, muscle, oral mucosa, pancreas,prostate, small intestine, spleen, thymus and heart.